Continental lithosphere of the Arabian Plate: A geologic, petrologic, and geophysical synthesis

Robert J. Stern [a,*], Peter Johnson [b]

[a] Geosciences Dept. U. Texas at Dallas Richardson TX 75080-0688, USA
[b] 1242 Tenth Street NW Washington DC 20001, USA

ARTICLE INFO

ABSTRACT

The Arabian Plate originated ~25 Ma ago by rifting of NE Africa to form the Gulf of Aden and Red Sea. It is one of the smaller and younger of the Earth's lithospheric plates. The upper part of its crust consists of crystalline Precambrian basement, Phanerozoic sedimentary cover as much as 10 km thick, and Cenozoic flood basalt (harrat). The distribution of these rocks and variations in elevation across the Plate cause a pronounced geologic and topographic asymmetry, with extensive basement exposures (the Arabian Shield) and elevations of as much as 3000 m in the west, and a Phanerozoic succession (Arabian Platform) that thickens, and a surface that descends to sea level, eastward between the Shield and the northeastern margin of the Plate. This tilt in the Plate is partly the result of marginal uplift during rifting in the south and west, and loading during collision with, and subduction beneath, the Eurasian Plate in the northeast. But a variety of evidence suggests that the asymmetry also reflects a fundamental crustal and mantle heterogeneity in the Plate that dates from Neoproterozoic time when the crust formed.

The bulk of the Plate's upper crystalline crust is Neoproterozoic in age (1000–540 Ma) reflecting, in the west, a 300-million year process of continental crustal growth between ~850 and 550 Ma represented by amalgamated juvenile magmatic arcs, post-amalgamation sedimentary and volcanic basins, and granitoid intrusions that make up as much as 50% of the Shield's surface. Locally, Archean and Paleoproterozoic rocks are structurally intercalated with the juvenile Neoproterozoic rocks in the southern and eastern parts of the Shield. The geologic dataset for the age, composition, and origin of the upper crust of the Plate in the east is smaller than the database for the Shield, and conclusions made about the crust in the east are correspondingly less definitive. In the absence of exposures, furthermore, nothing is known by direct observation about the composition of the crust north of the Shield. Nonetheless, available data indicate a geologic history for eastern Arabian crust different to that in the west. The Neoproterozoic crust (~815–785 Ma) is somewhat older than in the bulk of the Arabian Shield, and igneous and metamorphic activity was largely finished by 750 Ma. Thereafter, the eastern part of the Plate became the site of virtually continuous sedimentation from 725 Ma on and into the Phanerozoic. This implies that a relatively strong lithosphere was in place beneath eastern Arabia by 700 Ma in contrast to a lithospheric instability that persisted to ~550 Ma in the west. Lithospheric differentiation is further indicated by the Phanerozoic depositional history with steady subsidence and accumulation of a sedimentary succession 5–14 km thick in the east and a consistent high-stand and thin to no Phanerozoic accumulation over the Shield. Geophysical data likewise indicate east–west lithospheric differentiation. Overall, the crustal thickness of the Plate (depth to the Moho) is ~40 km, but there is a tendency for the crust to thicken eastward by as much as 10% from 35–40 km beneath the Shield to 40–45 km beneath eastern Arabia. The crust also becomes structurally more complex with as many as 5 seismically recognized layers in the east compared to 3 layers in the west. A coincident increase in velocity is noted in the upper-crust layers. Complementary changes are evidenced in some models of the Arabian Plate continental upper mantle, indicating eastward thickening of the lithospheric mantle from ~80 km beneath the Shield to ~120 km beneath the Platform, which corresponds to an overall lithospheric thickening (crust and upper mantle) from ~120 km to ~160 km eastward. The locus of these changes coincides with a prominent magnetic anomaly (Central Arabian Magnetic Anomaly, CAMA) in the extreme eastern part of the Arabian Shield that extends north across the north-central part of the Arabian Plate. The CAMA also coincides with a major structural boundary separating a region of northerly and northwesterly basement trends in the west from a region of northerly and northeasterly trends in the northeastern part of the Plate, and with the transition from high-stand buoyant Shield to subsided Platform. Its coincidence with geophysically indicated changes in the lower crust and mantle structure suggests that a

* Corresponding author.
  E-mail address: rjstern@utdallas.edu (R.J. Stern).

fundamental lithospheric boundary is present in the central part of the Arabian Plate. The ages and isotopic characteristics of xenoliths brought to the surface in Cenozoic basalt eruptions indicate that the lower crust and upper mantle are largely juvenile Neoproterozoic additions, meaning that the lower crust and upper mantle formed about the same time as the upper crust. This implies that the lithospheric boundary in the central part of the Arabian Plate dates from Neoproterozoic time. We conclude that lithospheric differentiation across the Arabian Plate is long lived and has controlled much of the Phanerozoic sedimentary history of the Plate.

Contents

1. Introduction

This paper is a review of public-domain information about the composition and structure of the continental lithosphere of the Arabian Plate (Fig. 1). This is the twelfth largest and one of the youngest of the Earth's lithospheric plates, having originated ~25 Ma ago when rifting to form the Gulf of Aden and Red Sea split off a fragment of the African continent. Its crust comprises Precambrian crystalline basement, well exposed in the west and locally exposed in the east, a Phanerozoic sedimentary succession that is up to 10 km thick, and fields of Cenozoic basalt (harrat) unconformable on the crystalline basement and Phanerozoic sedimentary rocks in the western and northwestern parts of the Plate. The Arabian Shield is mostly Neoproterozoic but locally contains tectonically intercalated Archean and Paleoproterozoic rocks. Crystalline basement in the east of the Plate is also Neoproterozoic, but appears to have a geologic history different to that of the Shield.

The primary objective of our review is to summarize current information about the continental lithosphere of the Arabian Plate with the aim of highlighting regional similarities and differences in composition and structure. This is done for two purposes. One is to determine whether lithospheric differences are discernable across the plate that may correlate with or point to tectonic boundaries within the Plate. The other is to consider possible causes for the topographic and geologic asymmetry of the Plate. The upper crust of the Plate displays a long and complex history of crustal accretion, mostly during Neoproterozoic time (1000–544 Ma). It evolved through a large variety of magmatic, depositional, structural, and metamorphic events, and has a large geographic extent. It is pertinent, therefore, to consider whether the lower crust and upper mantle are similarly complex and whether tectonic boundaries recognized in the upper crust are mirrored by variations in the lower crust and upper mantle. These variations in

lithospheric structure may be important for understanding along-strike variations in the Arabia–Eurasian convergence zone, as briefly discussed by Stern and Johnson (2008). It is also pertinent to question whether the geologic and topographic asymmetries of the Plate originated recently or reflect a long-lived cause. The Plate's surface lies 2000–3000 m above sea level on the eastern margin of the Red Sea and northern margin of the Gulf of Aden (Bosworth et al., 2005) and descends to sea level in the Gulf and near sea level in the Euphrates–Tigris valley. Precambrian rocks of the Arabian Shield dominate the western part of the Plate, but Phanerozoic rocks dominate elsewhere and form a succession that is progressively younger and thicker away from the Shield. The immediate cause of these asymmetries is marginal uplift associated with Red Sea and Gulf of Aden rifting and mantle processes which have operated during the past 25 million years since the onset of rifting, resulting in a gentle tilt of the Plate toward the north and east. But a further issue is whether the asymmetries also reflect a fundamental east–west contrast in crustal and upper-mantle structure and composition that pre-dates Cenozoic rifting and may have existed since at least the end of Precambrian time.

Geologic, petrologic, and geophysical data about the thickness, structure, and composition of the continental crust and upper mantle of the Arabian Plate are summarized and synthesized as a means of addressing these questions. Extensive geologic and geophysical, mainly magnetic, surveying over the Shield provides a rich multidisciplinary dataset constraining the origin and vertical structure for the continental crust in the western part of the Arabian Plate. Establishing the origin and structure of buried Arabian Plate continental crust is more problematic, at least partly because public-domain geologic and geophysical data are relatively sparse, and other datasets are proprietary, having been acquired during petroleum exploration over the Arabian Platform. Consequently, modeling the crust away from basement exposures
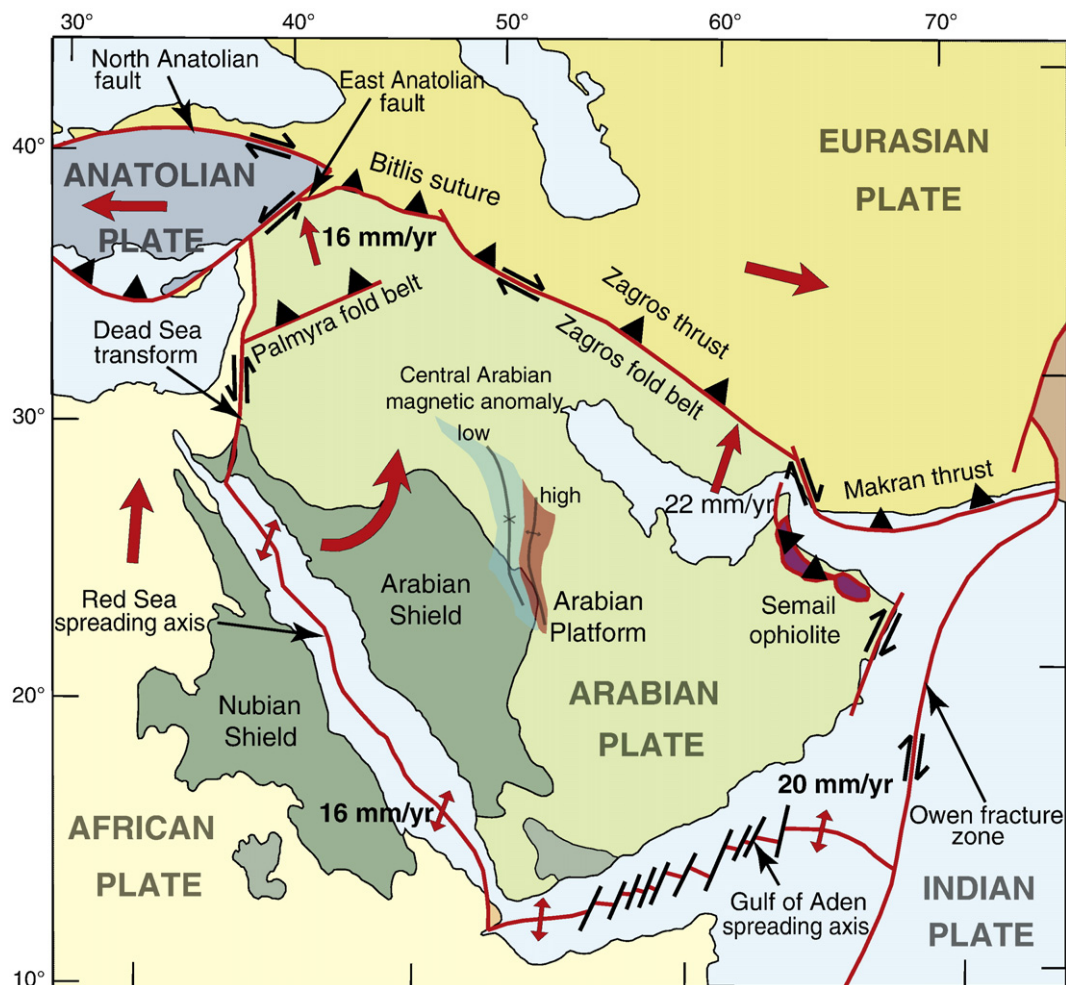
Fig. 1. Simplified map of the Arabian Plate, with plate boundaries, approximate plate convergence vectors, and principal geologic features. Note location of Central Arabian Magnetic Anomaly (CAMA).

depends on extrapolating insights from the exposed basement supplemented by the available published studies.

Fountain and Salisbury (1989), in reviewing the composition of the continental lithosphere of the coterminous United States, comment that "Models depicting the petrology, chemistry, and structure of the continental crust and upper mantle are … refined by integration of … geophysical data with the powerful constraints offered by geologic investigations … (and the) … study of xenoliths" (p. 711). In a similar vein, we present our review from the perspectives of four largely independent but complementary datasets: 1) near surface geologic and geochronologic studies on basement exposures in the Arabian Shield and Oman and the Phanerozoic succession; 2) heat flow measurements; 3) geophysical, principally seismic and some magnetic, studies of the lithosphere; and 4) mineralogical, geochemical, and isotopic studies of lower-crustal and upper-mantle xenoliths in Cenozoic basalt.

The first section of the review summarizes pertinent shallow-crustal geologic information obtained from the Arabian Shield, small exposures of Precambrian rock in the eastern part of the Plate, and the Phanerozoic succession covering the crystalline basement. We contrast the geologic history of the Shield with that of the eastern basement exposures and discuss insights about basement structures that are provided by features of the Phanerozoic succession. This is followed by a section describing the results of heat flow measurements across the Plate discussing both early suggestions of a "cold basement" and more recent estimates of a "warm basement". The third section summarizes geophysical information about variations in

crustal thickness and velocity and density structure across the Plate, and the fourth section summarizes and discusses crustal and lithospheric compositions gleaned from the mineralogical, geochemical, and isotopic study of Cenozoic basalt xenoliths.

In the following discussion, it should be noted that the terms "Arabian Plate", "Arabian Peninsula" and "Arabia" are synonyms, and that the waterway between the Arabian Peninsula and Iran is referred to as "the Gulf". Furthermore, geologic structures and units cut across, and may change names at, national boundaries: alternative names are given in parentheses. The lithosphere is the outer part of the solid Earth — the crust and upper mantle — but there is no common agreement about the exact meaning of the term (Anderson, 1995). It may be considered as a seismic layer in which earthquakes are generated; as a rheological layer, mechanically strong and rigid in comparison with the underlying asthenosphere; or as a thermal layer that is cooled by conduction and is below the temperature at which material become soft. In this discussion, we mostly follow the definition of thermal lithosphere referring to the outer part of the solid Earth that is cooled by conduction and moves coherently as a plate. The continental crust of the Arabian Plate is that part of the plate above the Mohorovičić discontinuity (Moho), and the term "continental crust" is mostly interchangeable with the term "crystalline basement" apart from instances where we specifically distinguish between the crystalline component of the crust and the overlying Phanerozoic sediments. Sedimentary rocks are considered part of the crystalline basement if they are deformed and metamorphosed and are of Neoproterozoic or older age.

The Arabian Plate measures ~2600 km north–south and ~3000 km east–west (Fig. 1). It is bounded on the west by the Dead Sea transform and Red Sea spreading/rifting axis; on the north by a zone of plate convergence made up of the East Anatolian fault, Bitlis suture, and Zagros collision zone; on the east by the Owen Fracture Zone; and on the south by the Gulf of Aden spreading axis (Sheba Ridge). Note that we do not discuss the oceanic realms around Arabia, even though these are important parts of the Arabian Plate *sensu stricto*. Since its separation from Africa, the plate has rotated anticlockwise and drifted north, currently at a rate of 2–3 cm/year (Bird, 2002). In the process of northward drift, the Plate closed the Tethys seaway as it subducted beneath Eurasia. There are strong along-strike variations in the style of Arabian–Eurasian convergence, ranging from current subduction of the Arabian Plate beneath Eurasia in the northeast associated with formation of the Zagros fold-and-thrust belt and ongoing arc volcanism in the Urumieh Dokhtar arc of Iran (Alavi, 2004), to oblique collision in
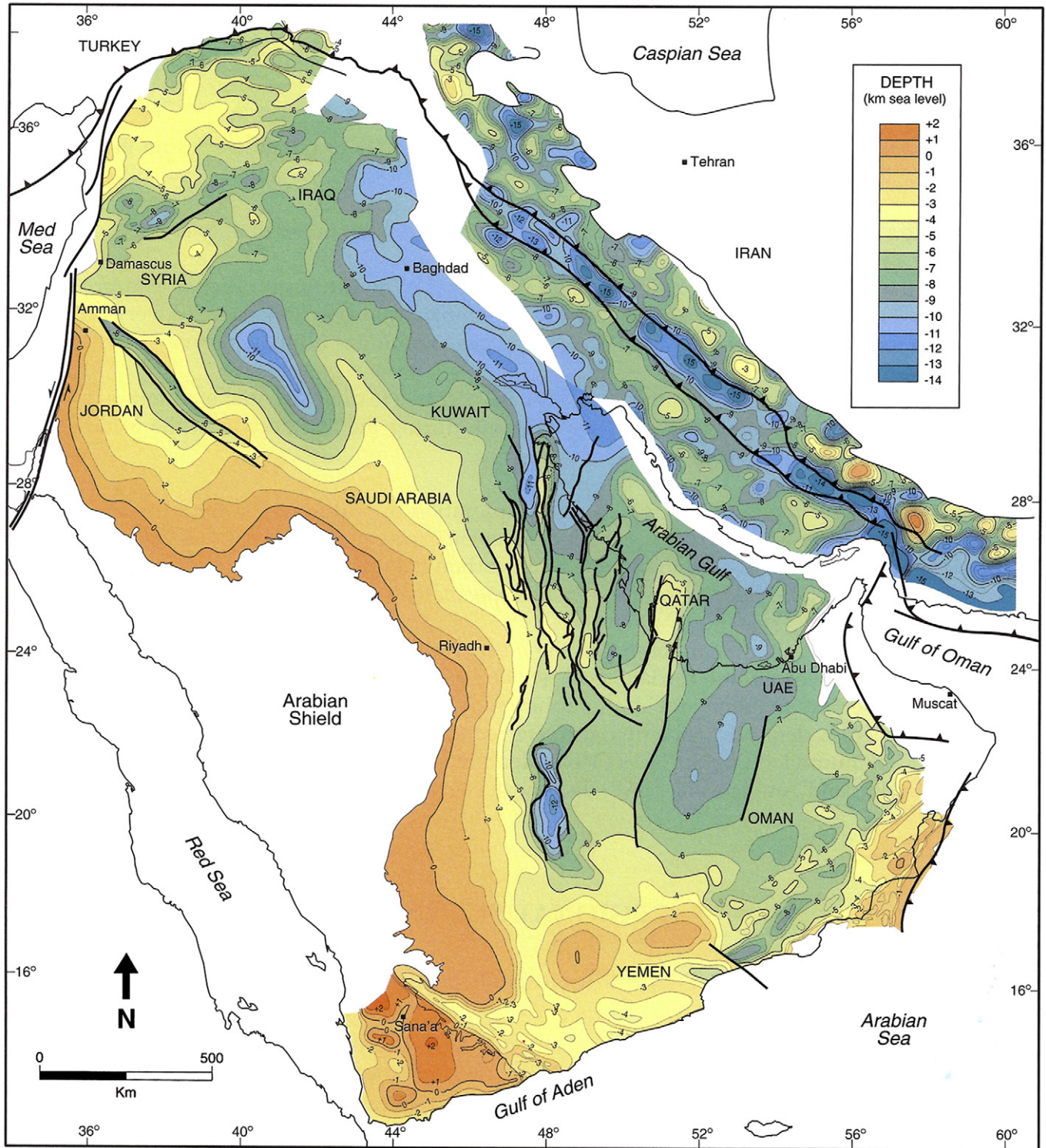

Fig. 2. Preliminary basement depth map of the Arabian Plate, after Konert et al. (2001), reproduced by permission of GeoArabia, showing the increasing thickness of Phanerozoic rocks away from the exposure of Precambrian rocks in the Arabian Shield.

the northwest associated with slip on the East Anatolian fault and post-collisional volcanism in eastern Anatolia (Keskin, 2003). Precambrian basement crops out in the west and south of the Plate, in parts of Jordan, Saudi Arabia, Yemen, and Oman, but the basement is mostly buried beneath several kilometers of Phanerozoic sediment in Syria, Iraq, southern Turkey, southwestern Iran, Kuwait, and United Arab Emirates, with the greatest thicknesses in the Gulf and Mesopotamian foredeep (Fig. 2). Between basement uplifts and foredeeps, the Phanerozoic cover defines a large stable platform that dominates eastern Arabia (Fig. 3).

2. Crustal geologic data

Exposures of upper continental crust dominate the geology of western Arabia as a result of Oligo-Miocene rift-flank uplift during formation of the Red Sea. Basement is also exposed in scattered outcrops in eastern Arabia adjacent to the Gulf of Aden and the Indian Ocean (Fig. 4). Radiometric crystallization ages for these rocks are overwhelmingly Neoproterozoic, and isotopic data confirm that the basement is mostly juvenile continental crust that formed during the Neoproterozoic (Stoeser and Frost, 2006),
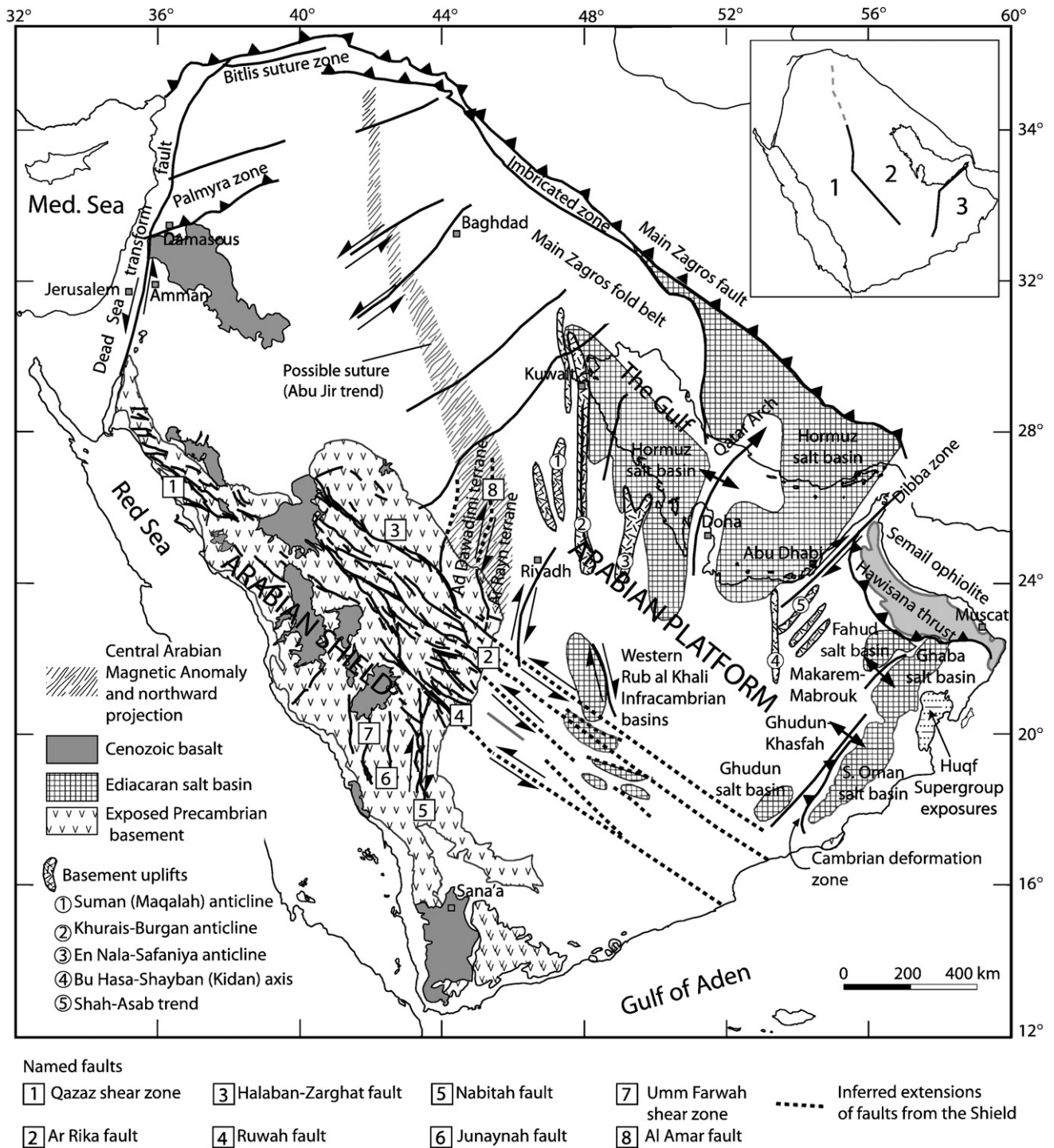
Fig. 3. Selected structural and tectonic features of the Arabian Plate, compiled after Sharland et al. (2001) and Johnson and Woldehaimanot (2003). Inset shows basement structural domains: see text for details.
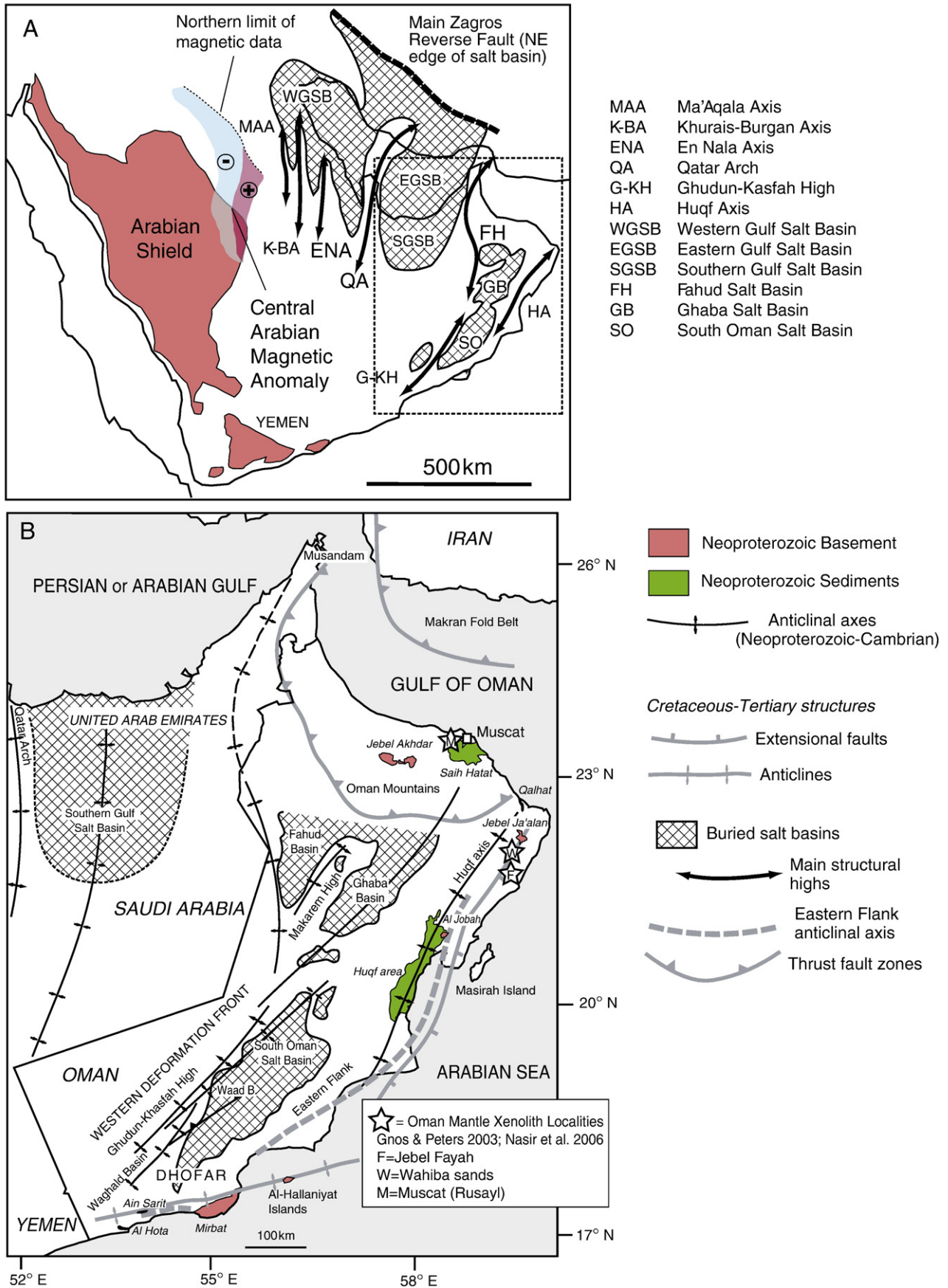
Fig. 4. (A) The main structural trends of eastern Arabia and the Gulf region showing the extent of the Ara–Hormuz salt basins. (B) Detail of the Oman area, with the main areas of Neoproterozoic outcrops, main structural trends and subsurface salt basins, from Allen (2007). Stars with letters in Oman correspond to locations of xenolith-bearing alkaline igneous rocks of Cenozoic age.

Fig. 5. Location (A) and evolution (B) of the East Africa–Antarctic Orogen (EAAO). A) Shows the reconstructed Gondwana supercontinent, modified after Meert and Lieberman (2008). Cratons of West Gondwana are shaded in light blue and those of East Gondwana are yellow. Neoproterozoic orogenic belts stitched Archean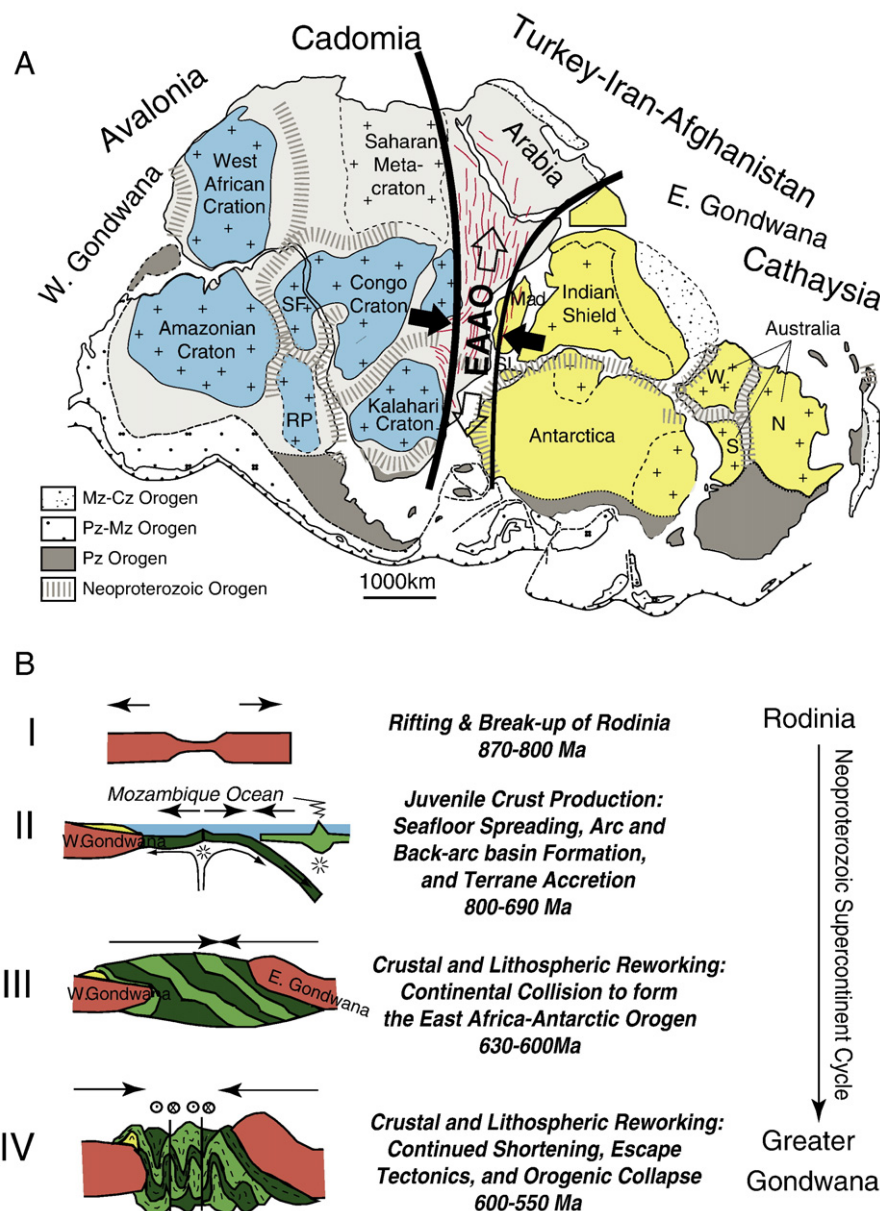 and Paleoproterozoic cratons together. Structural trends of the East Africa–Antarctic orogen are shown in red. Black arrows show inferred convergence and location of most intense continent–continent collision. Open arrow shows possible direction of tectonic escape. B) Shows greatly simplified evolution of the East Africa–Antarctic Orogen, modified after Stern (1994). EAAO evolution is tied to a Neoproterozoic "Supercontinent Cycle" (Worsley et al., 1986), beginning with the break-up of the supercontinent Rodinia (I), opening and closing of a wide "Mozambique Ocean" with associated formation of juvenile crust (II), collision between continental fragments (III), and continued convergence and tectonic escape (IV). By the end of Neoproterozoic time, a new supercontinent "Greater Gondwana" or "Pannotia" came into existence. Some of the crust that presently underlies the Arabian Peninsula may have been displaced northward (present coordinates) from the regions that experienced the most intense collision, in the vicinity of modern Madagascar, Kenya, and Tanzania.

apart from significant tracts of Paleoproterozoic and Archean crust in the southwest (Whitehouse et al., 2001b; Windley et al., 1996).

2.1. The Arabian Shield

The Arabian Shield encompasses ~770,000 km² (Gettings et al., 1986), an area about 15% larger than the US state of Texas and about twice the areas of Japan or Germany. The Shield surface is almost completely exposed in the hyper-arid environment of the Arabian Peninsula, with negligible soil and little windblown sand and provides an outstanding opportunity to examine how and when this part of Arabian Peninsula upper crust formed. It is estimated that the Shield exposes ~50% plutonic and ~50% volcanic and sedimentary rocks, and that granitic rocks make up ~70% of all plutons (Gettings et al., 1986).

Shield-like basement extends at least 200–300 km under Phanerozoic cover to the north and east (Johnson and Stewart, 1995), and similar rocks comprise the Nubian Shield in Egypt, Sudan, Eritrea, and Ethiopia. Together, these complementary tracts make up the Arabian–Nubian Shield (ANS). Comprehensive but slightly different reviews of the ANS and the Arabian Shield have recently been presented by Johnson and Woldehaimanot (2003) and Nehlig et al. (2002).

Juvenile Neoproterozoic crust of the Arabian Shield was mostly generated at primitive arc systems during the life of the Mozambique Ocean, which existed from ~870 Ma to ~630 Ma, widening until at least ~750 Ma (Stern, 1994) before closing. Collision between continental fragments occurred between 630 Ma and 600 Ma, and continued convergence and tectonic escape took place between 600 Ma and 550 Ma. Most Shield rocks were generated during the Cryogenian (850–630 Ma) although the Shield, as a whole, is the product of a cycle of continental accretion that lasted about 300 million years.

The ANS constitutes one of the largest, best exposed tracts of juvenile Precambrian continental crust on Earth and its history is intimately linked with a Neoproterozoic "Supercontinent Cycle" (Worsley et al., 1986) or Wilson Cycle (Fig. 5). This cycle began with the break-up of Rodinia in the early Cryogenian (Meert and Torsvik, 2003), continued with the opening and closing of one or two oceanic basins (Collins and Pisarevsky, 2005; Stern, 1994), and ended with the convergence of fragments of East and West Gondwana and the formation of the new supercontinent of "Greater Gondwana" (Stern, 1994) or "Pannotia" (Dalziel, 1997). The ANS is at the northern end (present-day coordinates) of the East Africa–Antarctic Orogen (EAAO; Jacobs and Thomas, 2004) (Fig. 5) formed by the East–West Gondwana collision. Although this supercontinent immediately began to break-up around its margins, a large portion remained intact for 300 m.y. as the Gondwana supercontinent. Some of the crust that presently underlies the Arabian Peninsula may have been displaced northward (present-day coordinates) from the regions that experienced the most intense Ediacaran collision, in the vicinity of modern Madagascar, Kenya, and Tanzania (Bonavia and Chorowicz, 1992). Crust in the southern part of the EAAO was displaced to the south (Jacobs and Thomas, 2004). Other portions of crust that originally fringed the northern margin of the supercontinent (again present-day coordinates) rifted off during the Paleozoic and drifted north to be incorporated in Laurasia as "Perigondwana" fragments (Keppie et al., 2003).

Although the EAAO was first thought to mark direct collision between E and W Gondwana with closure of a single ocean basin, more recently Collins and Pisarevsky (2005) infer an initial collision between a continental fragment "Azania" and NE Africa at ~630–650 Ma, followed by a later collision at ~550 Ma between composite NE Africa–Azania with E. Gondwana, implying the destruction of two oceanic basins. Whichever tectonic model is more correct, the EAAO is understood to mark a continental-scale suture zone between W. and E. Gondwana, and its creation implies that some eastern Arabia crust may be part of E. Gondwana.

The origin of the ANS is relatively well understood and its rocks have long been regarded as mostly formed in magmatic arcs (Gass, 1982). Exposed lithologic assemblages are dominated by ophiolites, primitive volcanics, calc-alkaline intrusives, and immature clastic sediments. Initial isotopic compositions of Sr and Nd (Stern, 2002a; Stoeser and Frost, 2006) indicate that these were new, juvenile additions from the mantle to the crust in Neoproterozoic time. Geochemical studies of the igneous rocks generally infer an arc setting for the tectonic environment of ANS crust-forming igneous activity (Gass, 1982; Khalil, 1997; Roobol et al., 1983), and ophiolitic components also testify to formation in a convergent-margin setting (Azer and Stern, 2007; Stern et al., 2004). Some workers suggest that accreted oceanic plateaux may be important juvenile crust-forming components (Stein, 2003), but no support for this hypothesis has been found in the composition of ANS igneous rocks.

The terrane concept (Howell, 1995) has been successfully applied to understanding how Arabian Shield crust was assembled from discrete arcs, beginning with Stoeser and Camp (1985). Recent reviews of Arabian Shield terranes (Johnson and Woldehaimanot, 2003; Nehlig et al., 2002) agree about the most important points, including the eight terranes themselves (Fig. 6). Most of the terrane boundaries are marked by ophiolite-decorated sutures (Johnson et al.,

2004). The ophiolites range in age from ~690 to ~870 Ma, and have a mean age of ~780 Ma that may approximate the onset of terrane accretion (Stern et al., 2004). Stoeser and Frost (2006) define Shield terranes differently and identify several more than those shown in Fig. 6. Stoeser and Frost (2006) concluded that the Shield has an older Neoproterozoic (>800 Ma) core of accreted intraoceanic arcs in the west, flanked by younger arc terranes (>740 Ma) to the east and north. The youngest arc assemblage (Ar Rayn terrane: 620–700 Ma) lies along the eastern flank of the Arabian Shield. Thus there appears to be a progressive younging of oceanic arcs eastwards across the Arabian Shield, but the significance of such younging is not yet clear.

In spite of consensus regarding the principal mechanisms of crustal growth in the Arabian Shield, questions remain about the role played by pre-Neoproterozoic crust elsewhere in the Plate. Intact Archean crust is known from exposures in Yemen (Whitehouse et al., 2001b) and Paleoproterozoic crust is preserved in the ~1.8 Ga Khida subterrane of the SE Shield (Fig. 6) (Stacey and Agar, 1985; Whitehouse et al., 2001a). Furthermore, ion-probe U–Pb dating of individual zircons reveals that even juvenile Neoproterozoic igneous rocks (as evidenced by low initial $^{87}Sr/^{86}Sr$ and high positive $\varepsilon_{Nd}(t)$), contain abundant xenocrysts with ages of especially ~1.9 and ~2.5 Ga (Hargrove et al., 2006a; Kennedy et al., 2004; Kennedy et al., 2005; Kennedy et al., 2009 in press). Curiously, such zircons are found even in rock samples that have geochemical and isotopic characteristics suggesting formation in an intra-oceanic arc, far from any continent Hargrove et al. (2006b). Moreover, xenocrystic zircons are proportionately most abundant in mafic lavas and unusual in felsic volcanic and plutonic rocks. These ancient xenocrysts are unlikely to have survived processing through a subduction zone. Ion-probe dating of more than 1000 zircons from igneous rocks of the modern Izu–Bonin–Mariana and Fiji intra-oceanic arcs, for example, reveals no zircons older than the age of the arc (K. Tani, e-mail comm., 2008). It may be that Arabian Shield lavas picked up ancient zircon xenocrysts by interacting briefly with clastic sediments shed from flanking ancient continents, but this remains to be demonstrated. The presence of ancient zircons in the Thurwah ophiolite (Fig. 6), identified by Pallister et al. (1988) and confirmed by Hargrove et al. (2006a), is very difficult to relate to sediment interaction. Another possibility is that disruption of Rodinia to open the Mozambique Ocean involved large scale delamination, introducing blocks of ancient lower crust into the asthenospheric source of future Arabian Shield melts. These observations and speculation indicate that the distribution and significance of xenocrystic zircons in the otherwise juvenile crust of the Arabian Shield merits further investigation.

Rb–Sr whole rock and U–Pb zircon radiometric ages for exposed basement of the Arabian Shield and Yemen yield a peak of ages in the range ~610–640 Ma, with smaller concentrations in the range 700–800 Ma (Fig. 7). It should be noted that the data may overemphasize the relative importance of younger rocks, because dating programs commonly preferentially sampled granitic plutons and felsic rocks that are more easily dated than the more mafic igneous rocks associated with earlier stages in crustal evolution. But the Neoproterozoic age range for basement rocks is a useful first-order approximation of overall Arabian Shield basement age, with the caveat that the mean age of the crust is somewhat older than can be inferred from the histogram pattern of Fig. 6 itself.

Isotopic data show that terranes in the western part of the Shield are of oceanic affinity, and have the least radiogenic Pb or Sr and most radiogenic Nd isotopic compositions and some of the lowest $\delta^{18}O$ values of any rocks in the Shield (Stoeser and Frost, 2006). The eastern terranes are also of oceanic affinity but their sources have slightly elevated $\delta^{18}O$ and Nd, Sr, and $^{208}Pb/^{206}Pb$ isotopic ratios. The Khida terrane between the western and eastern terranes is the only part of the Shield in Saudi Arabia to be underlain by Paleoproterozoic and Archean continental crust, and has negative ε_{Nd} compositions and radiogenic $^{207}Pb/^{204}Pb$ and $^{208}Pb/^{204}Pb$ (Stoeser and Frost, 2006). The
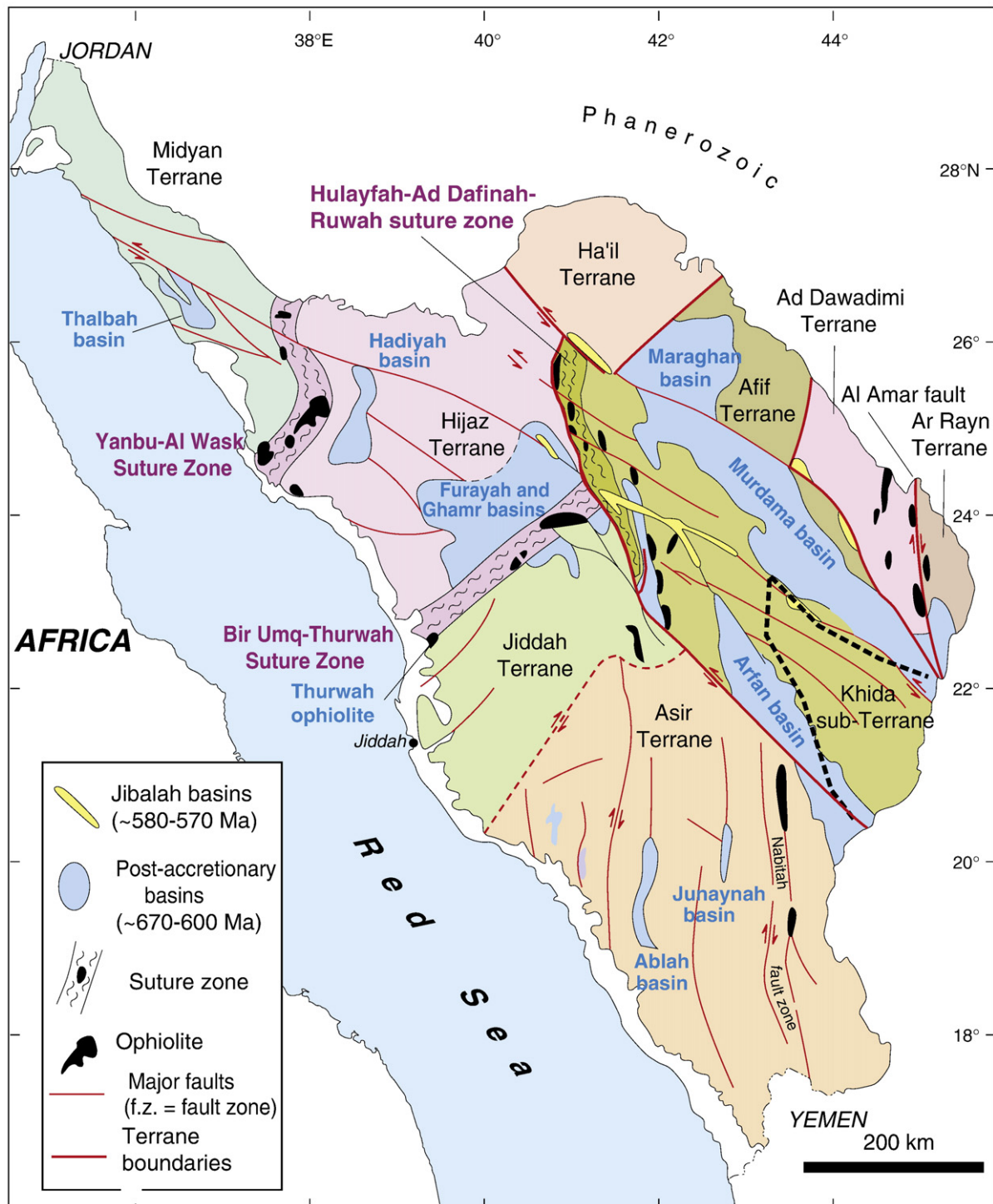
Fig. 6. Simplified map of the Arabian Shield, showing major tectonostratigraphic terranes, ophiolite belts, sutures and fault zones, and post-accretionary basins, modified after Nehlig et al. (2002) (reprinted by permission of GeoArabia) and Johnson and Woldehaimanot (2003). Location of Khida sub-terrane after Stoeser and Frost (2006).

presence of this E–W isotopic gradient identified in the provinciality of Pb isotopic compositions in feldspars and galenas in the Shield suggests that older crust could exist to the east of the Hulayfah–Ad Dafinah–Ruwah suture zone (Fig. 6), and led Stoeser and Frost (2006) to propose that the Khida terrane may belong to continental crust in the central and southern part of the Arabian Peninsula that was part of East Gondwana. However, this inference is not compelling. Stoeser and Frost (2006) concluded that the eastern terranes in the Arabian Shield formed as intraoceanic arcs but the mantle sources of the melts (with slightly enriched isotopic compositions compared to the

western-arc terranes) were less depleted than those that supplied the western-arc terranes, or that a small amount of older crust was incorporated in their formation.

2.2. Crystalline crust of Eastern Arabia

We are only starting to learn about the nature of continental crust east and north of the Arabian Shield. Some tectonic models suggest that juvenile "shield-type" rocks extend as far as the Zagros thrust. Other models suggest that the eastern limit of "shield type" rocks
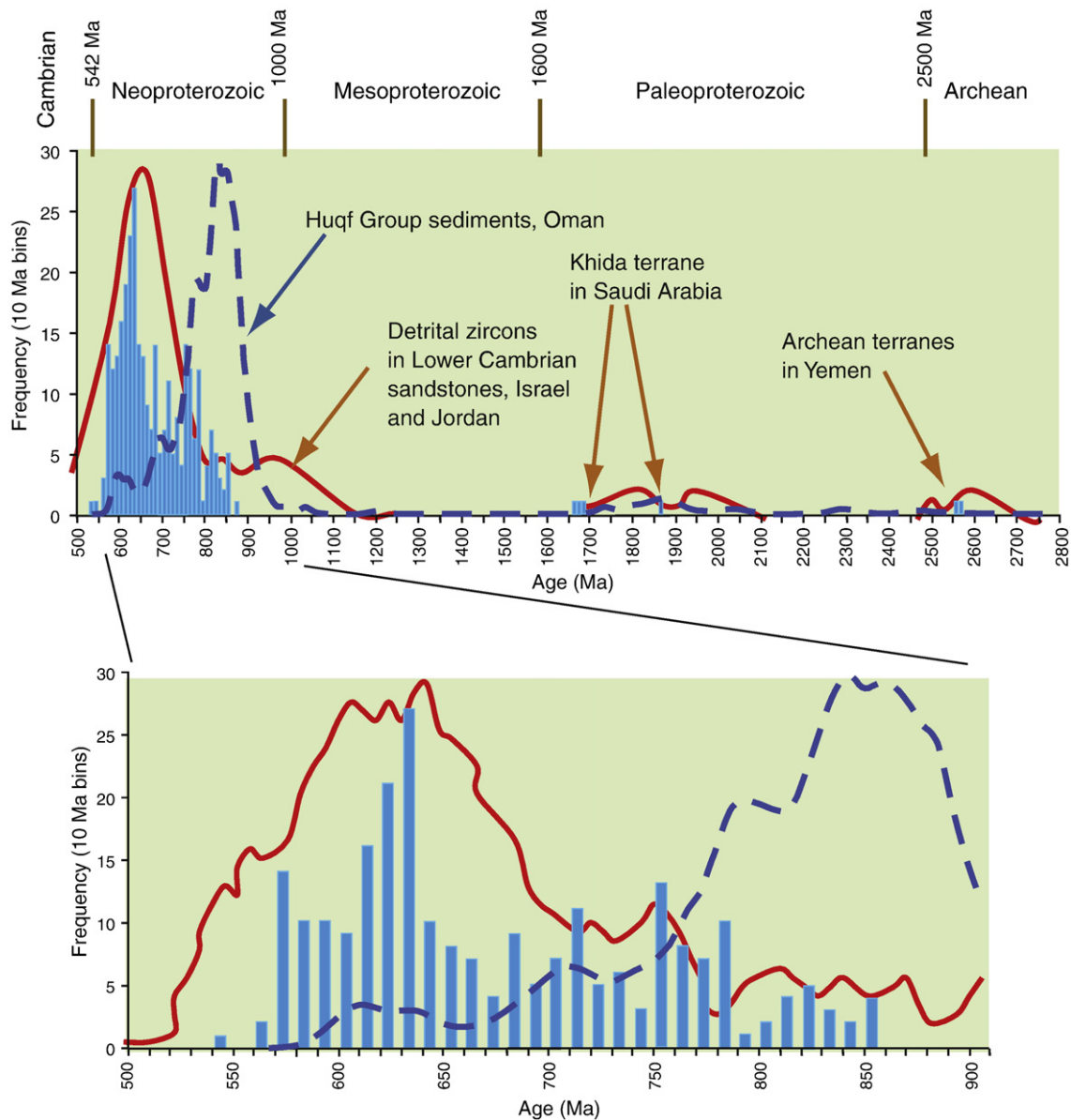
Fig. 7. Age histograms for exposed basement of Arabia (Johnson and Kattan, 2007) compared to U–Pb age probability curves for 386 detrital zircons from the Neoproterozoic Huqf Supergroup sediments of Oman (blue curve; Rieu et al., 2007; LeGuerroué et al., 2006) and detrital zircons from Lower Paleozoic sandstones from Israel and Jordan (red curve; Avigad et al., 2003, 2005; Kolodner et al., 2006). Upper panel (A) shows the entire age spectrum whereas the lower panel shows Neoproterozoic detail. The Lower Paleozoic detrital zircons show age distributions that are very similar to those of basement exposed in the Arabian Shield. Detrital zircons from the Huqf Group differ from both Arabian Shield ages and Lower Cambrian detrital zircons in showing an age peak ~850 Ma and few igneous rocks of <700 Ma age.

approximates the Shield/Platform contact and that a buried pre-Neoproterozoic craton may lie east and north of the Shield (Dixon and Golombek, 1988), but such speculation has found little support to date. The greatest hindrance to gaining a comprehensive understanding about the crystalline crust of eastern Arabia is that it is mostly buried by Phanerozoic formations and only crops out in small, scattered locations in Oman. Another hindrance is that the basement has been sampled by deep drilling and surveyed by geophysical methods during oil exploration, but the results of sampling and most surveys are proprietary and have not been released. The comments here are based on published datasets.

Despite the small size of basement exposures in Oman (Fig. 4), they have recently been scrutinized because they are critical to understanding the crust of the eastern half of the Arabian Plate. Most particularly, available geochronologic data indicate that igneous and metamorphic activity was Tonian (1000–850 Ma) and early Cryogen-

ian, and ended by ~700 Ma, in contrast to the prolonged period of magmatic and metamorphic events that characterized growth of the Arabian Shield. Subsequent Neoproterozoic activity in Oman took the form of Cryogenian–Ediacaran deposition of siliciclastic, glaciogenic, carbonate, and evaporite rocks (the Huqf Supergroup) unconformable on the crystalline basement. Gass et al. (1990) carried out Rb–Sr whole-rock dating of Precambrian exposures in Oman, including basement exposed on the Mirbat (Marbat) Peninsula, Al–Hallaniyat (Kuria Muria) Islands, and at Jebel Ja'alan (Fig. 4b). Four suites gave ages that ranged from 706 ± 40 Ma to 850 ± 27 Ma, with initial $^{87}Sr/$ ^{86}Sr from 0.7025 to 0.7041. Mercolli et al. (2006) carried out a detailed U–Pb zircon geochronologic study of basement on the Mirbat Peninsula, the largest (750 km^2) basement exposure in Oman and the best window that we have into eastern Arabian crust. Mercolli et al. (2006) defined three major units composed of metasedimentary mica-gneiss, amphibolite, and a few meta-ultramafic lenses; banded

gneiss; and tonalite, which were emplaced as igneous rocks or metamorphosed between 815 and 785 Ma. An independent U–Pb zircon dating program of granodiorite and metavolcanic rocks from the Al Jobah area and granitic rocks from Mirbat indicates that felsic magmatism occurred between ~840 Ma and ~810 Ma (Bowring et al., 2007). Late- to post-tectonic granites, pegmatite and mafic dikes intruded between 770 and 750 Ma. The younger (750–700 Ma?) emplacement of the Marbat Granodiorite, Shaat Dyke Swarm, and Leger Granite marked the end of magmatic and metamorphic evolution, and a Sm–Nd whole rock age of 757 ± 61 Ma for the dikes confirms that tectonic and magmatic activity was largely finished by ~750 Ma (Worthing, 2005). Post-tectonic magmatism continued for a short time after 750 Ma, nevertheless, as is shown by an age of ~730 Ma for the unfoliated Leger granite and a ~700 Ma syenite (Bowring et al., 2007).

A similar tectonomagmatic history is observed at the Al-Hallaniyat Islands east of Mirbat, where a calc-alkaline pluton yields an age of 780 Ma (Mercolli et al., 2006), similar to the Rb–Sr whole-rock age of 772 ± 8 Ma obtained by Gass et al. (1990). An Ar–Ar plateau age of 617 ± 3.5 Ma for a late mafic dike from these islands suggests late reheating (Mercolli et al., 2006).

Easternmost Oman has small (few km²) outcrops of Neoproterozoic crystalline basement at Al Jobah and around Jabal Ja'alan (Fig. 4b). Five samples of granodiorite from Al Jobah were dated using U–Pb zircon techniques, yielding ages that range from 802 to 826 Ma, with little evidence of any older crust (Allen and Leather, 2006). The Jabal Ja'alan exposures contain basement rocks coeval with, or slightly older than, the Mirbat basement, with undeformed calc-alkaline intrusions dating 834 ± 6 Ma (Pallister et al., 1990) and other intrusions giving ages of 824 ± 8 and 826 ± 9 Ma (Roger et al., 1991). Furthermore, micas have K/Ar cooling ages of ~815 Ma (Würsten et al., 1991), suggesting that the eastern Oman basement many not have experienced the main 815 and 780 Ma crust-forming events recorded in western Oman.

As noted above, these geochronologic studies are based on small, scattered exposures and form a small dataset relative to that available for the Arabian Shield. Nonetheless, the data consistently suggest that somewhat older Neoproterozoic crust is present beneath eastern Arabia than is present in the bulk of the Arabian Shield in the west. However, the data provide no evidence of significantly older basement that could be part of a pre-Neoproterozoic craton.

2.3. Insights from sedimentary history

Phanerozoic sedimentary rocks dominate the central and eastern parts of the Arabian Plate making up the thick succession of the Arabian Platform and the equally thick succession of the Mesopotamian/ Gulf foredeep (Fig. 2). The Platform rocks were deposited on a stable
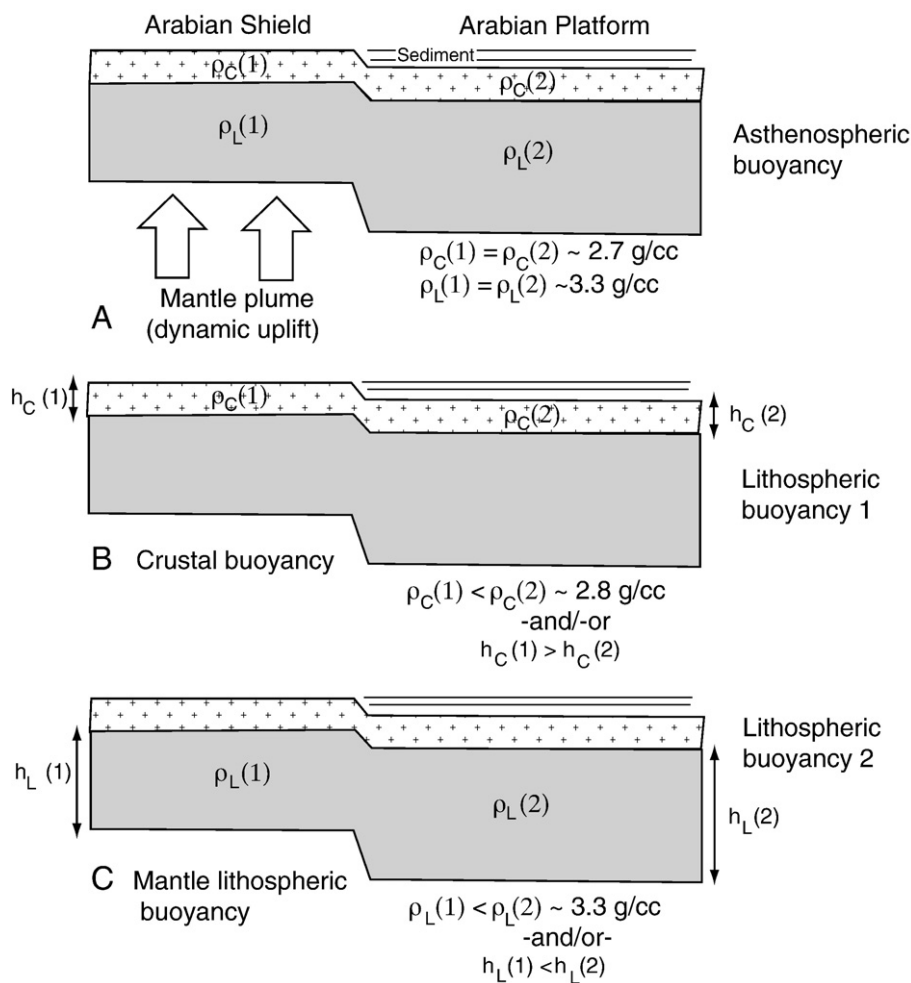
Fig. 8. Three plausible explanations for observed differential uplift observed in a simplified W–E section across Arabia, about 22°N. A) Dynamic uplift caused by (Cenozoic) asthenospheric upwelling or a mantle plume raising western Arabian lithosphere and elevating the Arabian Shield relative to the Arabian Platform. B) Greater buoyancy and uplift in the west caused by less dense and/or thicker crust relative to that in the east. C) Greater buoyancy and uplift in the west caused by less dense and/or thinner mantle lithosphere in the west relative to that in the east. A) Infers buoyancy reflects astheospheric activity, B) and C) Infer that buoyancy originates within the crust or mantle part of the lithosphere. These three causes may operate together. See text for further discussion.

basement: the foredeep rocks in a subduction-related trench. In contrast, only thin sequences of Phanerozoic rock are present across the Shield as isolated outliers of Lower Paleozoic sandstone and siltstone and some thin Cretaceous–Paleogene sandstone, mudstone, and limestone. An issue pertinent to this review is what geologic reasons account for the lack of, or only thin, Phanerozoic cover on the Shield. One reason may be that erosion due to dynamic uplift of the Shield by injection of hot asthenospheric mantle related to the Afar plume and/or to Red Sea rifting removed Phanerozoic strata during the Cenozoic (Daradich et al., 2003; Park et al., 2008). Another reason may be that the continental crust in western Arabia was never covered by a thick Phanerozoic succession because of long-lived lithospheric buoyancy. Buoyancy variations may derive from differences in thickness and (or) density of the lithosphere across the region, causing differentiation in terms of relative high-stand of the Shield and subsidence of the Platform and feedback between crustal structure and sediment loading. As summarized in Fig. 8, such variations could reflect: 1) similar crustal and mantle lithospheric thicknesses but denser lithosphere; or 2) similar crustal and mantle lithospheric densities but thinner crust and/or thicker mantle lithosphere. Because dynamic (rifting) "asthenospheric" causes should be relatively young whereas lithospheric buoyancy causes are likely to persist for much longer, these different explanations can be tested by considering when the Arabian Plate differentiated into western Shield and eastern Platform, and by examining the Phanerozoic sedimentary succession, which preserves the history of regional uplift and subsidence.

Sharland et al. (2001) reviewed Arabian Plate sequence stratigraphy and concluded that subsidence was mostly gentle during the Phanerozoic. They further concluded that accommodation space for sedimentation was chiefly created by a combination of sediment loading and global eustatic effects although locally, and for particular periods, subsidence was critical. The Plate subsided sufficiently during the Phanerozoic to accommodate more than 5 km of sediment over much of the Arabian Platform, and up to 10 or more km of sediment in the Mesopotamian/Gulf foredeep and some parts of the Platform (Fig. 2). Prominent regional unconformities, caused by inversions, uplifts, rifting, tilting and other types of plate structural reorganization as well as Late Ordovician–Early Silurian and Late Carboniferous–Early Permian glaciation, divide the preserved succession into large-scale sediment packages or tectonostratigraphic megasequences. As many as 11 megasequences are recognized (Sharland et al., 2001), which evolved through the various regional tectonic events that affected the Plate. The sediment packages are dominated by varying amounts of siliciclastic and carbonate deposits, with periodic concentrations of evaporites, and a common scenario over the central and eastern parts of the Arabian Plate during the Phanerozoic was the progradation of clastics from the west into a shallow-marine carbonate basin, driven by periodic uplift of the western hinterland (Sharland et al., 2001).

Sedimentation in eastern Arabia began with the deposition of the Huqf Supergroup, starting in middle Cryogenian time (~725 Ma). Structural differentiation between the eastern and western parts of the Arabian Plate and a recognizable contrast between a subsiding Arabian Platform and a high-stand Arabian Shield dates from that time. The Huqf Supergroup and associated end-Ediacaran to Early Cambrian salt basins (Allen, 2007; Husseini and Husseini, 1990) are unconformable on the early to middle Neoproterozoic (Tonian–Cryogenian) crystalline basement of Oman. It is believed that the Supergroup was deposited in a series of northeast-trending rift basins some of which were possibly contemporary with strike-slip faulting during an extensional phase of movements on the Najd faults in the Oman basement (Al-Husseini, 2000; Loosveld et al., 1996). This interpretation is unsatisfactory because the start of Huqf sedimentation predated Najd movements by ~100 m.y. The overall setting of the Supergroup was a subsiding, marine-shelf environment interrupted by periods of glaciation and dessication. The Supergroup commenced with the Abu Mahara Group, and passed up into the Nafun and Ara

Groups, and ranges in age from about 723 Ma in the Ghubrah Member in the basal Abu Mahara Group (Brasier et al., 2000) to 544 Ma in the Fara Formation (Ara Group) at the top (Brasier et al., 2000). The Abu Mahara Group consists of <1.5 km of marine sedimentary rocks, including glacial deposits. This is overlain by >1 km-thick carbonates and fine-grained clastic sediments, deposited during thermal subsidence following Abu Mahara rifting (Allen, 2007). The Nafun Group is a carbonate-rich sedimentary succession of Ediacaran age deposited in a continental-margin rim basin between about 600 Ma and 550 Ma, coeval with carbonate-rich units of the Jibalah group on the Shield. The Ara Group, deposited close to the Neoproterozoic/Cambrian boundary, is dominated by a chert–carbonate–evaporite succession. It is broadly correlative with the Hormuz evaporites of the Gulf region. Huqf Supergroup stratigraphy indicates that a broad, shallow sea inundated eastern Arabia throughout most of the last 200 m.y. of Neoproterozoic time and into the Phanerozoic.

Deposition of the Huqf Supergroup in a subsiding shallow marine environment that was structurally differentiated periodically into rift basins implies that a relatively strong lithosphere was in place beneath eastern Arabia by ~700 Ma ago, in contrast to the situation in western Arabia where lithospheric instability continued until the end of the Precambrian. The Shield was tectonically and magmatically active until well into the Ediacaran and was a region of internal structural differentiation, with parts emergent and eroding and other parts submerged below sea level, serving as sedimentary basins. Subduction-related arc activity continued into Late Cryogenian–Ediacaran time, as witnessed by the creation of the suprasubduction volcanic–plutonic assemblage of the Ar Rayn terrane in the eastern part of the Shield (Doebrich et al., 2007). Elsewhere, post-amalgamation basins developed unconformably on newly amalgamated arc terranes. The Thalbah group (<660 to <620 Ma) has abundant red sandstone, locally derived conglomerate, and alternating red/green siltstone that were deposited in a continental to shallow fluviatile/shallow marine environment (Johnson and Woldehaimanot, 2003). Other groups, such as the Murdama (~630 Ma Kennedy et al., in press), contain thick limestones and appear to have been deposited in mixed continental-marine basins (Johnson, 2003). Erosion occurred ~620–530 Ma in the northeastern part of the Shield and at other times elsewhere in the Shield, creating the unconformities observed at the base of post-amalgamation sedimentary units and the Lower Paleozoic succession. The youngest Neoproterozoic depositional units on the Shield include the <~600 Ma Abt formation near the eastern edge of the Shield and the Jibalah group (Johnson and Kattan, 2007). The Abt was likely deposited in a large, north-trending marine basin: the depositional environment and extent of the Jibalah is disputed. The Jibalah group is largely exposed in basins along or close to Ediacaran faults and many interpreters envisage that it was deposited in pull-apart basins. Nicholson et al. (2008), building on earlier work by Delfour (1970) and Hadley (1974), for example, identify a common stratigraphy in the various Jibalah basins, suggesting that this group was originally deposited in a single laterally continuous basin across much of the Arabian Shield and is merely preserved in downdropped fault basins. Zircons from tuff beds within the Jibalah group yield U–Pb ages of 588–600 Ma (Nicholson et al., 2008), and detrital zircons from sandstone suggest a maximum age of 599–570 Ma (Miller et al., 2008). The youngest Neoproterozoic sedimentary deposit on the Shield is the newly identified Kuraysh group in northwest Saudi Arabia, comprising terminal Neoproterozoic fluvial clastics and basalts unconformably overlying the Jibalah group (Nicholson et al., 2008).

By ~530 Ma, the Shield region was emergent, covered by Lower Paleozoic siliciclastic rocks of fluviatile origin (Siq and Saq Sandstones; Husseini, 1990; Kolodner et al., 2006), which transitioned into a marine environment to the north (Jordan) and to the east (Arabian Platform). Evidence that siliciclastic rocks covered the Shield is provided by Lower Paleozoic outliers scattered across it, as far as the Red Sea coastal plain and Gulf of Aqaba in the west, and from Yemen in the south to Jordan in the north. These outlier sequences are tens to

a few hundred meters thick and consist of Cambro-Ordovician sandstone that was deposited unconformably above the profound Shield-wide pediplane that developed toward the end of the Precambrian. However, sedimentation over the Shield did not persist, and thereafter the Shield appears to have been largely a region of non- or limited-continental deposition and above sea level (e.g., Konert et al., 2001; Ziegler, 2001). The Arabian Platform, in contrast, maintained marine to littoral conditions for most of Phanerozoic time, steadily subsiding to accommodate up to 14 km of sediment. Subsidence was periodically interrupted by block faulting, eustatic sealevel drops, and erosion, resulting in the unconformities that help divide the stratigraphy into sequences. Uplift of the Central Arabian Arch, for example, caused removal of Lower Paleozoic sedimentary rocks from parts of the eastern Shield so that the Permian Khuff Formation rests directly on basement rocks (Al-Aswad, 1997). Hercynian (~325 Ma) arching and block faulting resulted in vertical displacements of several km in the northern part of the Platform (Faqira et al., 2009), and local Cretaceous uplift and lateritic weathering produced the Az Zabirah paleobauxite close to, but east of, the Shield (Watson, 1994).

Overall, this geologic history suggests that the regions of Arabia now defined as Platform and Shield behaved similarly until ~750 Ma, with tectonics and sedimentation dominated by magmatic activity affecting a broad region. But starting at about 750 Ma, the region began to structurally differentiate. An increasingly stabilized neocraton developed in the eastern Arabian Plate and subsided more or less continuously for the rest of Neoproterozoic time, whereas igneous activity, as well as periodic uplift and erosion and the development of both continental and shallow-marine basins, continued in the western part of the Plate between 750 and 550 Ma. From Cambrian time onward, differentiation into subsided Platform and uplifted Shield became a permanent feature of Arabia, allowing for a thick sedimentary succession in the east and largely exposed Precambrian basement in the west. Persistence of differentiation between the subsided eastern Arabian basement and uplifted western Arabian basement for 550 million years of Phanerozoic time cannot only reflect recent uplift due to mantle-plume activity associated with Red Sea opening (Fig. 8A). Instead, we see such long-lived differential uplift as evidence of long-lived differences in crustal (Fig. 8B) or mantle lithospheric (Fig. 8C) density or thickness such that continental crust in western Arabia was a mostly positive feature during the Phanerozoic. Cenozoic uplift undoubtedly accentuates the high-stand character of the Shield but, in our opinion, is a recent reinforcement of what is fundamentally a Neoproterozoic lithospheric feature.

2.4. Erosion and detrital provenances

Detrital zircons in clastic sedimentary rocks provide a useful large-scale sample of provenance material. Accordingly, recent U–Pb dating of detrital zircons in Late Neoproterozoic sedimentary rocks of the Huqf Supergroup in Oman and in Lower Paleozoic sandstones in Israel and Jordan provide a perspective on the ages of basement rocks that were exposed and eroded at the end of the Precambrian in the eastern and western parts of the Arabian Plate alternative to the perspective provided by direct dating of the basement.

A result of detrital geochronologic studies in Oman is evidence that the source region of clastic material in the Huqf Supergroup (~725–540 Ma) was not much older than the deposition age. Glacial deposits of the Abu Mahara Group in the Oman Mountains (Ghubrah Formation) contain volcaniclastic rocks that have a crystallization age of approximately 713 Ma (Allen, 2007). Diamictite clasts from the same formation mostly yield ages of 777–832 Ma (Bowring et al., 2007) and relatively few have pre-Neoproterozoic ages. Younger synglacial turbiditic sandstones of the Fiq Formation (uppermost Fiq Formation was deposited <664 Ma; Bowring et al., 2007) yield Neoproterozoic

detrital-zircon ages ranging from 920 to 664 Ma (Allen, 2007), and volcaniclastic deposits intercalated with glaciogenic strata of the Fiq Formation in the South Oman Salt Basin, yield zircons as young as ~645 Ma. The overall detrital geochronology for the Huqf Supergroup is shown by the composite age curve plotted in Fig. 7. This shows a peak at ~850 Ma, progressively smaller peaks at ~780 Ma, ~720 Ma, and ~630 Ma, a small, broad Paleoproterozoic peak between about 1950 Ma and 1750 Ma, and a very small peak at about 2300 Ma.

Comparable U–Pb ages for detrital zircons in Lower Paleozoic sandstones in Israel and Jordan (Avigad et al., 2003, 2005; Kolodner et al., 2006) are shown by the dashed (red) curve in Fig. 7. The sandstones are part of the Lower Paleozoic siliciclastic succession that once blanketed Arabia above the major unconformity that resulted from deep erosion of the Precambrian basement between ~600 Ma and ~530 Ma. Lower Paleozoic sandstones are widespread in Gondwana fragments, and much of this detritus was probably derived from mountains of the EAAO to the south (Squire et al., 2006). Current directions for Lower Paleozoic sandstones on the Arabian Plate indicate that sedimentary sources were mostly to the south (Konert et al., 2001; Vaslet, 1987). Age information for detrital zircons in Cambro-Ordovician sandstones of Saudi Arabia is not available, but the Lower Paleozoic sandstone in Israel and Jordan show age distributions that are dominantly Neoproterozoic (Avigad et al., 2003, 2005; Kolodner et al., 2006). These are similar to the distribution of radiometric ages for igneous rocks of the Arabian Shield (Johnson and Kattan, 2007) (Fig. 7) with a large peak at ~650 Ma, moderate peaks at ~570 Ma, ~720 Ma and 755 Ma, and small peaks at 1.7–2.1 Ga and 2.4–2.7 Ga. The Lower Paleozoic detrital data differs from the Huqf Supergroup data however, in that the Huqf detrital zircons have a prominent peak at ~850 Ma but an insignificant peak in the 600–650 Ma range. The Lower Paleozoic data, furthermore, uniquely show a late Mesoproterozoic–early Neoproterozoic "Kibaran" peak in the range 1050 Ma to 900 Ma, for which a source has recently been reported in Sinai (Be'eri-Shlevin et al., 2009).

Caution is required in assigning significance to the relative sizes of the 600–650 Ma vs. 850 Ma peaks for the Huqf Supergroup detrital-zircon data because most of these data come from 650 to 720 Ma sedimentary rocks of the Abu Muhara Group at the base of the Huqf Supergroup and few come from younger Neoproterozoic sedimentary rocks higher in the Huqf. Nonetheless, it appears that the source region for the Huqf Supergroup detritus was overwhelmingly Neoproterozoic, especially Cryogenian. The small peaks between 1950–1750 Ma and 2300 Ma may indicate some Paleoproterozoic crust in the source region, but could equally reflect reworked xenocrysts of the type common, for example, in Neoproterozoic igneous rocks of the Shield. An immediate Neoproterozoic source region is evident in the Mirbat area where the Abu Muhara Group unconformably overlies 815–785 Ma crystalline basement (Mercolli et al., 2006), but there is no apparent immediate source for the 850 Ma detrital zircons. However, whether the immediate basement is the sole, or merely a local, source for detrital zircons for Abu Muhara Group sediments is not known.

2.5. Basement structural trends

Additional insight into differences between the eastern and western parts of the Arabian Plate comes from variations in basement structural trends. Basement structures, such as folds, faults, shear zones, elongate syntectonic plutons, and dikes, are well known on the Arabian Shield and their orientations can be determined by direct observation. Elsewhere, the basement is concealed and structural trends must be inferred from magnetic, gravity, and seismic data, and as a consequence, are less well known. Nonetheless, regional-scale contrasts in structural trends are apparent, and divide the Arabian Plate into three basement structural domains (Fig. 3): (1) a western domain comprising the Shield and the south-central part of the

Arabian Platform characterized by northerly and northwesterly trends; (2) a north-central domain dominated by northerly trends and a broad northeasterly trend; and (3) an eastern domain marked by northeasterly trends. Structural trends for the Arabian Shield shown in Fig. 3 are compiled from published geologic maps; basement trends east and north of the Shield are compiled from a limited amount of published geophysical information comprising aeromagnetic data in a 200-km wide belt flanking the exposed Arabian Shield in Saudi Arabia (Cowan et al., 2005; Zahran et al., 2003), and seismic, magnetic, and gravity data elsewhere (e.g., Loosveld et al, 1996; Faqira et al., 2009).

In the western domain, the oldest structures date from the Tonian to mid-Cryogenian accretionary phase of crustal growth. They include ophiolite-decorated sutures, tight, upright folds, and combinations of steeply dipping bedding and contacts, concordant contacts between bedding and pre- to syntectonic plutons, and bedding-parallel shear zones. These structures impart a conspicuous structural grain to much of the Shield. Structures of this age trend north–south in the southern Shield and northeast in the west-central part of the Shield. Younger, late Cryogenian to Ediacaran structures include north-trending belts of accreted magmatic and sedimentary rocks in the extreme eastern part of the Shield, north-trending shear zones in the southern Shield, and even more conspicuous northwest-trending 'Najd' sinistral shears. Late Cryogenian–Ediacaran north-trending shears in the southern Shield represent late Neoproterozoic reactivation of earlier shears, such as the final dextral strike-slip motion on the Nabitah fault (fault no. 5 in Fig. 3). This fault originated during the Nabitah orogeny (680–640 Ma; Stoeser and Stacey, 1988), but underwent renewed slip after intrusion of late-tectonic 640 Ma granite plutons and the deposition of post-640 Ma sandstone. A similar age is also known for final dextral slip on the Junaynah fault (fault no. 6), whereas final dextral slip on the Umm Farwah shear zone (fault no. 7) is somewhat younger and post-dated eruption of 640–613 Ma rhyolite of the Ablah group. Even younger Ediacaran north–south dextral shearing is evidenced for the Al Amar fault in the extreme eastern part of the Arabian Shield (fault no. 8 in Fig. 3). It is generally accepted that the Al Amar fault originated as a suture along the western margin of the Ar Rayn terrane, juxtaposing volcanic-arc rocks of the Al Amar group, belonging to the >689–625 Ma Ar Rayn terrane (Doebrich et al., 2007), with sandstone of the Abt formation, belonging to the Ad Dawadimi terrane. The fault is partly interpreted as a thrust but is currently exposed as a subvertical shear zone containing a few S–C fabrics indicating dextral strike-slip. Movement on the Al Amar fault deformed sedimentary rocks of the Hamir group (615–605 Ma), deposited in small basins along the fault, and the fault clearly developed late in the history of the Shield.

The broad zone of northwest-trending brittle–ductile shears that belong to the Najd Fault system is one of the most conspicuous Late Neoproterozoic structural elements of the Arabian Shield and south-central Arabian Platform. The zone is as much as 300 km wide and over 1100 km long. It crosses the entire central part of the Shield (Fig. 3), continues northwest into what, prior to opening of the Red Sea, were adjacent parts of the Nubian Shield, and is inferred, on the basis of magnetic and gravity data and paleogeographic reconstructions, to extend southeast across the concealed basement of the Arabian Plate into parts of India and the Lut block that were adjacent to Arabia as Gondwanan components at the end of the Precambrian (Al-Husseini, 2000). Individual structures within the Najd system are predominantly sinistral strike-slip, brittle to brittle–ductile shears a few meters to several kilometers wide. They form single, linear faults or broader sets of anastamosing shears, have metamorphic effects ranging from none to amphibolite-grade, and are associated with fault basins, domes and antiforms of mylonitic gneiss replete with S/C fabrics and fault-parallel dikes.

The age and origin of the Najd fault system are debated. In the literature, the faults are treated either as structures that origi-

nated during the final late Cryogenian–Ediacaran creation of the EAAO reflecting essentially east–west compression and north-directed tectonic escape (e.g., Stern, 1994), or as structures that originated during Ediacaran–Cambrian extension associated with collapse of the EAAO and rifting of the Gondwana margin (e.g., Al-Husseini, 2000). Given the age range and geographic scale of the fault system, both compression and extension may have operated (Sharland et al., 2001) depending on local thermal and mechanical conditions.

One of the principal Shield-wide Najd structures is the system of shears that extends from the Qazaz shear zone in the northwest (fault no. 1 on Fig. 3) to the Ar Rika fault (fault no. 2) in the southeast. The Qazaz, and adjacent Ajjaj, shear zones are anastomozing belts of amphibolite-grade mylonitic gneiss. The Ar Rika fault is characterized by an elongate mylonitic orthogneiss antiform, by kyanite-bearing paraschist, and by brittle–ductile deformation of conglomerate and sandstone, in which granite pebbles are stretched as much as 3 m. Initial movements on the Ar Rika fault followed deposition of the Murdama group (~630 Ma) and subsequent movements followed emplacement of 611 Ma granitoids. Movements on the Qazaz–Ajjaj shear zone are constrained to between ~635 and 573 Ma (Calvez et al., 1984; Kennedy et al., 2009, in press). Shorter — but still significant — Najd faults include the Halaban–Zarghat fault (Fig. 3 fault no. 3) and Ruwah fault (Fig. 3 fault no. 4), parts of which originated as ~680 Ma suture zones that were reactivated by Najd-type strike-slip shearing. As described above, many of the faults of the Najd system are associated with fault-bounded basins filled by sedimentary and volcanic rocks of the Jibalah group that either served as pull-apart depocenters or are younger fault basins in which remnants of the Jibalah group are preserved, or both.

Possible continuations of Najd shears to the south and east are hidden beneath Phanerozoic sediments, but geophysics and other expressions of structure can be used to infer their existence or absence. In central Arabia, northwest-trending basement faults assigned to the Najd system are associated with elongate basins recognized on seismic profiles (Western Rub al Khali Infracambrian Basins) filled by clastic sedimentary rocks and evaporites (Dyer and Husseini, 1991; Faqira and Al-Hawuaj, 1998; Blood, 2000). The Western Rub al Khali Infracambrian Basins are interpreted by Sharland et al. (2001) as a linked series of intracratonic rift basins filled by syn-rift sediment assigned to the AP1 tectonostratigraphic megasequence of the Arabian Plate (~610–520 Ma). The syn-rift fill itself is not directly dated, but is correlated with the Hormuz Group and upper part of the Huqf Supergroup.

A region in the northeastern part of the Arabian Plate dominated by north- and northeast-trending structures is the second of the three structural domains. These structures were identified during geophysical investigations in eastern Saudi Arabia, which revealed that the N-trending onshore oilfields are underlain by faulted Precambrian basement blocks comprising N-trending horsts and grabens. The N–S pattern is variably referred to as the "old grain" of the Arabian Peninsula, the "El Nala trend" (Ayres et al., 1982), the "Arabian Trend" (Edgell, 1992), or "Rayn anticlines" (Al-Husseini, 2000). It is now known that these N–S structures are superimposed on the earlier formed, but still Hercynian, northeast-trending Al-Batin Arch. The arch is one of three mid-Carboniferous Hercynian arches newly recognized in the Arabian Plate (Faqira et al., 2009), and part of a set of NE-trending Hercynian arches and basin throughout Arabia and North Africa. The Levant Arch extends from Egypt to northern Syria and is present in the northwesternmost corner of the Arabian Plate. The Hadhramaout–Oman Arch runs along the coast of the Arabian Sea. The Al-Batin Arch is the central Hercynian upswell in the Arabian Plate, extending from the eastern part of the Shield to southwestern Iran (Fig. 3). The presence of N-trending basement highs bounded by steeply dipping basement

faults results in positive gravity anomalies coincident with the oil fields. The crestal Phanerozoic stratigraphic sequences of the oil fields indicate repeated rejuvenation of the basement highs (Edgell, 1992). When these structures formed and their tectonic significance are not certain. Noting that the prevailing northerly trends have the same orientation as the Ar Rayn and Ad Dawadimi terranes and the intervening Al Amar fault in the eastern Arabian Shield, Al-Husseini (2000) proposed that the N-trending horsts and grabens originated as a series of anticlines or westerly-vergent fold-thrust belts during the same late Neoproterozoic east–west compression contemporary with collision between the Ar Rayn terrane and terranes farther west in the Shield. Conversely, Edgell (1992), citing Henson (1951), envisages that Arabian Trend horsts and grabens formed during Late Neoproterozoic east–west extension. Faqira et al. (2009) question the details of Al-Husseini's model, but recognize that recently-acquired but unpublished aeromagnetic data substantiate the presence of N-trending Neoproterozoic terrane boundaries in the basement of eastern Saudi Arabia, which broadly parallel the horsts and grabens. Faqira et al. (2009) envisage that the master bounding faults are basement faults that were reactivated during the Hercynican Orogeny, causing a suprimposition of northerly structural trends on the broader NE-structural trend of the Al-Batin Arch. We note with interest that the western margin of the Al-Batin Arch shown by Faqira et al. (2009) is coincident with the magnetically inferred northerly extension of the Al Amar fault at the boundary between the Ar Rayn and Ad Dawadmi terranes.

As this discussion highlights, Neoproterozoic basement structures exerted important controls on Phanerozoic structures and associated sedimentation throughout northeastern Arabia (Sharland et al., 2001) in a region referred to as the East Arabian–Zagros Block (Bahroudi and Talbot, 2004). The westernmost representatives of the north-trending structures are exposed on the Shield as the Ar Rayn and Ad Dawadimi terranes (Figs. 3 and 6), the reference area for the Rayn anticlines of Al-Husseini (2000). The terranes coincide with a prominent magnetic anomaly (the Central Arabian Magnetic Anomaly, discussed below) that continues beneath the Arabian Platform north of the Shield, and projects along the line of the "Possible suture" or CAMA trend shown on Fig. 3 (Abu Jir trend of Sharland et al., 2001). The southeastern limit of this domain is the Oman line or Dibba zone (Derakshani and Faroudi, 2005).

The third basement structural domain is the southeastern part of the Arabian Plate, south of the Dibba zone and east of the Bu Hasa–Shayban axis (uplift no. 4 on Fig. 3). It is characterized by northeasterly trends formed by highs such as the Shah–Asab trend in UAE and the Ghudun–Khasfah and Makarem–Mabrouk basement highs in Oman, and the general trends of the Huqf Supergroups basins. Northeast–southwest trends are the dominant grain picked out by geophysical surveys in Oman (Loosveld et al., 1996).

Periodic reactivation of basement structures in central and eastern Arabia is demonstrated by the offset of Phanerozoic strata by faulting or the thickening and thinning of formations between basement highs and lows and the erosional removal of formations over basement highs. Phanerozoic reactivation of Neoproterozoic structures on the Arabian Shield has not been identified because Phanerozoic marker beds that would demonstrate offset or thickening and thinning of strata across the structures are not present. In principle, Phanerozoic reactivation of basement structures in the Shield is expected to the same extent that reactivation has occurred farther east, and finding examples of reactivation would be an important future task for geologic investigation. Pertinent to this review, however, is the observation that the basement structures were in place before the end of the Precambrian and are therefore a feature of the Precambrian crust. Also pertinent is the recognition of at least three structural domains in the basement on the basis of variations in structural orientations. The exact reason why such domains are present is not certain but they suggest a structural differentiation of

the Precambrian basement that is compatible with other types of differentiation noted in this review.

3. Heat-flow measurements

Heat flow is the outward flow of heat across the Earth's surface Morgan and Gosnold (1989). It is estimated that a few to more than 65% of continental heat flow results from the radioactive decay of uranium, thorium, and potassium isotopes in the upper crust (Morgan and Grosnold, 1989); the balance comes from radioactive decay in the mantle and fossil heat from the deep Earth. The heat flowing out of the Earth is not uniform and, on a global scale is mostly released by volcanism associated with mid-ocean ridges, subduction zones, rifts, and hot spots. In a continental environment, variations in surface heat flow may reflect contrasting thermal regimes in different tectonic environments and variations in lithospheric composition. In principle, measurements of heat flow across the Arabian Plate are expected to reveal whether the plate has a uniform or variable lithospheric structure, composition, or age (Förster et al., 2009). Unfortunately, public domain heat-flow measurements are only available for western Arabia, and are neither uniformly distributed nor consistent with expected heat-flow values. Despite this limitation, the available heat-flow studies are summarized here because they highlight an important field of lithospheric study that, if expanded, may contribute further insight into lithospheric variability in the Arabian Plate.

A significant portion of heat transfer may be convective, but surface heat-flow measurements typically record conducted heat flow (Morgan and Gosnold, 1989. At equilibrium, conductive heat flow measured in boreholes results from crustal heat production and heat flowing out of the mantle. A broad measure of conductive heat flow at the surface (Q_0, in mW m^{-2}) is given by:

$$Q_0 = Q_r + DA_0 \tag{1}$$

Q_r refers to "reduced" heat flow (mostly heating of the base of the lithosphere by the asthenosphere), A_0 refers to radioactive heat production (mostly by radioactive decay of ^{40}K, ^{235}U, ^{238}U, and ^{232}Th, measured in mW m^{-3}) measured in the upper crust, and D is the characteristic depth (in meters) for which heat-producing elements are found. In detail, the equation is an oversimplification because other radioactive elements are present in the upper crust and heat production is not restricted to the upper crust, but these other sources contribute little to the total heat production.

A global compilation by Rudnick et al. (1998) shows that Archean cratons average low heat flow (41 ± 11 mW m^{-2}), Early Proterozoic crustal tracts show slightly higher heat flow (46 ± 15 mW m^{-2}), Late Proterozoic crust (away from Archean cratons) averages 55 ± 17 mW m^{-2}, and Phanerozoic crust averages 49–55 mW m^{-2}. This yields a weighted average continental conductive heat flow of 47–49 mW m^{-2}, similar to the average heat flow of 48 mW m^{-2} for regions of Precambrian crust determined by Mclennan et al. (2005). Although direct correlation between surface heat flow, the geotherm, and tectonic age (time since the last major tectonic and thermal event) is not straightforward because of the chemical heterogeneity of the continental crust Morgan and Gosnold (1989), Nyblade (1999) concluded that heat flow varies inversely with age of the crust and that the simple cooling and thickening of the thermal boundary layer (the thermal lithosphere) predicts that heat flow should be constant for crust >1.5 Ga old.

Given its Neoproterozoic age, these considerations predict relatively high, uniform conductive heat flow for the crystalline basement of Arabia, but the dataset that exists does not show this. Heat flow (obtained over areas where the upper crust was not affected by Cenozoic reheating) is reported to be high for southern Syria (50–88 mW m^{-2}; Matviyenko et al., 1993), but lower for Jordan (42–

65 mW m^{-2}; Galanis et al., 1985), and significantly lower for the southern Arabian Shield (36–45 mW m^{-2}; Gettings, 1982; Gettings and Showail, 1982). Because the Neoproterozoic crust in western Arabia is generally uniform, it is difficult to accept these variations as real. Förster et al. (2007), in fact, challenged their validity by arguing that these measurements were made with unreliable techniques, are inconsistent with expected heat flow, and likely underestimate true heat flow. Förster et al. (2007) went on to report a new average heat flow for Jordan of 60.3 ± 3.4 mW m^{-2}, significantly higher than the earlier estimates obtained for Jordan and Saudi Arabia and much closer to the global prediction of 60 mW m^{-2} for 700 Ma Neoproterozoic lithosphere given by Artemieva and Mooney (2001). Förster et al. (2007) noted that Arabian lithosphere structure and crustal composition are broadly similar over the region where heat flow measurements have been reported and concluded that conductive heat flow should also be uniform. The Neoproterozoic crust exposed in southern Jordan is dominated by igneous rocks of intermediate composition, such as monzogranites and monzonites/granodiorites. These rocks contain abundances of heat producing elements (K, U, and Th) that yield typical values of radiogenic heat-production for upper crustal rocks, between 1 and 2 mW m^{-3}, with some areas of increased heat production, between 2 and 4 mW m^{-3}, associated with less abundant rhyolites and alkali-feldspar granites. The conclusion of Förster et al. (2007) (p. 281) that "… a value of 60 mW m^{-2}… typifies the Arabian Shield unaffected by younger geodynamic reactivation" is consistent with these heat-production values.

The earlier measurements are not only lower than expected for Neoproterozoic crust on the basis of the global heat flow database, but are actually similar to those typical of Archean regions. Low heat flow through Archean cratons is largely ascribed to very thick lithosphere (200–250 km) combined with low crustal heat production (Jackson et al., 2008; Nyblade, 1999; Rudnick et al., 1998). Neither factor applies to the Arabian Shield, which is characterized by lithospheric thicknesses of ~100 km (see below) and contains a large proportion of granitic material. Recently, Förster et al. (2009) modeled pre-Miocene geotherms for the continental lithosphere in Jordan based on surface conductive heat flow of 55 and 60 mW m^{-2} down to a depth of 65 km. The results contradict the earlier view that the Neoproterozoic/Cambrian lithosphere of the stabilized Arabian Shield has anomalously low heat flow and show that a "cold" thermal structure is inconsistent with the thickness, composition, and petrophysical properties of the stable lithosphere of the Shield.

4. Geophysical study of the lithosphere

The composition and structure of the Arabian Plate lithosphere are constrained by a wide range of geophysical data. Large tracts are covered by regional magnetic and gravity surveys, and smaller areas are covered by airborne electromagnetic and ground electrical and electromagnetic measurements. Considerable amounts of proprietary gravity, magnetic, and seismic data were acquired during hydrocarbon exploration in the Phanerozoic rocks in the eastern and northern parts of Saudi Arabia, and along the Red Sea coast, but the results of these surveys are not publically available. Published investigations include magnetic-anomaly maps of western Saudi Arabia, Jordan, and Syria, the results of seismic-refraction profiling in the southwestern and northwestern parts of the Plate, and multiple analyses of earthquake seismic waveforms and velocities.

4.1. The Central Arabian Magnetic Anomaly

Among the public-domain geophysical datasets available for the Arabian Plate, the most comprehensive is coverage provided by magnetic surveys of the Arabian Shield and adjacent Phanerozoic rocks in an area extending from the Yemen border with Saudi Arabia

in the south to the Jordan and Iraq border in the north (Fig. 9; modified from Zahran et al., 2003). A prominent feature of the magnetic data is the north-trending anomaly in central Saudi Arabia, at about 45°E. This anomaly, referred to here as the Central Arabian Magnetic Anomaly (CAMA), is a magnetic couplet, high in the east and low in the west, that extends as much as 900 km north–south and 200 km east–west. Johnson and Stewart (1995) reported that the anomaly could be traced due north across the Saudi Arabia–Iraq border to the Zagros thrust and its projection (as well as unpublished gravity data; I.C. Stewart, written communication, 2009) is the presumed basis of the structure shown on Fig. 3, after Sharland et al. (2001), as a "Possible suture". The high part of the couplet consists of numerous large-amplitude, short-wavelength anomalies, the low comprises broad-wavelength, low-amplitude anomalies (Gettings et al., 1986). Johnson and Stewart (1995) originally referred the anomaly to the magnetic-high part of the couplet, but the term is expanded here to include the high and the low.

In the extreme eastern part of the Arabian Shield, the CAMA correlates with rocks of the Ar Rayn and Ad Dawadimi terranes. The magnetic high correlates with the dominantly igneous rocks of the Al Amar group and associated plutons; the low with granites and thick sedimentary rocks of the Abt formation of the Ad Dawadimi terrane. The magnetic gradient between the two correlates with the Al Amar fault. A domain of high-frequency anomalies west of the CAMA corresponds to amalgamated western terranes in the Shield; a domain of subdued magnetic values to the east reflects basement beneath Phanerozoic cover (Johnson and Stewart, 1995). The mutual parallelism of CAMA magnetic high and low and their discordance with the terranes farther west suggest that these westerly terranes had already accreted and behaved coherently at the time of emplacement of the Ad Dawadimi and Ar Rayn terranes. This implies that the CAMA is the magnetic expression of a major crustal discontinuity that developed relatively late in the history of the Plate, consistent with the <~600 Ma age of the Abt formation (Johnson and Kattan, 2007) and multi-stage collisional models for this part of the Arabian Plate proposed by Al-Husseini (2000); the Amar collision and Collins and Pisarevsky (2005). In this regard, the anomaly is effectively the boundary between the western and central basement structural domains described above. The CAMA can be traced on the magnetic anomaly map as far south as the NW-trending Najd fault that appears to truncate the structure between 21°N and 22°N. Either the fault displaces the CAMA sinistrally on the south side of the fault, and the CAMA continues in modified fashion along N–S anomaly at about 46°50′ E, or the fault marks a major tectonic boundary terminating the Ar Rayn and Ad Dawadimi terranes.

A recent study by Doebrich et al. (2007) demonstrates that the Ar Rayn terrane — the exposed equivalent of the CAMA magnetic high — is a >689–625 Ma magmatic arc complex. Doebrich et al. (2007) and Al-Saleh and Boyle (2001) interpret the arc as formed at a convergent-margin above a west-dipping subduction zone from a trench east of the terrane. Other workers (e.g. Stacey et al., 1984) relate the arc to an east-dipping subduction zone. Doebrich et al. (2007) compared the geotectonic evolution of the Ar Rayn terrane to the modern Andean continental margin, suggesting that west-directed oblique subduction and collision between the western terranes of the Shield and a block to the east caused sinistral displacement along the Al Amar fault. The present-day exposure of the fault is a sub-vertical, dextral strike-slip shear zone enclosing discontinuous lenses of carbonate-altered serpentinite. Its overall dip is uncertain and it is just as plausible that the Al Amar fault marks an east-dipping subduction zone.

Al-Husseini (2000) treats the Ar Rayn terrane as the westernmost of a set of north–south anticlines or westerly-vergent fold-thrust belts present throughout the basement of central and eastern Arabia. As described above, the N–S structures are thought to have formed as a response to late Neoproterozoic east–west compression contemporary
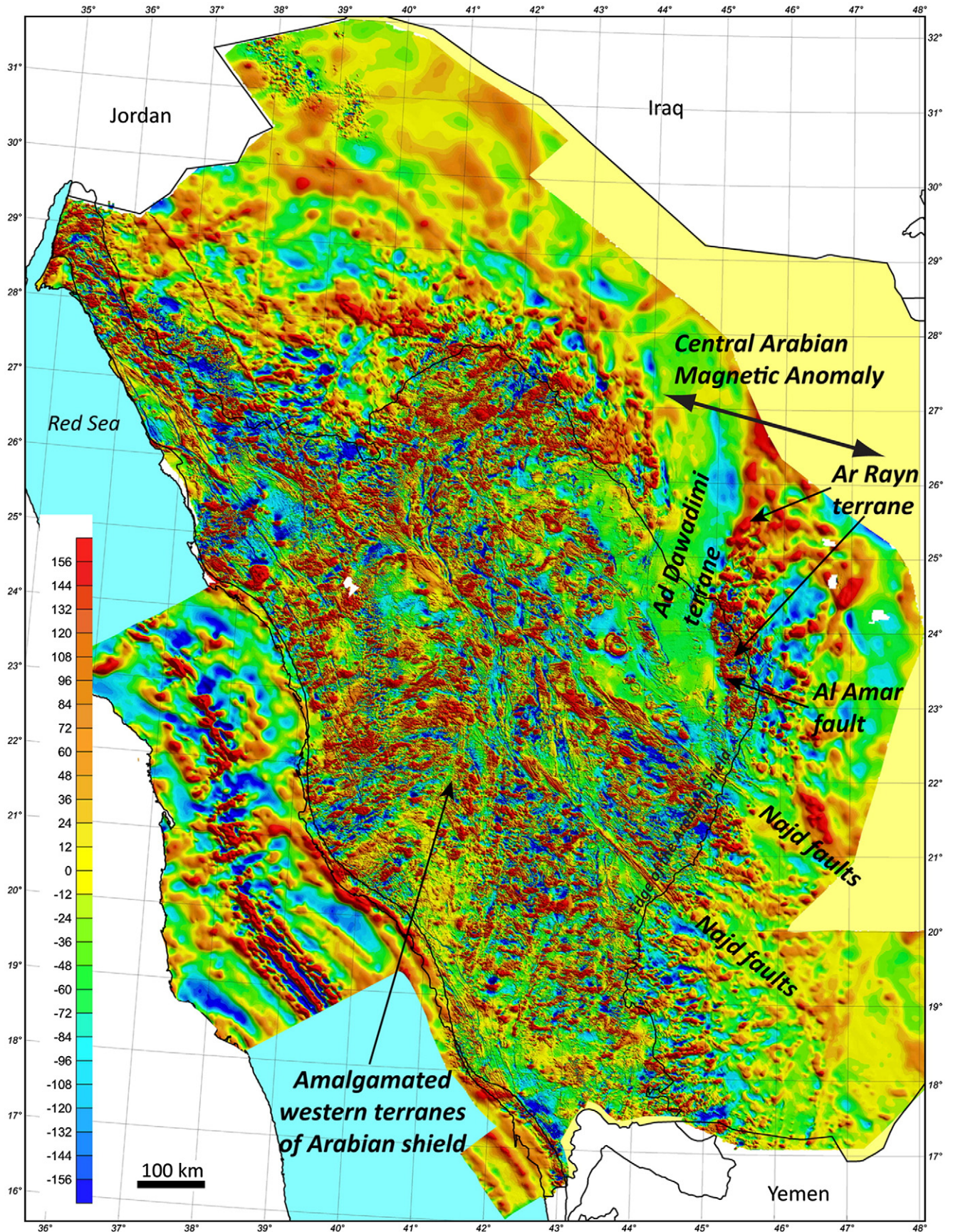
Fig. 9. Reduced-to-the-pole magnetic anomaly map over the Arabian Shield (inside solid black line) and surrounding regions (modified after Zahran et al., 2003). Selected features, referred to in text, are identified. Note that the western part of the map clearly shows some of the late Neoproterozoic NW–SE Najd shear zones and N–S Asir structures, but that terrane boundaries are not well-defined. For completeness, the map shows magnetic anomalies over portions of the Red Sea, but these are not discussed in the text. Additional magnetic data east of the Shield are shown by Johnson and Stewart (1995) extending as far east as longitude 51°E.

with collision between terranes in the western Shield and the Ar Rayn terrane and a block farther east (Al-Husseini, 2000) although the exact nature of the colliding block to the east is poorly known. The magnetic expression of this potential block east of CAMA is the region of broad-wavelength, low-amplitude anomalies east of CAMA shown in the magnetic-anomaly map published by Johnson and Stewart (1995), their Fig. 2 and Al-Husseini (2000), his Fig. 4. Despite the poor quality of the ground magnetic data on which these figures are based, and the strong attenuation effects that reduce the amplitude and detail seen in the data to the east, where depths to magnetic sources (crystalline basement) are generally more than 5 km, this eastern region appears to show a real contrast in magnetic signature to that of the Ar Rayn terrane, consistent with the change in basement composition proposed by Johnson and Stewart (1995).

4.2. Crustal thickness

Continental crust comprises continental lithosphere above the Moho. On a global scale, models such as CRUST 5.1 (Mooney et al., 1998) (http://earthquake.usgs.gov/research/structure/crust/data-base.php) and CRUST 2.0 (http://igppweb.ucsd.edu/~gabi/rem.dir/crust/crust2.html) suggest a mean global thickness of 41.9 km beneath shield areas (exposed stable crust) and 41.4 km beneath platforms (buried stable crust). CRUST 5.1 has a resolution of $5° \times 5°$ and CRUST 2.0, an updated version of CRUST 5.1, has a resolution of $2° \times 2°$ binned with 5 km thickness steps. The models are suitable for regional studies and at this scale closely agree with the known ~40 km thickness of the Arabian crust. However, the models lack sufficient resolution to reveal subtle variations in crustal structure. For information about fine crustal detail in Arabia, it is necessary to resort to regional and local investigations, principally the results of seismic-refraction profiling using controlled, active (man-made) sources, and the results of teleseismic-receiver-function analysis and surface-wave studies using natural (earthquake) sources. These studies show (Table 1) that the Arabian Plate, in fact, has a range of crustal thicknesses, varying across the Plate from 22 km (near the Red Sea) to 53 km in the east. In the context of this review, we note that these variations amount to a modest step in general crustal thickness beneath central Arabia, increasing from ~32–46 km in the west to 35–50 km in the east. The step is emphasized in Table 1 by dividing the data into results from the Plate west and east of the CAMA: a separate set of two results come from the far northern part of the Plate, north of the Palmyrides and along the Bitlis suture. We note, moreover, within the broad spatial parameters of Table 1, that the step occurs close to the Shield/Platform boundary. It is broadly coincident with the Al Amar fault and the CAMA and with the tectonic boundary at this location envisaged in this paper.

The most detailed public-domain crustal-thickness information comes from a seismic-refraction experiment in the southwestern part of the Plate west of the CAMA carried out in 1978 (Healy et al., 1982). Several interpretations of the profile have been reported (Badri, 1991; Gettings et al., 1986; Mechie et al., 1986; Mooney et al., 1985) and the well-known model of Mooney et al. (1985) is shown in Fig. 10. The refraction measurements were made on a southwest-trending, 1000-km-long profile across the Arabian Shield, from just west of Riyadh, on the Arabian Platform, to the Farasan Islands in the Red Sea, 30 km offshore from southern Saudi Arabia. The results reveal a crust that is generally about 40 km thick but with significant variations. According to Mooney et al. (1985), the crust is 43 km thick east of the CAMA, near Riyadh, and 38 km thick west of the CAMA (Fig. 10), whereas Prodehl (1985) models the crust–mantle boundary at a common depth of 40 km with a maximum of 50 km beneath the southwestern

Table 1
Geophysical crustal-thickness estimates for the Arabian Plate.

| Source	Thickness (km)	Location	Method
West of CAMA	**Shield/western part of Plate**		
Mooney et al. (1985)	38	Western part of shield	Seismic-refraction profile
El-Isa et al. (1987)	32	Jordan, adjacent to Dead Sea Transform	Seismic-refraction profile
El-Isa et al. (1987)	37	Jordan, east of Dead Sea Transform	Seismic-refraction profile
Kumar et al. (2002)	35–38	Beneath the Shield	Teleseismic receiver function
Al-Damegh et al. (2005)	39	Average beneeath the shield	Teleseismic receiver function
Hansen et al. (2007)	35	Beneath southern shield	Teleseismic receiver function
Hansen et al. (2007)	40–45	Beneath central shield	Teleseismic receiver function
Hansen et al. (2007)	22–25	Beneath western part of shield	Teleseismic receiver function
Mohsen et al. (2005)	30–38	Jordan, north of exposed shield	Teleseismic receiver function
Sandvol et al. (1998)	40–43	Arabian shield	Teleseismic receiver function
Al-Saad et al. (1992)	~32	Syria	Gravity modeling
Brew et al. (2001)	~35	Southern Syria	Gravity and receiver function
Mokhtar et al. (2001)	41–46	Beneath the shield	Surface wave study
Al-Heety (2002)	36.5	Iraq	
Northern part of Plate	**Bitlis and north of Palmyrides**		
Brew et al. (2001)	~25	Syria, north of Palmyrides	Gravity and receiver function
Angus et al. (2006)	~40	Bitlis suture	Receiver function
East of CAMA	**Platform/eastern side of Plate**		
Mooney et al. (1985)	43	East of CAMA, near Riyadh	Seismic-refraction profile
Al-Damegh et al. (2005)	41–49	Northern Oman	Teleseismic receiver function
Al-Damegh et al. (2005)	41–53	Three stations between Shield and Bahrain	Teleseismic receiver function
Midzi (2005)	~43	Crust beneath Kuwait	Teleseismic receiver function
Sandvol et al. (1998)	45–46	Shield and Platform	Teleseismic receiver function
Hansen et al. (2007)	40–45	Beneath Platform	Teleseismic receiver function
Hansen et al. (2007)	35–40	Beneath eastern edge of shield	Teleseismic receiver function
Al-Lazki et al. (2002)	40	Oman Arabian Platform	Gravity and receiver function
Al-Lazki et al. (2002)	45	Oman beneath Semail ophiolite	Gravity and receiver function
Gok et al. (2008)	39	Crust near Mosul	Receiver function and surface wave study
Gok et al. (2008)	43	Mesopotamian Foredeep	Receiver function and surface wave study
Pasyanos et al. (2007)	37	Crust beneath Kuwait	Receiver function and surface wave study
Al-Amri (1999)	46	Platform east of Riyadh	P-wave study
Rodgers et al. (1999)	40	Beneath the Platform	Surface wave study
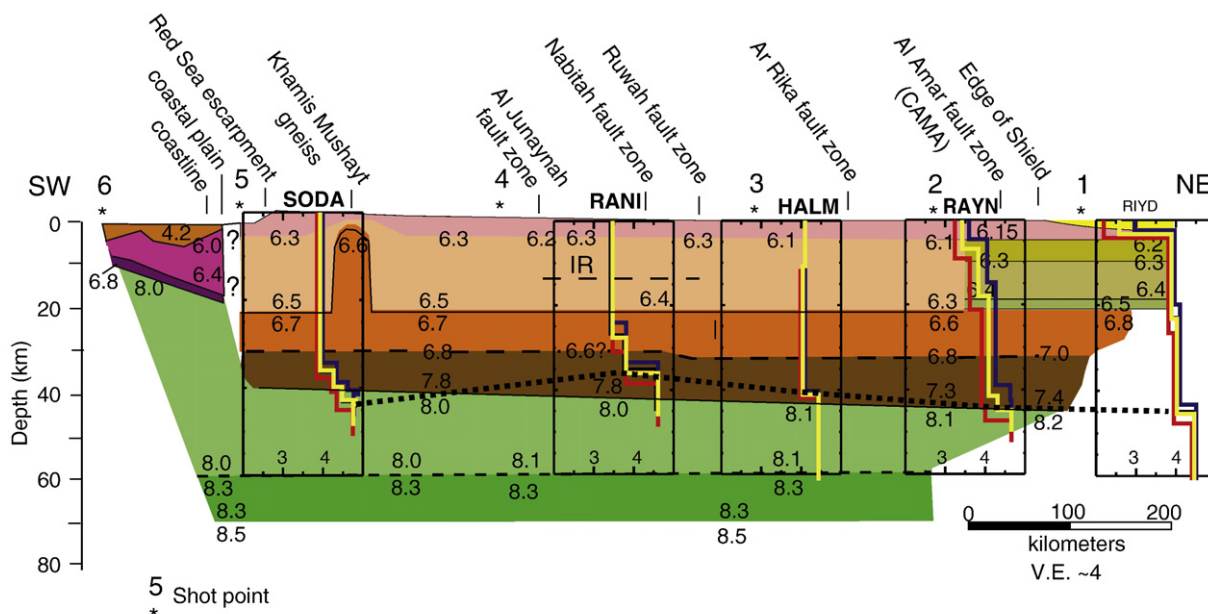
Fig. 10. Interpretive crustal section along the 1978 seismic-refraction profile, Saudi Arabia (Mooney et al., 1985). This composite section is based on crustal and upper mantle P-wave velocity structure, from the Red Sea to slightly east of the Arabian Shield. Velocities for each layer are given in km/s. Numbers above asterisks = shot points. Overlain on this is shear-wave velocity structure from receiver-function stacks of Sandvol et al. (1998) for seismic stations at SODA, RANI, HALM, RAYN, and RIYD (see Sandvol et al., 1998 for locations). The yellow line is the optimal receiver function S-wave mode assuming a Poisson's ratio of 0.25. The red and blue are jackknife (2 SD) error (re-sampling procedure) ranges. Sandvol et al. (1998) noted that P-wave velocity structure inferred from refraction studies are not clear on receiver function stacks, possibly because these features are subtle (<0.15 km/s P wave velocity contrast). Only beneath station RAYN and perhaps RANI did they observe clear infra-crustal velocity contrasts of 0.3 km/s or more in shear-wave velocity. Note the similarities and differences between the Moho determined by the seismic-refraction profile, placed at the boundary between $V_p \sim 7.4$–7.8 km/s and ~8 km/s (boundary between brown and green), and the Moho determined by receiver function, drawn where $V_s = \sim 4.6$ km/s (short dashed line).

part of the Shield. The Moho is a broad transition zone, perhaps 2–5 km thick, underlain by mantle with P-wave velocities of 8.0–8.2 km/s. Abundant pyroxene-rich rocks in both the lower crust and upper mantle are probably responsible for this transition zone, as discussed below in the section on xenoliths. The Mooney et al. (1985) interpretation shows a significant change in crustal structure beneath the CAMA, comprising a major lateral crustal discontinuity at which the velocities in both the upper and lower parts of the crust increase to the northeast by about 0.2 km/s. The discontinuity is located west of the Al Amar fault, beneath the magnetic-low part of the CAMA anomaly. Badri (1991) models a discontinuity in the same part of the refraction profile, but infers a system of thrusts rather than a vertical boundary, in which east-directed nappes are placed on the Ar Rayn terrane.

A seismic-refraction study by El-Isa et al. (1987) farther north in the Arabian Plate, west of the projected line of the CAMA, reveals the crust is less than 32 km thick adjacent to the Dead Sea Transform but thickens eastward to 37 km, where it is underlain by uppermost mantle with $V_p \sim 8.0$–8.1 km/s. The result is supported by gravity modeling studies of Al-Zoubi and Ben-Avraham (2002). The DEad SEa Rift Transect (DESERT) from Israel to Jordan, begun in 2000, included a 260 km long wide-angle reflection/refraction profile (WRR), half of which imaged the Arabian Plate (Fig. 11A,B), and a near-vertical seismic reflection profile (NVR) that coincided with the inner 100 km of the WRR across the Dead Sea Transform, 50 km of which imaged the Arabian Plate. Assuming a velocity of 6.9 km/s for the lower crust, the results of DESERT-Group (2004) indicate that the crust is ~39 km thick beneath Jordan, with only minor thinning of the crust beneath the transform.

In addition to seismic-refraction profiling, Arabian Plate crustal thicknesses have also been estimated using teleseismic S-wave receiver function studies, particularly in areas west of the CAMA. A study by Kumar et al. (2002) of receiver functions from eight stations on the Shield, identified a Moho discontinuity at a depth of 35–38 km,

and a study by Al-Damegh et al. (2005) of receiver functions from 23 stations showed an average crustal thickness beneath the Arabian Shield of 39 km. More recently, Hansen et al. (2007) used S-wave receiver functions supplemented with modeling of gravity data obtained from the Gravity Recovery and Climate Experiment (GRACE) to estimate the depth to the Moho (Fig. 12B,C). It was found that the Moho beneath southern Arabia deepened from about 12 to 35 km inland from the Red Sea, mostly deepening beneath stations on higher topography in the southern Shield. Crustal thickening along profile H2 (Fig. 12A) continues ENE until an average Moho depth of about 40–45 km is reached beneath both the central Arabian Shield and Platform, with the greatest depth (47 km) in the vicinity of Riyadh, east of the CAMA. Moho depths along profile H1 are comparable to those at similar distances from the coast along profile H2. The Moho near the coast lies about 22–25 km deep, and the crust continues to thicken until an average Moho depth of about 35–40 km is reached beneath the eastern edge of the Arabian Shield. Al-Amri et al. (2008) report a similar eastward increase in crustal thickness, inferred from P-wave receiver functions, with a change from 35–40 km beneath the interior of the Shield to 40–45 km beneath the Platform. Sandvol et al. (1998), also on the basis of P-wave receiver functions, reports a comparable change from 35–40 km crustal thickness in the west, adjacent to the Red Sea, to 45 km beneath central Arabia. Surface-wave dispersion measurements, which are sensitive to vertical shear-wave velocity variations, were made by Mokhtar et al. (2001) for parts of the Arabian Plate west of the CAMA, and show a Moho depth beneath the Shield of 41 km to 46 km (Fig. 13A), somewhat deeper than inferences from either refraction or receiver-function studies.

In the northern part of the Arabian Plate, in Jordan, but still west of the projected trend of CAMA, Mohsen et al. (2006) used receiver function analysis to trace the depth of the Moho across the Dead Sea transform. They obtained depths ranging from 30 km to 34–38 km, a result similar to the range of 35–37 km obtained from active seismic
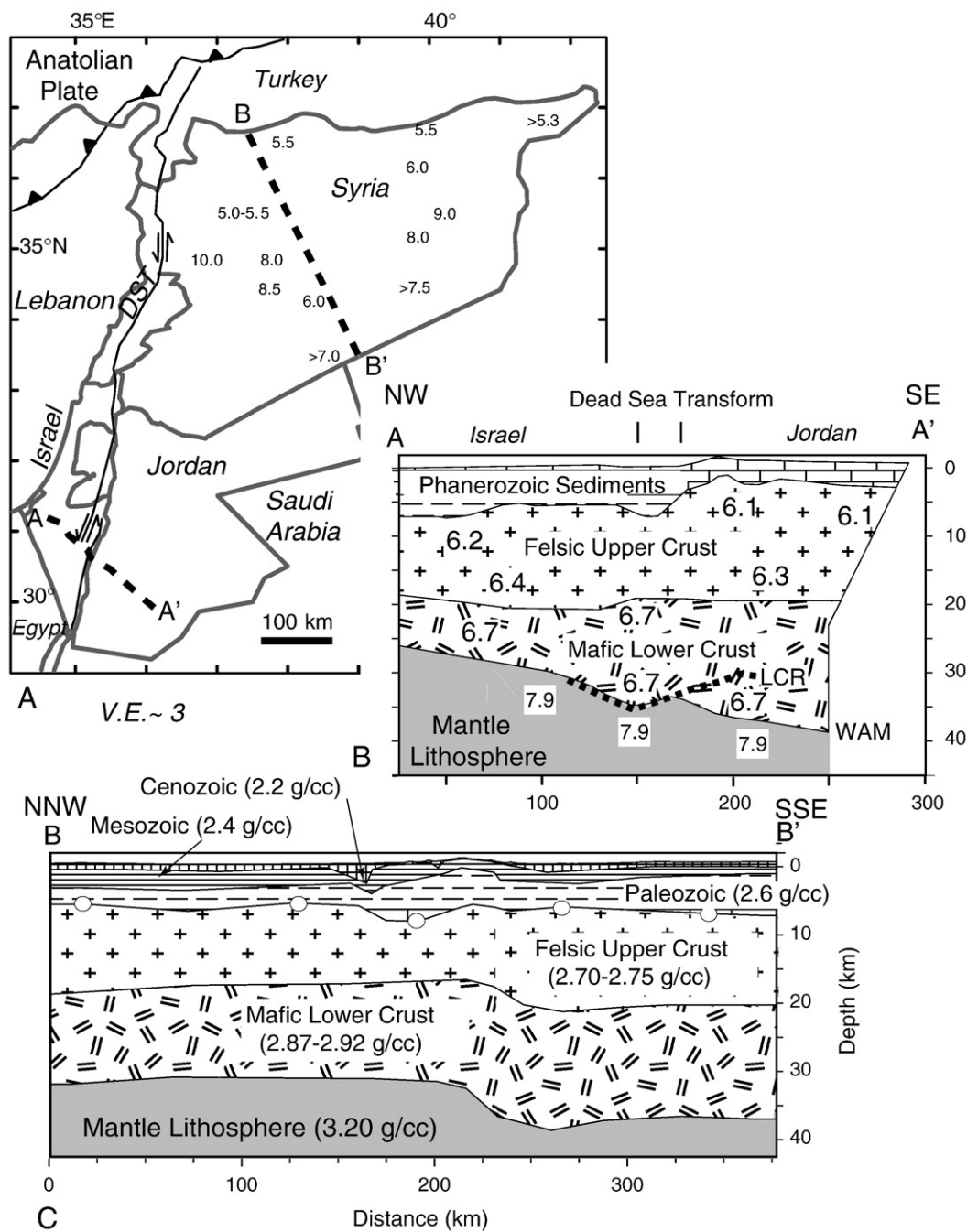
Fig. 11. Crustal structure beneath Syria and Jordan. A: Locality map of Syria and Jordan, showing depth to basement in Syria from drillholes (in km). Dashed lines show locations of profiles A–A′ and B–B′. B) 2-D P-wave velocity model (velocities in km s^{-1}) across Jordan and Israel (profile A–A′; DESERT-Group, 2004). The thick dashed line near the Moho indicates the location of bands of strong reflections (LCR = Lower crustal reflectors; WAM — Moho inferred from wide-angle seismic profiling). C). Model of crustal structure in Syria, from gravity modeling and other constraints by Brew et al. (2001). Densities in g cm^{-3} in parentheses; position of Moho was determined independently by receiver function analysis. Open circles indicate top of crystalline basement from seismic-refraction studies.

profiling (El-Isa et al., 1987). In Syria, the crust appears to be significantly thinner. Al-Saad et al. (1992) used gravity modeling to estimate ~32 km thick crust and Brew et al. (2001) combined gravity modeling and receiver-function analysis to show that Syrian crust north of the Palmyrides is significantly thinner (~25 km) than that to the south (~35 km; Fig. 11C). The crust beneath the northernmost Arabia Plate thickens somewhat near the Bitlis suture, where a thickness of ~40 km was determined by receiver function studies (Angus et al., 2006). Surface-wave dispersion measurements, which are sensitive to vertical shear-wave velocity averages, were made by Mokhtar et al. (2001) for parts of the Arabian Plate west of the CAMA, and show a Moho depth beneath the Shield of 41 km to 46 km

(Fig. 13A), somewhat deeper than inferences from either refraction or receiver-function studies.

The crust of the Arabian Plate east of the CAMA has been sounded at locations from Oman, to Saudi Arabia, to northern Iraq. The ratio of vertical and horizontal components of long-period P-waves generated by earthquakes was used by Al-Amri (1999) to build a forward model of crustal structure beneath the Arabian Platform east of Riyadh. The study gives a preferred Moho depth of 46 km, underlain by mantle with $V_p = 8.3$ km/s, similar to depths of 44.6, 45.0, and 41–53 km obtained from teleseismic receiver functions for 23 stations between the Arabian Shield and Bahrain (Al-Damegh et al., 2005). The results suggest that the crust beneath the southeastern Arabian Platform is
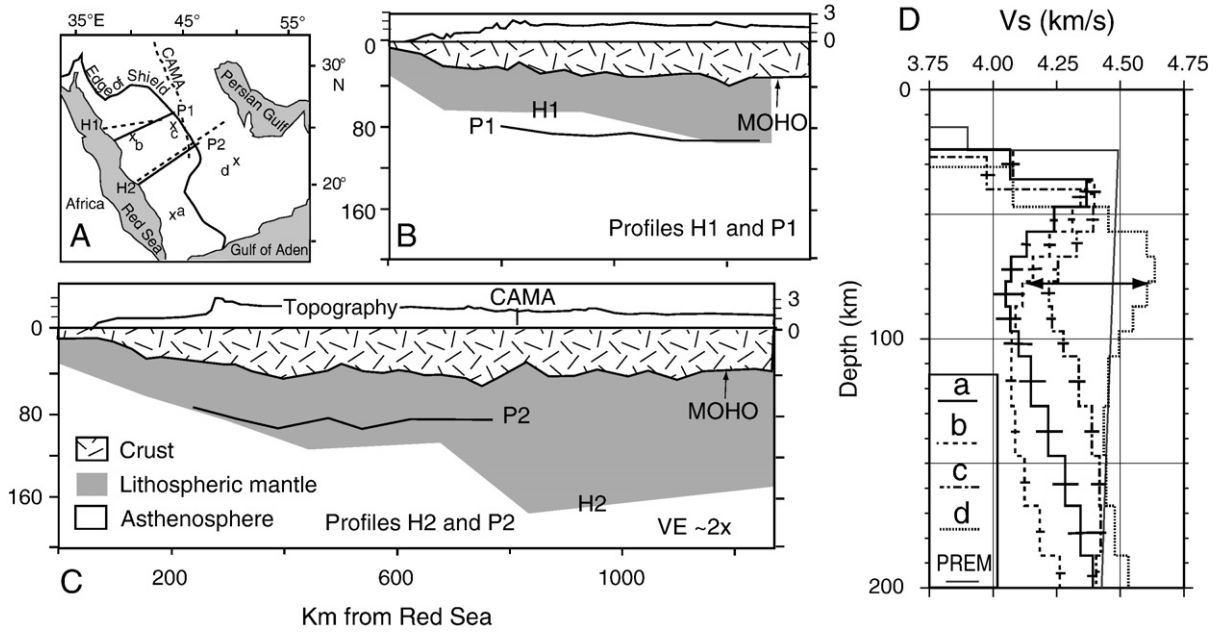
Fig. 12. Thickness of crust and lithospheric mantle beneath western Arabia, from Hansen et al. (2007) and Park et al. (2008). A) Locations of profiles from Hansen et al. (H1 and H2), and Park et al. (P1 and P2), and stations for shear-wave velocity profile (a–d). B) Location of the Moho and lithosphere–asthenosphere boundary (LAB) beneath the northern shield, determined by Hansen et al. (2007); profile H1 and Park et al. (2008); profile P1. C) Location of the Moho and LAB beneath the central shield, determined by Hansen et al. (2007); profile H2 and Park et al. (2008); profile P2. The solid vertical line approximates the boundary between the shield and the platform, also the position of CAMA. D) Shear-wave velocity profile beneath stations a–d, locations shown in A (from Park et al., 2008). Double-arrowed line shows difference of V_s at 80 km depth beneath shield (slow) and platform (fast). Note that the depth to the low-velocity zone (asthenosphere) beneath the three Shield stations is ~80–100 km and ~150 km beneath the Platform station.

thicker (41–53 km) than beneath the Shield, consistent with results of a surface-wave study by Rodgers et al. (1999), which was the first study to show a clear geophysical distinction between Arabian Platform and Shield crusts. Rodgers and his colleagues used surface-wave data to develop an initial model that was refined using teleseismic body-wave arrivals to constrain upper-mantle velocities (although sediment thicknesses must be subtracted). They found that the crust beneath the Platform is slightly thicker (40 km) than the Shield, is slower ($V_p = 6.07$ km/s), and does not have a strong velocity gradient, and suggested that these results are consistent with an overall felsic composition. A reconnaissance study by Al-Lazki et al. (2002) using receiver-function analysis and forward modeling of gravity on a 225-km-long, NE–SW transect across the Semail ophiolite and onto the Arabian Platform estimated a crustal root ~45 km thick beneath the Oman Mountains, and ~10 km of sediment overlying a ~30 km thick crust beneath the Platform.

In the northeastern part of the Arabian Plate, Al-Heety (2002) examined the crust and uppermost mantle beneath Iraq using spectral
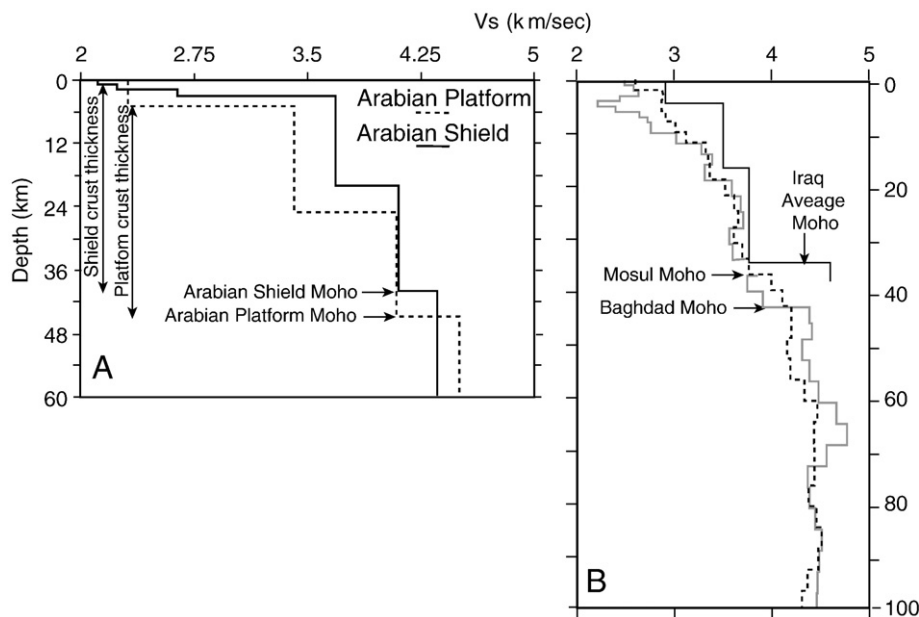

Fig. 13. Crustal structure for (A) Arabian Shield and Platform compared with (B) crustal structure beneath the northernmost Arabian Plate (Iraq). A: Shear-wave velocity models from surface wave analysis of Mokhtar et al. (2001). B: Crustal models beneath Iraq. Three models include average Iraq crustal model based on spectral analysis of long period P-wave amplitude ratios (Al-Heety, 2002) and two models based on receiver function analyses for teleseismic arrivals at Baghdad and Mosul (Gok et al., 2008).

analysis of long period P-wave amplitude ratios from 9 earthquakes recorded at Baghdad (BHD) and Rutbah (RTB) stations (Fig. 13B). A depth of 36.5 km for the Moho and a velocity of 7.8 km/s for the uppermost mantle were indicated. Alsinawi (2003) reported crustal thicknesses of 38 km near Baghdad, 31–34 km near Mosul, and 41–43 km in the Sulaymania region. Gok et al. (2008) used combined P-wave receiver functions and surface (Rayleigh) waves to estimate crustal thicknesses of 39 km beneath Mosul (near the Zagros Fold Belt) and 43 km at Baghdad (in the Mesopotamian Foredeep). On the basis of this study, it was concluded that the two regions had similar crustal structure (Fig. 13B).

Crustal thickness beneath Kuwait has been studied by Midzi (2005) and Pasyanos et al. (2007). Midzi (2005) applied receiver-function techniques to teleseismic arrivals at six seismic stations, and concluded that the crust beneath Kuwait was 42.6 ± 1.8 km thick, similar to Iraq. Pasyanos et al. (2007) used surface waves and receiver-function data to obtain a model of 8 km sediments overlying 37 km thick crust. This study also found that that mantle beneath Kuwait has a P-wave velocity of 7.84 km/s, which is significantly lower than is found for the mantle immediately beneath the Arabian Shield and beneath stable platforms globally.

Overall, these results indicate that, away from the Bitlis–Zagros–Oman convergence zone, Arabian Plate continental crust is ~40 km thick, similar to the CRUST 5.1 and 2.0 models. However, there is a tendency for the crust to thicken eastward beneath the Shield and Platform, particularly at their contact, so that Platform crust is ~10% thicker than that beneath the Shield. This thickening coincides approximately with the CAMA and with the marked lateral changes in crustal structure identified at the northeastern end in the Saudi Arabian seismic-refraction profile.

4.3. Crustal structure

Because it is nowhere exposed, the structure and composition of Arabian Plate lower-continental crust, in addition to its thickness, must be inferred geophysically. A common feature of most Arabian Plate crustal structure models is horizontal layering defined by velocity steps. Layering, in fact, is observed in many tracts of continental crust, and a well-known first-order layered structure in many of these is a sub-horizontal mid-crustal velocity step, referred to as the "Conrad discontinuity" (Wever, 1989). Globally, the discontinuity is not as prominent as the Moho and is often absent. Where it is found, the Conrad occurs 15 to 20 km deep. It is conventionally drawn to separate slower felsic upper crust from faster mafic lower crust, and may coincide with the transition from brittle to ductile deformation. However, as for other lithospheric discontinuities, the exact significance of the Conrad discontinuity is not certain, and alternative interpretations are that it may reflect partial melting zones in the continental crust or changes in metamorphic grade.

A Conrad-like mid-crustal discontinuity is reported from a number of crustal studies in the western and northwestern parts of the Arabian Plate west of the CAMA. The most extensive discontinuity, recognized beneath the entire Arabian Shield, is the velocity step about 20-km deep, apparent in the 1978 1000-km-long Saudi Arabian seismic-refraction profile (Fig. 10). The step separates two 20-km-thick layers, with average P-wave velocities of about 6.3 and 7.0 km/s, respectively (Gettings et al., 1986; Mooney et al., 1985). The lower crust, in turn, is further divided on the basis of a change in velocity gradient along the profile, at about 30 km depth, into two layers each about 10 km thick (Gettings et al., 1986). Surface-wave data (Mokhtar et al., 2001) also shows a mid-crustal velocity step 20–25 km beneath the Shield, and Rayleigh wave velocity inversion indicates a two-layer crust as well, each layer about 20 km thick. A mid-crustal velocity step 18–20 km deep was also identified in a refraction study in Jordan (El-Isa et al., 1987). A similar step was identified in the DESERT NVR and WRR experiments (DESERT-Group, 2004) (Fig. 11B), and was modeled in the gravity study of Al-Zoubi and Ben-Avraham (2002).

Modeling of gravity beneath Syria likewise favors a relatively simple layered crust. Al-Saad et al. (1992) describes ~12 km of relatively low density (ρ~2.67–2.73 g/cc) upper crust underlain by ~19 km of denser (ρ~2.86–2.92 g/cc) lower crust. Brew et al. (2001) (Fig. 11C) model an upper-crustal felsic layer about 12 km thick (2.7–2.75 g/cc), overlain by sedimentary rocks as much as 8 km thick, and a lower-crustal mafic layer about 15 km thick (2.87–2.92 g/cc). These densities are significantly lower than the ~3.0 g/cc expected for tholeiitic gabbro at ~1 GPa, 800 °C, and the overall crustal thickness (32 km) is somewhat thinner than other crustal estimates for the western part of the Arabian Plate. Whether these differences are a real feature of the lower crust beneath Syria is not certain.

In detail, the lower-crustal layer recognized along the Saudi Arabian seismic-refraction profile (Fig. 10) between depths of ~20 and 40 km, has V_p ranging from 6.6–6.8 km/s at the top to 7.3–7.8 km/s at the base, which suggests a mafic composition. Tholeiitic gabbro at 1 GPa and 800 °C, for example, is expected to have V_p~7.1–7.2 km/s, with relatively small effects ($\pm$ 0.1 km/s) reflecting variations in P or T (Hacker et al., 2003). It is reasonable therefore to infer that the lower crust beneath the Arabian Shield has a broadly gabbroic composition, although second-order compositional variations such as increased plagioclase content upwards and increased pyroxene content downwards may be present, as discussed in the section on xenoliths.

Crustal structure in the eastern part of the Arabian Plate is not well known, but appears to be more complicated than in the west. This is evident at the northeastern end of the Saudi Arabian seismic-refraction profile, northeast of the lateral discontinuity referred to in the previous section. Three upper-crust sub-layers are recognized, and velocities increase to 6.2–6.5 km/s in the upper crust and are high (6.8–7.4 km/s) in the lower crust (20–40 km). The causes of this complexity are not certain. Gettings et al. (1986) comment that the different velocity–depth functions in this part of the seismic profile are not surprising given the geologic evidence that the Ar Rayn terrane is allochthonous with respect to terranes farther west and that its crustal layers may well have different compositions than those to southwest. A high-velocity upper layer in the lower crust may reflect the presence of more mafic rocks in the amphibolite facies than the adjacent part of the lower crust to the southwest. Seber et al. (2001), in the context of gravity calculated for well-constrained crustal models, noted a large difference between the observed and the modeled gravity in the northern part of the Arabian Plate, but since there are reasonably good observations in this region, the difference is not easily attributed to error in the model. Possible explanations are that higher-density material is present at subcrustal (mantle) levels or that the crust is denser than allowed for in the gravity model.

Farther east in the Arabian Plate, east of Riyadh, the crust is modeled as a five-layered structure (Al-Amri, 1999), with thicknesses and velocities varying, top to bottom, from 3 km and 5.6 km/s, to 10 km and 6.3 km/s, 8 km and 6.6 km/s, 15 km and 6.9 km/s, and 10 km and 7.6 km/s. Kuwait crustal structure was investigated by Pasyanos et al. (2007). They used surface waves and receiver-function data to generate a preferred model with three crustal layers; upper crust ~17 km thick characterized by V_p~5.9 km/s; 9-km-thick intermediate crust with V_p~6.4 km/s; and 11-km-thick lower crust with V_p~7 km/s. In Iraq, the crust appears to have three distinct layers, with an upper layer 4–10 km thick characterized by V_p ranging from 4.9 to 5.2 km/s; an intermediate layer 11–14 km thick with V_p ranging from 6.0 to 6.6 km/s; and a lower layer 16–18 km thick and marked by V_p 6.4 to 6.8 km/s (Al-Heety, 2002).

4.4. Lithospheric thickness and structure

As previously noted, there is no agreed definition of the lithosphere because of the varying seismic, thermal, or mechanical criteria that may be used (Anderson, 1995), other than the standard definition that it includes the crust and the upper part of the mantle.

The crust is, of course, the upper part of the lithosphere, but for purposes of description and analysis may be treated as a separate layer in Earth structure, as is done here. From a seismic point of view, the base of the lithosphere — the contact with the asthenosphere, or lithosphere–asthenosphere boundary (LAB) — is a "low-velocity zone" (LVZ) at depths of about 200 km in continental tracts where velocity either decreases slightly downward, or at least does not increase as rapidly as it does above the LVZ (Rogers and Santosh, 2004). From a thermal point of view, the base of the lithosphere is conventionally defined as the 1300 °C isotherm since mantle rocks above this temperature are partially molten (www.geolsoc.org.uk/gsl/null/lang/en/page2675.html; Artemieva and Mooney, 2001).

Continental lithosphere of the Arabian Plate extends from the contacts with new ocean crust in the Gulf of Aden, Red Sea, and Indian Ocean in the south, west, and east, to the Bitlis suture and Main Zagros Thrust in the north and northeast, and to the Dead Sea Transform in the northwest, and its thickness is mostly estimated between 100 and 160 km. This thickness is close to that expected from a compilation by Artemieva and Mooney (2001) of 300 thermal lithospheric-thickness estimates. The compilation indicates an age dependence of continental lithospheric thickness, with covariation of age and thermal lithospheric thickness, from 250 ± 70 km for Archean lithosphere to 200 ± 50 km for Paleoproterozoic lithosphere, to 140 ± 40 km for Mesoproterozoic and Neoproterozoic lithosphere.

In practice, it is difficult to seismically determine the thickness of the lithosphere because velocity contrasts across the LAB are small and recourse is mostly made to shear wave velocity variations because these are sensitive to the presence of small amounts of melt, which is one of the means of differentiating between asthenosphere and lithosphere. Several methods are available to determine V_s structure. Seber and Mitchell (1992) were the first to do this for the southern part of the Arabian Plate. They studied surface wave dispersion across the Arabian Peninsula and inferred that the LAB lay ~120 km deep beneath western Arabia. Hansen et al. (2007), using S-wave receiver functions and GRACE gravity, estimated depth to the LAB along profiles approximately perpendicular to the coast (Fig. 12B,C). These profiles are referred to, above, in the section on crustal thickness: here, the emphasis is on the overall thickness of lithosphere (crust + upper mantle). Along profile H2, the LAB rapidly thickens inland from the Red Sea, increasing, from ~50 km near the coast to ~120 km beneath the Shield, 300 km from the Red Sea, a depth comparable to the global depth compiled by Artemieva and Mooney (2001) and the depth result of Seber and Mitchell (1992). A similar result was observed by Hansen et al. (2007) along profile H1, with the LAB near the Red Sea ~55 km deep and beneath the Shield 100–110 km deep. The shallow depth of the LAB close to the Red Sea is confirmed in a receiver-function and fundamental-mode group velocity analysis by Juliá et al. (2003), which indicates a possible lithospheric thickness of as little as 50–60 km some 120 km inland from the coast.

East of the CAMA, across the Shield/Platform boundary and broadly coincident with the location of changes in structure and thickness of the crust described above, Hansen et al. (2007) found that the LAB on profile H2 deepens to about 160 km. Profile H1 of Hansen et al. (2007) suggests a comparable lithospheric-thickness increase eastward but the profile, unfortunately, does not extend far enough to the east to confirm this. Significantly, however, a similar step of 20–40 km in lithospheric thickness across the Shield/Platform boundary is reported by Al-Amri et al. (2008).

These results further emphasize the significance of CAMA as the magnetic expression of a fundamental boundary in the Arabian Plate, separating thinner lithosphere to the west from thicker lithosphere to the east. However, caution is needed in interpreting the estimates of lithospheric thickness, because they depend on the method adopted. Park et al. (2008), for example, approaching the issue from a different geophysical perspective, estimated shallower depths to the LAB than did Hansen et al. (2007) (Fig. 12). Park et al. (2008) used Rayleigh wave phase and group velocities to constrain the shear-wave velocity

structure of the shallow mantle in the region. They found ~90–100 km thick lithosphere beneath the southern and northern Shield, similar to lithospheric thicknesses determined by Hansen et al. (2007), but obtained a depth of as little as ~80 km for LAB beneath the eastern Shield, near CAMA (profile P2 in Fig. 12C), in contrast to the eastward increase in depth to ~130 km and ~160 km farther east shown by Hansen et al. (2007). Nonetheless, the results of Park et al. (2008) distinguish different lithospheric structures beneath Shield and Platform consistent with inferences of a major discontinuity near CAMA and the Shield/Platform boundary. Three vertical profiles beneath the Shield (a–c in Fig. 12D) contrast with the profile beneath the Platform (d in Fig. 12D), which shows significantly (up to 0.5 km/s) faster uppermost mantle velocities, consistent with thicker, colder mantle lithosphere. The most striking differences are observed ~80 km deep, where the slower sub-Shield velocities indicate mantle temperatures that are ~300 °C warmer than those beneath the Platform (Park et al., 2008). This lithospheric structure should be shown by a strong gradient in heat flow across Arabia and should be testable by a heat-flow survey.

Structure in the lithosphere below the Moho is not widely reported for Arabia. One of the earliest studies was by Knopoff and Fouda (1975), who measured phase velocity of Rayleigh waves for three profiles across the Peninsula. A pronounced low-velocity channel for S-waves was found throughout the region with its top at depths of 100–140 km, and crustal thickness of 35 ± 8 km. In a later work, Prodehl (1985) used the results of the 1978 Saudi Arabian seismic-refraction study over the SW Arabian Shield to model traveltimes and amplitudes. The work yielded velocity–depth profiles down to ~80 km and indicated alternating layered high- and low-velocity zones in the upper mantle lithosphere. Mooney et al. (1985) inferred a P-wave velocity jump in the upper mantle at a depth of about 65 km, from $V_p = 8.1$ to 8.4 km/s, about 25 km beneath the Moho but well above the LAB. Rodgers et al. (1999) found that sub-Moho V_p was slower beneath the Shield than beneath the Platform (7.9 vs. 8.1 km/s) and Seber and Mitchell (1992), on the basis of a surface-wave study, identified a low-velocity zone ~70 km deep beneath western Arabia and a smaller low-velocity zone ~100 km beneath eastern Arabia. An upper-mantle interface was also observed using receiver functions for teleseismic arrivals at RAYN on the eastern edge of the Arabian Shield (Levin and Park, 2000). This revealed a well-defined "Hales discontinuity" ~70 km deep, which Levin and Park (2000) interpreted as marking the upper boundary of a zone of depth-dependent anisotropy within the upper mantle. They further argued that shear was guided by depth-dependant rheologies in the lithosphere, concentrating shear near the Moho and Hales discontinuities. Because the anisotropy at these two discontinuities was similar, they inferred that both were caused by the same process, which they further suggested to be large-scale lithospheric shearing during the Neoproterozoic episode of tectonic escape. Petrologic data from mantle xenoliths, discussed in a later section, suggest that the Moho may also reflect a change from pyroxene-rich lithologies above to more peridotitic mantle below. Deeper structure in the Arabian continental lithosphere is little known. By inverting Rayleigh wave phase velocity measurements, Park et al. (2008) found a broad LVZ to depths of ~150 km in the mantle beneath the Shield. It is unknown whether the LVZ persists at this depth across the entire Plate or deepens to 180–220 km similar to the depths found in other continental tracts. Tkalcic et al. (2006) describes shear-wave velocity models that suggest mantle lithospheric thickness varies regionally with the LVZ varying from 47–140 km deep close to the Red Sea, to 67–80 km deep beneath the northern Shield, and to 120 km deep beneath the eastern part of the Plate.

In the northeastern Arabian Plate, Kaviani et al. (2007) carried out a high-resolution study of lithospheric structure along a 620-km temporary seismic profile across the Zagros belt in Iran, using surface-wave dispersion and inversion of teleseismic P-wave traveltime residuals. They identified a strong lateral change of both P- and S-wave velocities in the shallow mantle beneath the profile, with the Main Zagros Thrust (MZT) marking the surface trace of the mantle

seismic discontinuity. The mantle of the Arabian Platform beneath Zagros has Shield-like S-wave velocity structure, whereas the mantle to the north has V_s as much as 0.5 km/s slower. The 0.5 km/s difference between sub-Moho V_s was interpreted by Kaviani et al. (2007) to be due to a compositional change, for example the presence of hydrated minerals in subduction-affected mantle north of the MZT. Along the Dead Sea Transform, at the northwestern Plate margin, Mohsen et al. (2006) estimated the depth to the LAB using teleseismic-receiver functions. West of the Dead Sea transform, the LAB was found to be ~67 km deep, whereas east of it, the lithosphere thickness varies from ~80 km north of the Dead Sea to 67 km in the south. These are broadly compatible with the depth to the LAB measured near the Red Sea coast by Hansen et al. (2007), but are less than lithospheric thickness in the interior of the Plate and may reflect Cenozoic lithospheric thinning in the vicinity of the rifted Arabian Plate margins (Hansen et al., 2007).

4.5. Shear-wave splitting

The azimuthal variation of material properties reveals much about lithospheric deformation and perhaps asthenospheric flow. It is known that much of the lithospheric mantle is anisotropic — largely reflecting the preferred orientations of olivines — and that upper mantle and crustal anisotropy can be quantified by measuring the splitting (birefringence) of teleseismic shear waves, especially SKS splitting. It is controversial, however, whether the observed anisotropy resides entirely in the lithosphere. Fouch and Rondenay (2006) concluded from studies of four stable continental interiors (E. North America, Canadian Shield, Australia, and South Africa) that the upper part of the mantle lithosphere has moderate to strong anisotropy (typically 3–5%) whereas the lower mantle lithosphere and asthenosphere has weak to moderate anisotropy (<3%).

A range of studies show that the Arabian Plate has well-developed and systematic mantle anisotropy (Fig. 14), although it is not clear at what depth the anisotropy is located. Wolfe (1999) measured shear-wave splitting across western Saudi Arabia, using data from eight temporary broadband stations, and found that the fast polarization is north–south, with splits of 1.0 to 1.5 s. Interestingly, the shear-wave splitting times were ~1.5 s beneath the western part of the Shield, decreasing systematically to 0.5 s beneath the Platform, which suggests a systematic change in mantle anisotropy across the Shield/Platform boundary. However, it was not possible to determine whether the splitting is a fossil, upper-mantle anisotropy associated with the dominantly east–west compression that formed the lithosphere in late Neoproterozoic time or whether it is caused by Cenozoic and current northward motion of the Plate or northward asthenospheric flow from an Ethiopian mantle plume.
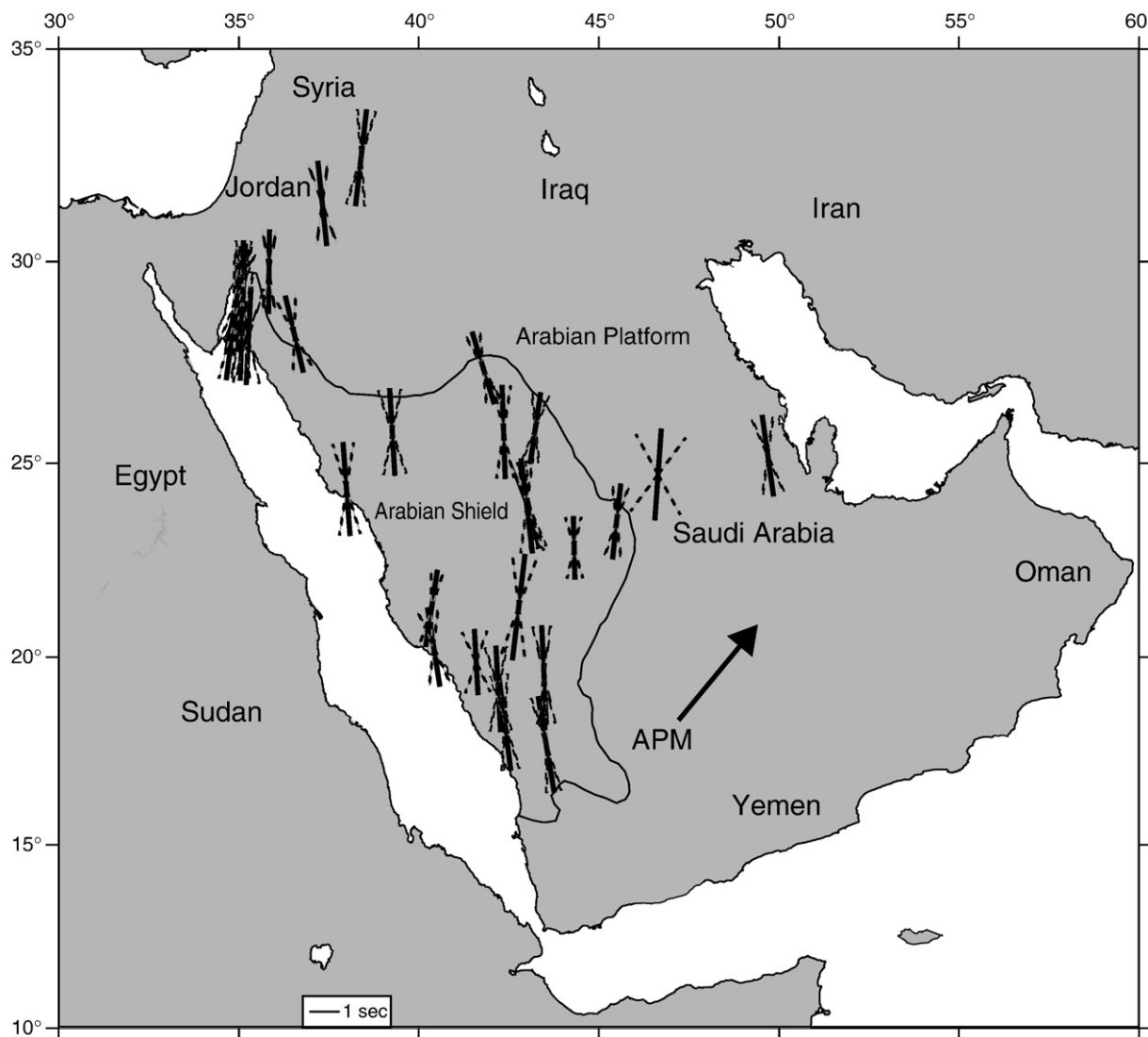

Fig. 14. Map showing average shear wave splitting parameters for Arabia, from Hansen et al. (2006). Bold, center lines at each station are oriented in station's average and length of line is scaled to average δt. Dashed "fans" show one standard deviation of fast angle. Black arrow shows average absolute plate motion (APM).

As previously discussed, Levin and Park (2000) noted that teleseismic receiver functions for station RAYN on the eastern edge of the Arabian Shield contain strong converted-phase P-wave phases. They inferred that these phases arise from the Hales discontinuity within the lithosphere at a depth of ~70 km. On the basis of the polarization, azimuthal behavior, and frequency dependence of the
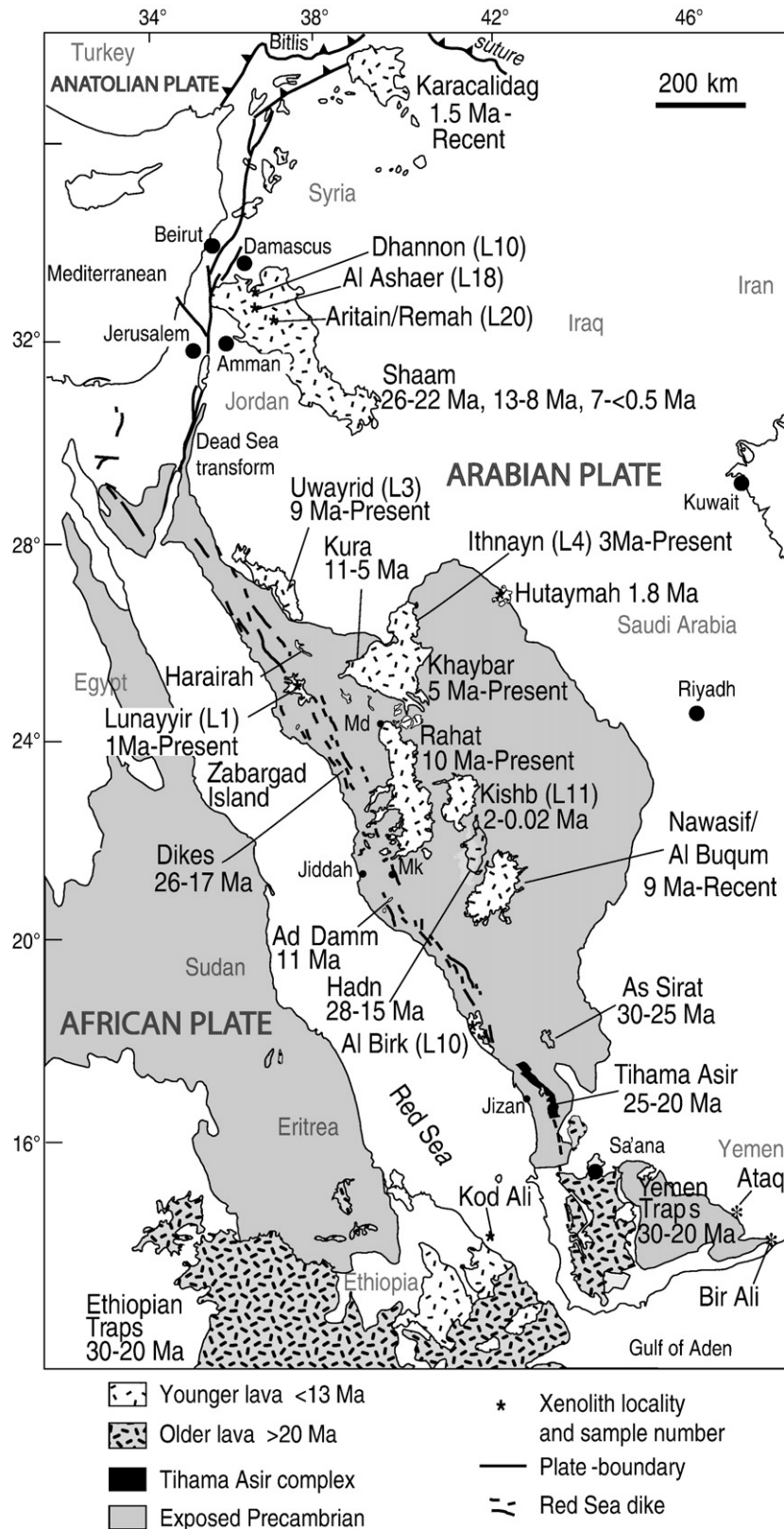

Fig. 15. Map of Cenozoic volcanic fields (harrats) of the western Arabian Plate and the northern extremity of the East African Rift system (lava fields modified from Coleman 1993). The volcanic fields are named and the age or age range of volcanism indicated, after Coleman (1993). Locations of sites with lower-crustal xenoliths (LC) discussed here are shown with the number of samples analyzed by Ghent et al. (1980), McGuire and Stern (1993), Nasir (1995), and/or Al-Mishwat and Nasir (2004) in parentheses following the "LC"; e.g., (LC5). Md = Medinah, Mk = Makkah.

phases, they characterized the Hales discontinuity as marking the upper boundary of a zone of depth-dependent anisotropy within the upper mantle, and proposed a similar zone just below the Moho. They further found that the anisotropy trended N–S and plunged ~50°south. They proposed that the regions of coherent fabric in the upper mantle implied by the anisotropy represent fossil lithospheric shear zones developed during Neoproterozoic continent–continent collision, when the easternmost Shield underwent northward 'escape' along the northern flank of the Najd fault system.

Hansen et al. (2006) studied shear-wave splitting beneath Arabia, using data from 33 Saudi Arabian and 2 Jordanian stations. Their results confirm N–S fast directions with an average split of 1.4 s, similar to previous findings, although splits from sites adjacent to the Gulf of Aqaba are deflected sligly to the NNE, parallel to the Dead Sea Transform. Levin et al. (2006) analyzed SKS splits for 5 stations around the Dead Sea Transform and found that the fabric was partitioned into an upper layer, subparallel to both modern transform motions and fossil Arabian Shield fabrics, whereas the lower layer showed anisotropy consistent with contemporary relative plate motions. The remainder of their observations show north–south-oriented fast directions and splits averaging 1.4 s. Hansen et al. (2006) argued that neither fossil lithospheric anisotropy nor present-day asthenospheric flow fully explain the

observed splitting. Instead, they preferred to explain it as due to northeast-oriented flow associated with absolute plate motion combined with northwest-oriented flow associated with the channelized Afar plume. More recently, Al-Amri et al. (2008) made similar comments about shear wave splitting, noting a splitting time of approximately 1.4 s with the fast axis slightly east of north. They confirmed the remarkably consistent nature of splitting across the Arabian Peninsula with a slight clockwise rotation parallel to the Dead Sea Transform (Fig. 14).

5. Lower crustal and mantle xenoliths

It is well known that xenoliths transported to the surface by alkali basalts provide a direct means of studying the lower crust and upper mantle by constraining the composition of the lower crust and upper mantle, and allowing their heterogeneity and origin to be assessed. In the Arabian Plate, mafic and ultramafic xenoliths are abundant in Cenozoic alkali-basalt fields (harrats). These eruptions were especially common in the western part of the Plate (Fig. 15) as a result of rifting and separation from Africa. Arabian Plate harrats are all west of the CAMA, are younger than ~30 Ma old, and stretch discontinuously N–S for ~2500 km. Harrat xenoliths provide a remarkable glimpse of the lower-crustal and upper-mantle lithosphere beneath the Plate. The
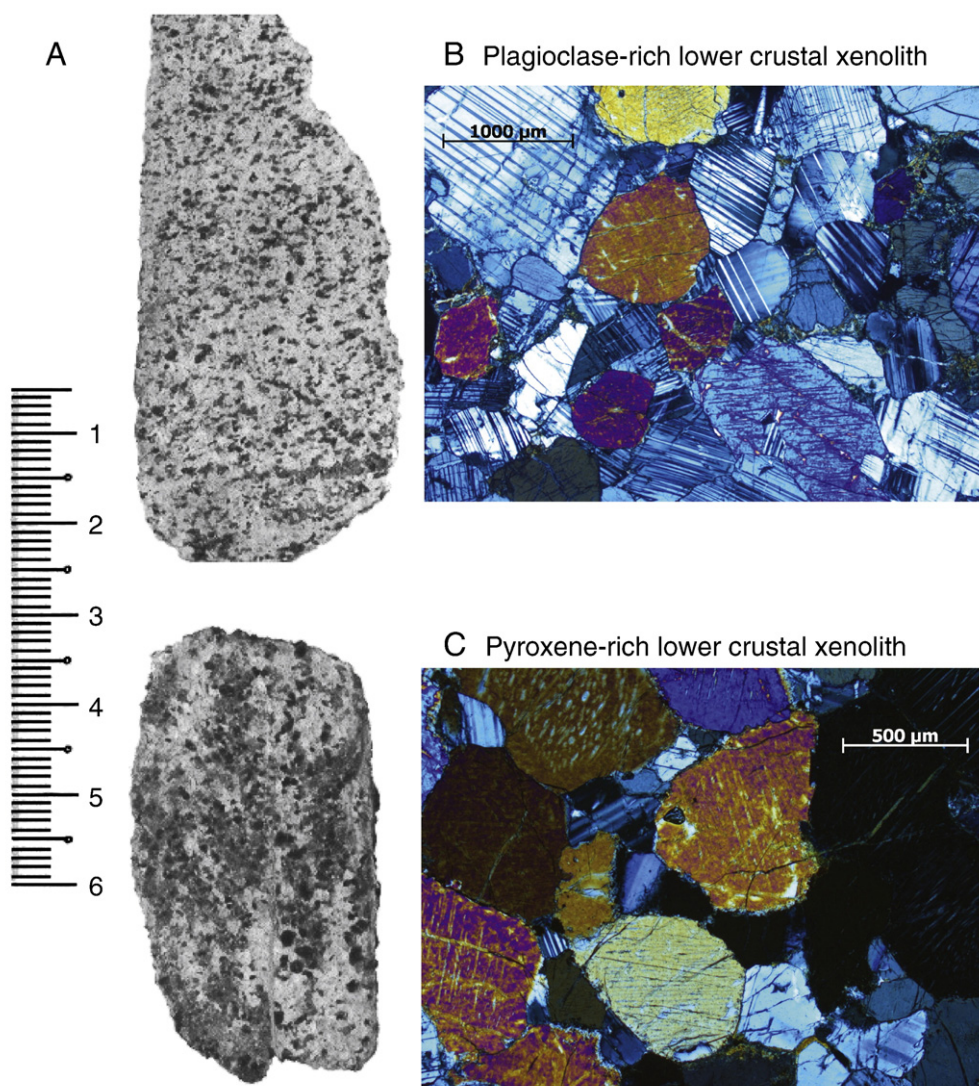

Fig. 16. Typical lower-crustal xenoliths from western Arabian Plate harrats. A) Typical hand specimens of plagioclase rich (upper) and pyroxene-rich (lower) xenoliths (Safarjalani et al., 2009). B) Photomicrograph (crossed nicols) of typical plagioclase-rich xenolith, from Aritain volcano, Jordan; C) Photomicrograph (crossed nicols) of typical pyroxene-rich xenolith, from Dhannon volcano, Syria (Al-Mishwat and Nasir, 2004). Note OPX exsolution in large CPX.

northern Harrat Ash Sham (Shaam) in Syria alone has 24 volcanoes with xenolith-bearing alkaline basalt lavas. In addition, the northern segment of the Dead Sea Transform in western Syria hosts 36 explosive kimberlite-volcanic pipes containing various mantle xenoliths such as peridotite, pyroxenite, and eclogite (G. Syada, pers. comm. 2008). Mantle xenoliths also occur in Paleogene mafic plugs and dikes in the far east of the Plate, in Oman (Fig. 4). Much less work has been done on these xenoliths, and we focus on the harrat xenolith suite here.

McGuire (1988) noted that most Arabian xenoliths are found in alkali basalts that are younger than ~5 Ma. The xenoliths include plagioclase- and pyroxene-bearing mafic granulites, rarer garnet-bearing granulites, gabbro, spinel lherzolite, dunite, wehrlite, clinopyroxenite, and megacrysts of clinopyroxene and amphibole. A division into lower-crustal and upper-mantle xenoliths is largely done on the basis of whether or not the xenoliths contain plagioclase (presence of plagioclase distinguishes lower-crustal rocks from mantle rocks), but a further distinction can be made using whole-rock compositions and the T conditions that the xenoliths record. Lower-crustal xenoliths generally are characterized by lower Mg# $(=100\,Mg/(Mg+Fe))$, Ni, and Cr contents, and yield lower mineral equilibration temperatures (~700–900 °C) than do upper-mantle xenoliths (~800–1050 °C). In spite of these distinctions, there is considerable overlap in composition and T between especially pyroxene-rich xenoliths of inferred lower-crustal and upper-mantle origins. There are many fewer estimates of xenolith pressure, but 1–1.2 GPa (33–40 km) are estimated for the garnet-bearing lower-crustal granulite xenoliths, whereas 1–3.3 GPa (33–100 km depth) is estimated for mantle xenoliths.

5.1. Lower-crustal xenoliths

The study of Arabian Plate lower-crustal xenoliths began with gabbroic inclusions found in Harrat Al Birk, in the southwestern part of the Plate (Fig. 15), by Ghent et al. (1980). Plagioclase-bearing mafic lower-crustal xenoliths have since been reported from 7 localities scattered ~1700 km N–S across Saudi Arabia, Jordan and Syria. Al-Mishwat and Nasir (2004) examined more than 200 lower-crustal xenoliths from Harrat Kishb in Saudi Arabia and Harrat Ash Sham in

Jordan (Aritain) and Syria (Dhannon). Similar xenoliths found at Harrats Ithnayn, Uwayrid, Harairah and Lunayyir in northwestern Saudi Arabia have been studied by McGuire and Stern (1993). The xenoliths are 1 to 20 cm in diameter (Fig. 16). All sample the lower crust of the Arabian Plate west of CAMA.

Mineralogically, the xenoliths contain plagioclase and pyroxene, and a few contain garnet and rare amphibole, but olivine and spinel are absent. They are divisible into pyroxene-rich varieties and plagioclase-rich varieties, both with many samples, and a rare garnet-bearing group (Table 2). This pyroxene/plagioclase distinction is based on work by Al-Mishwat and Nasir (2004), who divided >200 lower-crustal xenoliths into: (1) pyroxene-rich samples, composed of two pyroxenes and plagioclase in subequal proportions; and (2) plagioclase-rich samples containing significant orthopyroxene and clinopyroxene (Fig. 16). They concluded that pyroxene-rich xenoliths were more common than plagioclase-rich xenoliths, although McGuire and Stern (1993), conversely, found that most of the smaller group of xenoliths they studied contained 70–80% plagioclase. The minor garnet-bearing class of xenoliths is based on three samples described by McGuire and Stern (1993) from Harrat Al-Birk in southwestern Arabia and a few xenoliths from Harrat Shaam (Safarjalani et al., 2009)(Fig. 15). Other garnet-bearing granulite xenoliths in the region are reported from Birkat Ram in Israel (Esperanca and Garfunkel, 1986) and at Nabi Matta in NW Syria (Sharkov et al., 1993) but these are west of the Dead Sea Transform, outside the Arabian Plate.

Comparing the major element data of Al-Mishwat and Nasir (2004) with their petrographic subdivisions indicates that plagioclase-rich xenoliths contain >16% Al_2O_3, whereas the pyroxene-rich group contains <16% Al_2O_3. Because of the large size (N>200) of their sample population, we use their Al_2O_3 thresholds to classify xenoliths for which modal estimates are not available, and on this basis we have assigned Arabian Plate lower-crustal xenoliths with major element or modal data to one of the three groups: pyroxene-rich, plagioclase-rich, or garnet-bearing (note: data from Safarjalani et al., 2009 are not included in this compilation because this suite is compositionally distinct). Chemical, modal, and mineral data for these three suites are summarized in Table 2, including the means of major element

Table 2
Summary of major oxide contents[a] and mineral and modal data for crustal xenoliths from western Arabia.

	Pyroxene-rich			Plagioclase-rich			Garnet-bearing		
	Composition	1 SD	N	Composition	1SD	N	Composition	1 SD	N
SiO_2	49.95	1.60	25	50.73	3.05	39	50.55	2.90	3
TiO_2	1.05	0.40		0.91	0.46		0.82	0.33	
Al_2O_3	13.15	1.76		18.67	1.54		15.11	2.62	
FeO*	9.88	1.69		8.93	2.08		9.86	2.00	
MnO	0.21	0.09		0.16	0.06		0.21	0.08	
MgO	11.23	1.75		6.89	2.54		9.41	0.25	
CaO	12.44	1.48		9.99	1.49		10.95	1.52	
Na_2O	1.62	0.40		3.06	1.07		2.75	0.90	
K_2O	0.29	0.27		0.43	0.25		0.27	0.09	
P_2O_5	0.22	0.13		0.21	0.14		0.07	0.05	
Mg#	66.8	4.8		55.1	6.8		63.3	4.6	
Ni (ppm)	169	64	25	66	52	22	160	10	2
Cr(ppm)	435	214	25	117	74	22	780	390	2
Mode									
PLAG	37	5	25	61	7	25			
CPX	31	9	25	13	8	25			
OPX	27	7	25	23	4	25			
AMPH	3.2	4.4	25	1.7	2.0	25			
Mineral compositions									
PLAG AN	65.8	9.9	9	49.5	9.8	16	70.0	2.2	2
OPX EN	65.2	4.9	7	57.1	6.8	16	45.2	1.4	2
CPX WO	47.2	1.3	7	45.3	2.3	16	41.9	1.1	2
CPX EN	36.2	1.8	7	36.1	2.7	16	13.0	2.5	2
CPX FS	16.6	3.9	7	18.6	12.3	16	70.0	2.2	2

[a] Recalculated 100% anhydrous.

compositions; Mg#; Ni and Cr contents; modal compositions; and compositions of plagioclase, orthopyroxene, and clinopyroxene, as determined by electron microprobe analysis. These data are compiled from several studies (Al-Mishwat and Nasir, 2004; Ghent et al., 1980; McGuire and Stern, 1993; Nasir, 1992, 1995; Nasir and Safarjalani, 2000), and are based on the analyses of 67 lower-crustal xenoliths from 8 localities stretching ~1500 km from Al Birk, in the south, to Kishb, Ithnayan, Harairah, and Uwayrid, in Saudi Arabia; Aritain and Remah, in Jordan; and Dhannon, in Syria (Fig. 15). Using the Al_2O_3 thresholds mentioned above, the 67 lower-crustal xenoliths summarized in Table 2 are 37% pyroxene-rich, 58% plagioclase-rich and 5% garnet-bearing. Table 2 also shows that the mean pyroxene-rich xenolith contains ~1/3 each of plagioclase, clinopyroxene, and orthopyroxene, whereas the mean plagioclase-rich xenolith contains twice as much plagioclase as pyroxene, with the ratio of clinopyroxene:orthopyroxene ~2:1 (Fig. 16). Both varieties sometimes also contain subordinate (few %) amphibole. No major systematic variations in the mineralogic compositions are observed.

The pyroxene-rich and plagioclase-rich lower-crustal xenoliths have mean Al_2O_3 contents of 13% and 19%, respectively: otherwise the two groups have similar elemental compositions. Both contain ~50% SiO_2 and ~1% TiO_2, with low K_2O (<0.5%) and Na_2O (1–3%). Both groups show tholeiitic affinities and are quite distinct from their alkali basalt hosts. Mean pyroxene-rich and plagioclase-rich samples differ significantly in their extent of fractionation, as indicated by MgO contents (11% vs. 7%), Mg# (67 vs. 55), and contents of compatible elements Ni (169 vs. 66 ppm) and Cr (435 vs. 117 ppm). Despite high Mg# in pyroxene-rich xenoliths, mineral compositions of labradoritic plagioclase (mean ~ An_{64}) and relatively Fe-rich pyroxenes (mean $OPX \sim En_{63}$; mean $CPX \sim Wo_{48}En_{35}Fs_{17}$) indicate that these are somewhat fractionated. Plagioclase-rich varieties are significantly more fractionated, with a mean mineral composition of andesine–labradorite (mean ~ An_{50}) and more Fe-rich pyroxene (mean $OPX \sim En_{57}$; mean $CPX \sim WO_{45}En_{36}Fs_{19}$). There is likely a compositional continuum among the lower-crust xenolith suites, from the most fractionated plagioclase-rich to more primitive pyroxene-rich lower-crustal suites to pyroxenites of presumed mantle origin, discussed in the next section. Such a compositional spectrum could reflect gross layering in the lower crust and upper mantle beneath W. Arabia. We speculate that density variations among these lithologies may reflect plagioclase-rich lower-crustal types concentrated at the top of the lower crust, pyroxene-rich lower-crustal types concentrated at the base of the lower crust, and mantle pyroxenites concentrated at and just beneath the Moho (Fig. 17).

Temperature estimates for the pyroxene- and plagioclase-rich xenolith groups have been made on the basis of the compositions of coexisting minerals. Temperature estimates using the pyroxene geothermometers of Wells (1977), Brey and Köhler (1990), and Anderson and Lindsley (1988) are reported by Ghent et al. (1980), Nasir (1992), Nasir (1995), and Nasir and Safarjalani (2000). The Wells (1977) 2-pyroxene thermometry gives temperatures ranging from 775 °C to 1015 °C; estimates by Nasir (1995) and Nasir and Safarjalani (2000) are up to 880 °C; and two estimates by Ghent et al. (1980) yield higher temperatures of 1010 °C and 1015 °C. McGuire and Stern (1993) quoted a range of 830°–980 °C based on Wells (1977) thermometry and a range of 680 °C to 885 °C based on Brey and Köhler (1990) thermometry for the lower-crustal 2-pyroxene granulite xenoliths they studied. Seven pyroxene-rich granulite xenoliths give mean T estimates of 786 ± 25 °C (Wells, 1977) and 710 ± 76 °C (Brey and Köhler 1990) whereas 11 plagioclase-rich granulites yield 857 ± 78 °C (Wells, 1977) and 776 ± 75 °C (Brey and Köhler, 1990). The higher temperatures for the plagioclase-rich group relative to the pyroxene-rich group are surprising, given the likelihood referred to above of a density-stratified lower crust and the more fractionated nature of the plagioclase-rich lower crustal suite; this apparent paradox requires further investigation.

Garnet-bearing lower-crustal xenoliths are rare and easily confused with rare upper-mantle garnet-pyroxenites, discussed in the next section. The three known garnet-bearing mafic-granulite varieties inferred to have been derived from the lower crust (McGuire and Stern, 1993) show a large compositional range. Compared to the much more abundant plagioclase-rich and pyroxene-rich lower crustal types, the garnetiferous lower-crustal xenoliths have similar mean SiO_2 and TiO_2 contents, intermediate Al_2O_3 (15%) and Na_2O contents (2.7%), and slightly lower K_2O contents (0.27%). McGuire and Stern (1993) reported Wells (1977) temperatures of 900°–1010 °C, garnet-clinopyroxene T of 930°–1100° (Ellis and Green, 1979), and P of 10–12 kbar (Wood and Banno, 1973), consistent with an origin in the lower crust. The small number of garnet-bearing xenoliths, and the large compositional variations observed, dissuade further speculation about their significance.

The mafic xenoliths considered here have textures as well as compositions consistent with a magmatic origin. Al-Mishwat and Nasir (2004) noted that granoblastic textures dominate lower-crustal xenoliths, but that relict cumulate textures, such as orthopyroxene oikocrysts enclosing plagioclase, are also common. Nasir (1995) and Al-Mishwat and Nasir (2004) concluded that the mafic xenoliths were basaltic cumulates that crystallized in the lower crust, and that the
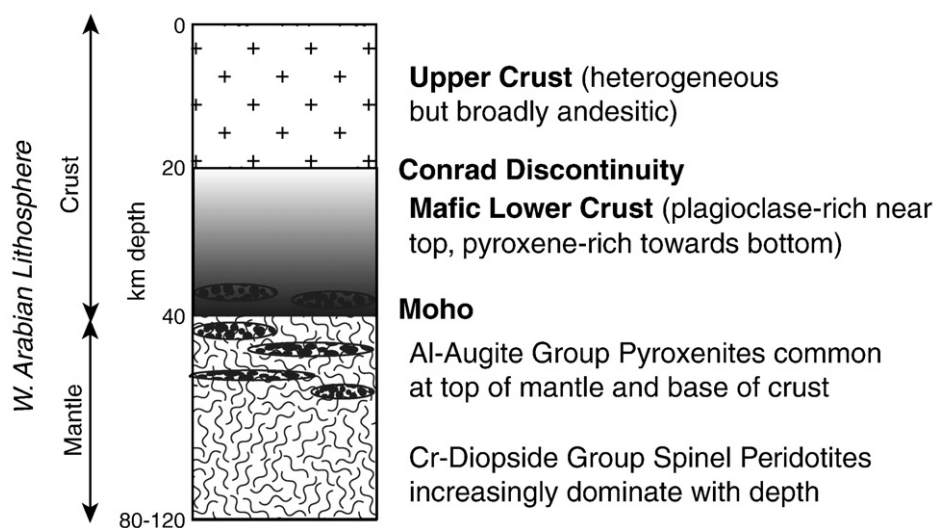

Fig. 17. Generalized lithospheric structure for W. Arabia as inferred from xenoliths recovered from Neogene harrats in the western part of the Arabian Plate (see text for discussion).

lower crust of, at least, western Arabia is made up of gabbroic intrusive complexes. Metasedimentary xenoliths are noticeably missing from the lower crustal suite, although Safarjalani et al. (2009) infer that SW Syria lower crust formed from a mixture of metamorphosed marls and within-plate basalts.

The trace-element signature of Arabian lower-crustal xenoliths (Fig. 18) reveals further details. MORB-normalized trace-element patterns for both plagioclase- and pyroxene-rich xenoliths varieties are enriched in the most incompatible elements (e.g., Rb and Ba) and are depleted in the moderately incompatible elements (Y, Yb and Lu). Positive anomalies of Ba, Sr, and Eu are observed, as well as a modest Nb depletion. A trace-element pattern of this type is commonly observed for convergent-margin magmatic suites (Stern, 2002b) in which the trace-element contents reflect enrichment in fluid-mobile elements (Rb, Ba and Sr) derived from subducted crust and sediments, coupled with an unusually high degree of mantle melting causing relatively low concentrations of high-field strength cations (HFSC) such as Nb and HREE. In comparison with a recent estimate of the bulk Earth $^{147}Sm/^{144}Nd$ value of 0.1941 ± 0.0059 (Amelin and Rotenberg, 2004), 19 Arabian lower-crustal xenoliths have a slight LREE enrichment with a mean (± 1 std. dev.) $^{147}Sm/^{144}Nd = 0.1833 \pm 0.0475$.

Isotopic compositions of Sr and Nd have been determined for 20 and 19 (respectively) mafic lower-crust xenoliths from six harrats in Saudi Arabia (Henjes-Kunst et al., 1990; McGuire and Stern, 1993) as well as for two xenoliths, uncorrected for radiogenic growth, from Yemen (Baker et al., 2002). Assuming 750 m.y. of radiogenic growth, 19 of these xenoliths have initial $^{87}Sr/^{86}Sr$ ranging from 0.70257 to 0.70332, with a mean of 0.70299 (Fig. 19A). This range matches the initial $^{87}Sr/^{86}Sr$ expected for 750 Ma depleted mantle, further confirmation that the lower crust of this region is largely a juvenile Neoproterozoic addition from the mantle. An exception is indicated by somewhat more radiogenic initial $^{87}Sr/^{86}Sr$ for one sample from each of two locations in the southern part of the Arabian Plate.
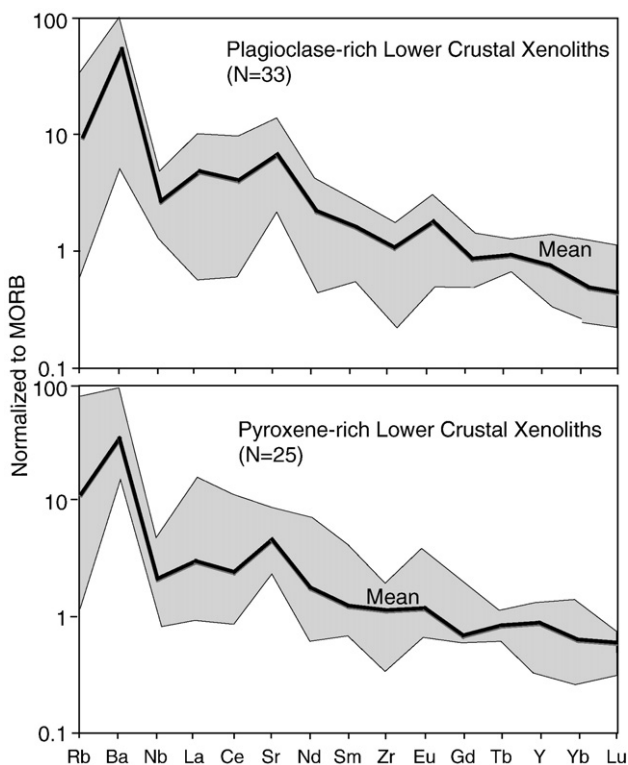

Fig. 18. Incompatible trace-element patterns for A) plagioclase-rich and B) pyroxene-rich lower-crustal xenoliths, compiled from McGuire and Stern (1993), Nasir (1995), and Al-Mishwat and Nasir (2004). More incompatible elements plot to the left, whereas more compatible elements plot to the right. Grey pattern indicates total range, solid line indicates mean. Element order and N-MORB normalization are from Hofmann (1988).
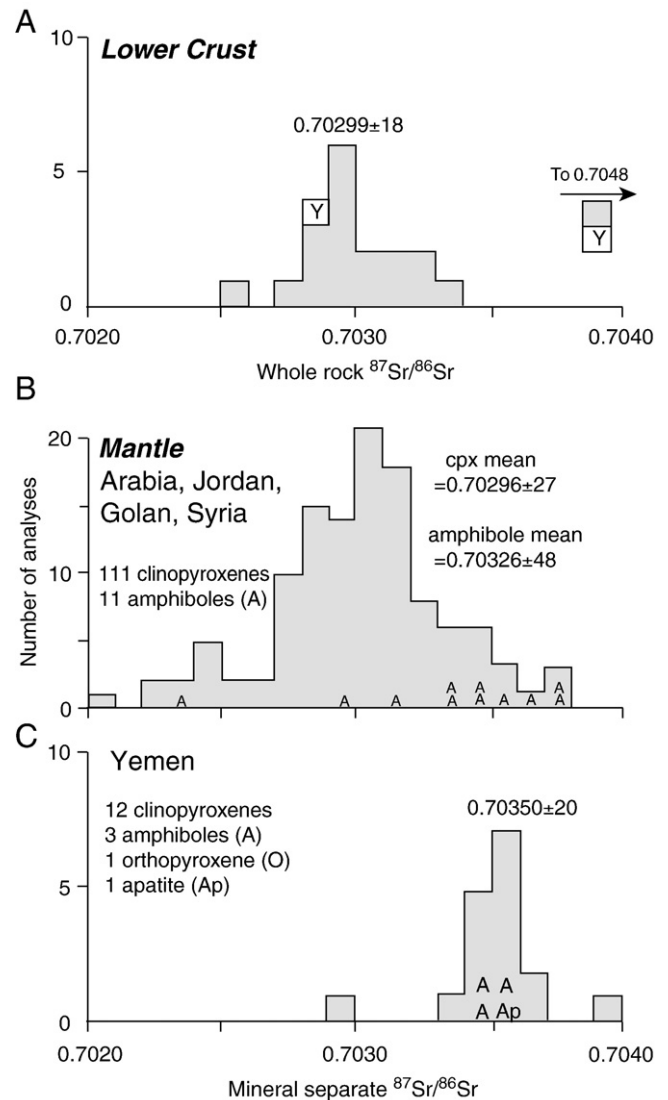

Fig. 19. Initial Sr isotopic compositions of Arabian Plate lower crust and upper mantle. Each panel reports mean and 1-standard deviation. A) 19 whole-rock samples (corrected for 750 m.y. of radiogenic growth) of Arabian lower crust (McGuire and Stern (1993) and 2 (uncorrected) whole-rock samples of Yemen lower crust (granulite, labeled "Y", from Baker et al., 2002). Mean for lower crust excludes one sample with high initial $^{87}Sr/^{86}Sr$.; B) 111 clinopyroxene (uncorrected for radiogenic growth) and 11 amphibole separates ("A"; 7 corrected and 4 uncorrected for radiogenic growth), from mantle xenoliths (Henjes-Kunst et al., 1990; Thornber 1992; Stein et al. 1993; Blusztajn et al., 1995; Shaw et al., 2007; Nasir and Rollinson, 2009). Note that the initial isotopic composition of lower crust and mantle peridotite clinopyroxene north of Yemen are both ~0.7030. C) 10 clinopyroxene, 3 amphibole, 1 orthopyroxene, and one apatite (Baker et al., 2002). Yemen upper mantle is distinctly more radiogenic than the rest of the western Arabian upper mantle, consistent with the presence of pre-Neoproterozoic crust in Yemen. See text for further discussion.

Xenolith sample # 93751-A, from Harrat Al Birk has a significantly higher initial $^{87}Sr/^{86}Sr$ of 0.70486, and a clinopyroxene separated from a lower-crustal xenolith in Oligocene–Miocene flood basalt at Bir Ali in Yemen (Baker et al., 2002) has an initial ratio of 0.70476; these results suggest that pre-Neproterozoic material may locally be preserved in the lower crust of the SW Arabian Plate. A second clinopyroxene separate from Bir Ali has a typical juvenile Neoproterozoic initial $^{87}Sr/^{86}Sr$ of 0.70285, suggesting that the lower crust from this region is heterogeneous and at least partly juvenile Neoproterozoic material. Certainly, the possibility that pre-Neoproterozoic lower crust is preserved beneath the Arabian Plate warrants further investigation.
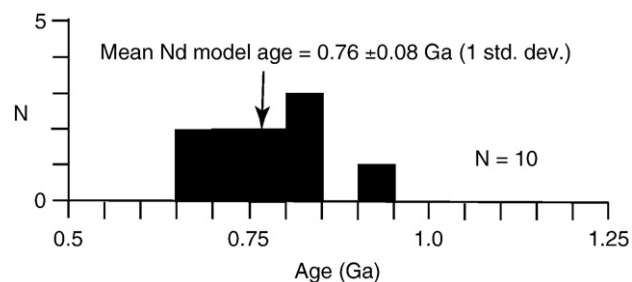
Fig 20. Nd-model ages for lower-crustal xenoliths (using Nelson and DePaolo, 1984 model for depleted mantle). Data from McGuire and Stern (1993). Only whole-rock samples with $^{147}Sm/^{144}Nd<0.17$ are plotted. Note the similarity of lower-crust model ages to crystallization ages of Arabian Shield upper crust summarized in Fig. 7.

Nd-isotopic data consistently support a juvenile origin for the lower crust, with Nd-model ages of 10 samples that have $^{147}Sm/^{144}Nd$ <0.17 clustering between 0.66 and 0.92 Ga and a mean of 0.76 ± 0.08 Ga (using the model of Nelson and DePaolo (1984) for inferring the Nd-isotopic composition of primitive mantle; Fig. 20). Correcting for radiogenic growth using an age of 750 Ma yields initial ε_{Nd} values between +1.5 and +7.3, with a mean of +5.5, consistent with that expected for depleted mantle at that time (+6.4, according to the model of Nelson and DePaolo, 1984). A plot of $^{147}Sm/^{144}Nd$ vs. $^{143}Nd/^{144}Nd$ (isochron plot) (Fig. 21) does not yield a good age, but comparison of the data with 500 Ma, 700 Ma, and 1000 Ma reference lines is consistent with formation in Neoproterozoic time, and high-lights the isotopic similarity of lower crust and lithospheric mantle. A plot of $^{87}Rb/^{86}Sr$ vs. $^{87}Sr/^{86}Sr$ does not result in any age information.

As noted above, the trace-element patterns of the plagioclase- and pyroxene-rich lower-crustal xenoliths share the characteristic features of arc magmas. This is strong evidence that the Arabian lower continental crust formed from ponding and/or fractionation of arc-related magmas. This conclusion contrasts somewhat with inferences

from global xenolith compositions, which indicate that about one third of post-Archean lower continental crust is composed of mafic rocks from mantle-plume sources (accreted oceanic plateaus or mafic underplating) with only some two thirds from arc sources (Condie, 1999). A genetic link between subduction-related igneous activity and lower crust formation in the Arabian Plate is consistent with what is known about the convergent-margin, terrane-accretion, magmatic–tectonic origin of the upper crust. Such a link implies, moreover, that the lower crust originated prior to the cessation of subduction-related igneous activity in the upper crust of the ANS at about 630 Ma. However, whether there is a temporal relationship between lower-crust formation and terrane-accretion events cannot yet be demon-strated. Age information for Arabian Shield lower crust is complicated by steep thermal gradients that existed in the region at ~600 Ma. Such gradients are estimated at ~30 to 50 °C/km (Abd-El-Naby et al., 2008; Abu-El-Enen, 2008; Reymer et al., 1984), and imply temperatures >600–1000 °C in the lower crust. On this basis, it is conceivable that large parts of the lower crust remained very hot, perhaps partially molten, well after subduction-related magmas were emplaced, and in such a hot environment, the Sm–Nd system may have remained isotopically open until relatively late in the history of the Arabian continental crust west of CAMA.

5.2. Mantle xenoliths

Many inclusions in Cenozoic basalt erupted onto the Arabian Plate appear to sample its upper-mantle continental lithospheric "keel". These include some peridotite and pyroxene-rich xenoliths as well as megacrysts. The samples mostly come from Yemen, Saudi Arabia, Jordan, and Syria, in the western part of the Plate, but some have also been collected from Oman. No Cenozoic lava fields occur between the Arabian Shield and Oman, so there are no samples of mantle lithosphere from beneath the Platform in central Arabia.

The abundance of mantle xenoliths in the Arabian Plate provides a wealth of information about the lithospheric mantle, especially lithologic, chemical, and isotopic compositions and its P–T environment.
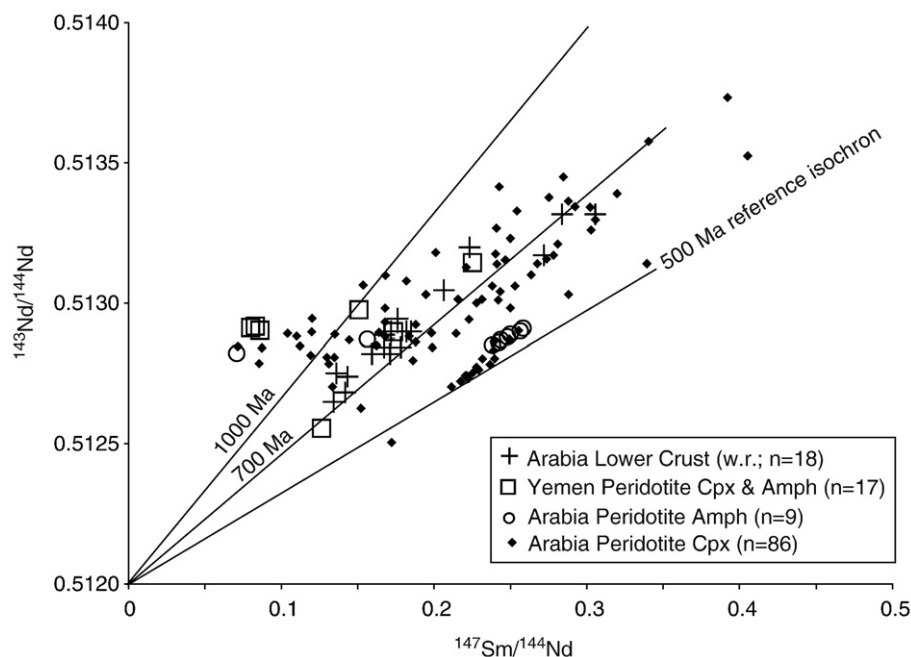

Fig. 21. A) An isochron plot for $^{147}Sm/^{144}Nd$ vs. $^{143}Nd/^{144}Nd$ for 18 whole rock mafic lower-crust xenoliths from six harrats in Saudi Arabia (Henjes-Kunst et al., 1990; McGuire and Stern, 1993) and for 71 mineral separates (mostly clinopyroxene but also including 1 apatite, 1 orthopyroxene, and 2 amphiboles from mantle xenoliths of Jordan, Golan Heights, western Arabia, and Yemen. Data scatter greatly ($r^2\sim 0.7$), forming no isochron, so no age information can be obtained. A 500 Ma reference line is shown, suggesting that isotopic closure may have been reached at the end of Neoproterozoic time. Data are from Henjes-Kunst et al. (1990), Thornber (1992), Stein et al. (1993), Baker et al. (2002), and Shaw et al. (2007).

Key studiess include Ghent et al. (1980), Kuo and Essene (1986), Nasir and Al-Fuqha (1988), McGuire (1988a), Stein and Katz (1989), Henjes-Kunst et al. (1990), Thornber (1992), Nasir (1992), Medaris and Syada (1998, 1999), Nasir and Safarjalani (2000), Kaliwoda et al. (2007), Al-Amaireh (2007), Shaw et al. (2007), Ismail et al. (2008), and Nasir and Rollinson (2009). Complementary studies of Yemen (Chazot et al., 1996, Ali and Arai, 2007, Baker et al., 2002) and Oman xenoliths (Gnos and Peters, 2003; Nasir et al., 2006; Grégoire et al., 2009) are also reported.

Arabian Plate mantle xenoliths are lithologically diverse. McGuire (1988a) described four types from Harrats Al Birk, Kishb, and Hutaymah, and Thornber (1992) identified 25 different varieties among 709 mantle xenoliths and megacrysts collected from Harrat Hutaymah (Fig. 15). However, most mantle xenoliths can be assigned to either a Cr-diopside suite or an Al-augite suite (following the major subdivisions of Wilshire and Shervais (1975)), depending on mineral compositions. The Cr-diopside suite is characterized by Mg–Cr-rich pyroxene and spinel and Mg-rich olivine. Lithologically, this suite includes peridotite (lherzolite, harzburgite, and minor dunite) with some websterite (pyroxenites composed of both orthopyroxene and clinopyroxene) and subordinate pyroxenite (McGuire, 1988a). Cr-diopside-suite samples show either igneous or porphyroclastic textures such as kink banding. The Al-augite suite comprises pyroxene-rich lithologies characterized by aluminous pyroxenes, Mg–Al-rich spinel, and a higher Fe content of all minerals relative to the Cr-diopside suite. It includes spinel websterites, garnet–spinel websterites, and garnet-bearing spinel clinopyroxenites. For simplicity, all pyroxene-rich mantle xenoliths are referred to as "pyroxenites". Composite xenoliths described by McGuire (1988a) show that Cr-diopside-group websterites and lherzolites coexist, and that Cr-diopside lherzolite was intruded by and partially equilibrated with Al-augite pyroxenite. McGuire (1988b) suggested that Cr-diopside peridotites mostly represent residues after melt extraction, whereas the Al-augite group crystallized from basaltic magma.

Using slightly different terminology, Thornber (1992) divided the Harrat Hutaymah xenolith and megacryst suite into Mg–Cr-group mantle peridotites (with minor pyroxenite, equivalent to Cr-diopside suite) and Al–Fe–Ti-group pyroxenites (equivalent to Al-augite suite). Hutaymah xenoliths are 31% spinel peridotite, 58% pyroxenite, and 9% amphibolite (which are probably samples of the lower crust); another 2% are composite xenoliths: peridotite in contact with pyroxenite or amphibolite. Hutaymah pyroxenites include all Al–Fe–Ti-group samples as well as a subordinate number of Mg–Cr-group samples. Thornber (1992) inferred from phase equilibria that the Al–Fe–Ti-group pyroxenites crystallized in the uppermost ~10 km of the mantle, and represent a crust–mantle transition zone (Fig. 17). He also noted garnet in 14 Al–Ti–Fe-group metamorphic pyroxenites but not among the Mg–Cr peridotites.

Farther north in the Arabian Plate, Al-augite-group, spinel- and garnet-bearing pyroxenites are described from the Al Ashaer volcano in Harrat Shaam, Syria (Medaris and Syada, 1999), and bombs of lherzolite and minor harzburgite, dunite, clinopyroxenite, and websterite, as much as 14 cm across, are described from pyroclastic beds around the Aritain and Jebel Hassan volcanoes in NE Jordan (Nasir and Al-Fuqha, 1988) (Fig. 15). Aritain lherzolite xenoliths have average modal abundances of 67% OL, 23% OPX, 9% CPX, and 2% SP, and are inferred to represent the uppermost mantle (Nasir and Al-Fuqha, 1988). In the Al Ashaer xenolith suite, 95% of the samples represent shallow upper-mantle material, but some 5%, comprising gabbro and diabase, represent the lower crust (Medaris and Syada, 1999). The upper-mantle xenoliths are 75% spinel + Cr-diopside-bearing peridotite and 20% Al-augite-bearing pyroxenite. In a related study, Nasir and Safarjalani (2000) divided xenoliths from Harrat Shaam (Syria) into four groups: (1) Type I Cr-diopside xenoliths with protogranular to porphyroclastic textures, including anhydrous (IA) and hydrous (IB) subtypes; (2) Type II Al-augite, spinel and garnet pyroxenite and websterite with igneous and/or porphyroclastic textures and abundant phlogopite and/or amphibole; (3) Type III Cr-poor megacrysts; and (4) Type IV mafic lower crust. Type IA xenoliths have low REE concentrations (La/Yb = 1–2 and Sm = 0.7–1.1 × chondrite), whereas Type IB xenoliths are LREE enriched (La/Yb = 6–9 and Sm = 1.1–1.3 × chondrite). Type II xenoliths have higher overall LREE enrichment. Similar observations and conclusions were recently reported by Nasir and Rollinson (2009) for mantle xenoliths from Harrat Shaam, Syria.

Oman mantle xenoliths come from small mafic plugs and dikes that have K–Ar ages of 37 to 44 Ma and intrude sedimentary rocks as young as Paleocene. The 14 studied xenoliths comprise 14 spinel lherzolites, 6 spinel harzburgites, 4 dunites, and 4 wehrlites (Gnos and Peters, 2003; Grégoire et al., 2009; Nasir et al., 2006) and are all Cr-diopside-group ultramafics. Al-augite-group ultramafics are absent which, if indicative of the eastern Arabian lithosphere, suggests a significant difference with the lithosphere in the west that contains abundant Al-augite pyroxene-rich rocks. Grégoire et al. (2009) suggest that the Oman mantle xenoliths formed by two processes; (1) relatively old (early Neoproterozoic?) ~1 to 13% partial melting, followed by (2) Cenozoic metasomatism perhaps related to interaction with host basanites.

Chemical information about Arabian Plate mantle xenoliths is summarized in Table 3 as means of major elements, mineral compositions, and mineral modes (Sources: Ghent et al., 1980; Kuo and Essene, 1986; Nasir and Al-Fuqha, 1988; McGuire, 1988a,b; Stein

Table 3

Major oxide contents, and mineral and modal data for mantle xenoliths from western Arabia.

	Peridote[a]		"Pyroxenite"[b]		Ave. W. Arab.	Primitive
	Mean	1 SD	Mean	1 SD	Upper Mantle	mantle
SiO$_2$	44.13	1.66	46.95	4.07	45.34	46
TiO$_2$	0.14	0.18	0.86	0.89	0.45	0.18
Al$_2$O$_3$	2.02	1.15	9.52	3.92	5.23	4.06
Feo*	8.63	0.73	8.95	2.97	8.77	7.54
MnO	0.15	0.07	0.17	0.05	0.16	
MgO	42.23	4.46	19.75	6.36	32.61	37.8
CaO	2.21	2.09	12.61	4.06	6.66	3.23
Na$_2$O	0.26	0.24	0.97	0.4	0.56	0.33
K$_2$O	0.10	0.05	0.18	0.47	0.14	0.03
P$_2$O$_5$	0.05	0.03	0.05	0.03	0.05	
Mg#	88.8	5.8	78.8	7.3	86.70	89.7
Ni(ppm)	2111	522	724	1912	1517.36	2080
Cr(ppm)	2792	915	827	1761	1950.98	
Mode %						
OL	69.4	10.8	24.1	27.4	49.99	
CPX	7.5	5.6	57.8	21.9	29.01	
OPX	15.1	8.36	8.9	8.2	12.44	
SP	2.2	2.8	5.5	6.8	3.60	
AMPH	4.1	1.98	0.3	0.75	2.46	
PHL	1.6	2.2	1.4	2.7	1.52	
GA	0.0	0	2.2	6.6	0.94	
Mineral compositions						
OL	90.1	0.89	83.4	4.5		
OPX EN	90.3	1.2	82	5.6		
CPX WO	46.1	1.8	44.6	2.7		
CPX EN	49.2	1.4	50.6	13.5		
CPX FS	4.6	1.3	10.3	3.9		
SP Or#	23	14.7	12.2	16.5		
AMPH Mg#	83.8	13.9	77.2	10.7		
PHL Mg#			84.7	4.7		
GA Ca			14.5	53.2		
GA Mg			53.2	3.4		
GA Fe			32.3	3.4		

Average W. Arabian upper mantle is weighted (by sample %) average of peridotite and "pyroxenite".
Primitive mantle from Hofmann (1988).
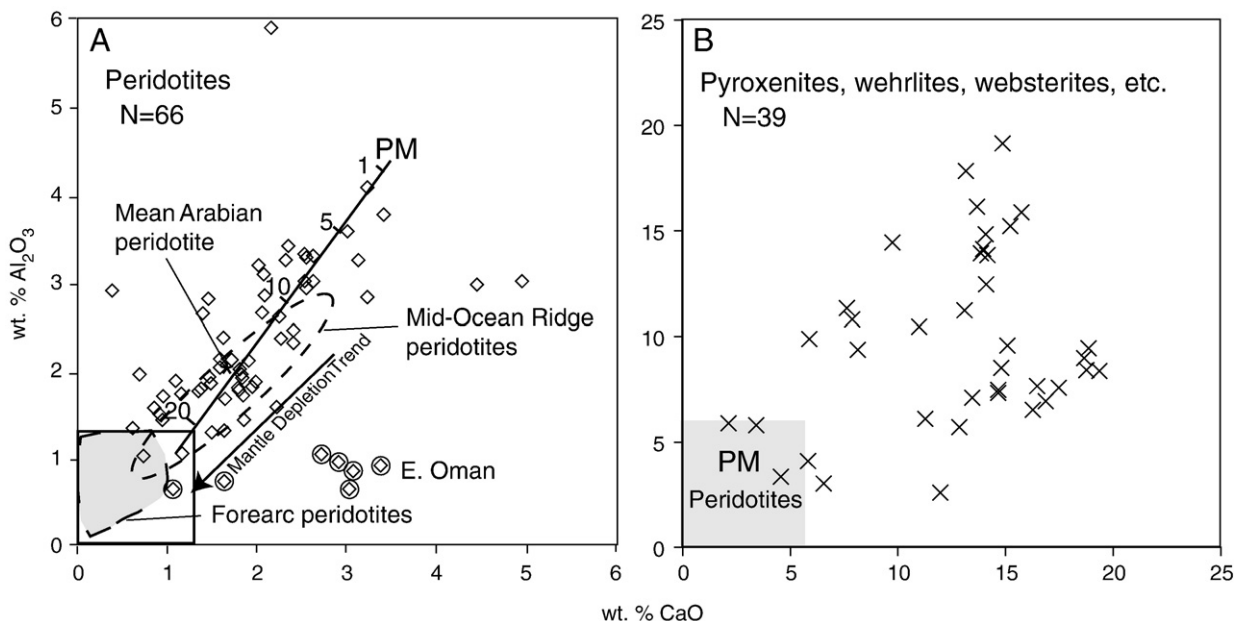
[a] 147 total samples.
[b] 110 total samples.

Fig. 22. CaO–Al₂O₃ plot for Arabian mantle xenoliths (after Ishiwatari, 1985) showing the composition of A) spinel peridotites, and B) pyroxene-rich mantle xenoliths such as pyroxenites, wehrlites, and websterites. Grey area in B outlines relative position of A. A) CaO–Al₂O₃ plot for 66 spinel peridotite xenoliths. PM = composition of primitive (undepleted) mantle (McDonough and Sun, 1995). Seven circled diamonds are xenoliths from eastern Oman (Nasir et al., 2006), other peridotites are from three W. Arabia harrats: 35 from Harrat Shaam (Al-Amaireh, 2007; Medaris and Syada, 1998; Nasir and Al-Fuqha, 1988; Nasir and Safarjalani, 2000); 23 from Harrat Hutaymah (Thornber, 1992), and one from Harrat Kishb (Kuo and Essene, 1986). Compositional fields for forearc peridotites and mid-ocean ridge peridotites are from Azer and Stern (2007). Also shown is a melting-depletion trajectory, showing expected CaO and Al₂O₃ contents for residual peridotites after 1%, 5%, 10% and 20% melting to generate basalt; composition of the "Mean Arabian Peridotite" corresponds to ~15% melt depletion. B) CaO–Al₂O₃ plot for 39 pyroxene-rich xenoliths, including 7 from Harrat Shaam (Nasir and Safarjalani, 2000) and 32 from Harrat Hutaymah (Thornber, 1992). Note strong enrichment of "pyroxenites" in CaO and Al₂O₃ contents.

and Katz, 1989; Henjes-Kunst et al., 1990; Thornber, 1992; Nasir, 1992; Medaris and Syada 1998, 1999; Nasir and Safarjalani, 2000; Kaliwoda et al., 2007; Al-Amaireh, 2007; Shaw et al., 2007; Ismail et al., 2008). The peridotites are relatively homogeneous, consisting of ~70% olivine (Fo₉₀), ~15% orthopyroxene (En₉₀), ~7% diopsidic clinopyroxene, 4% amphibole and ~2% spinel with relatively low Cr# (=100Cr/Cr + Al)~23. Note that the group "Pyroxenite" in Table 3 is very heterogeneous, including clinopyroxenites, amphibole-pyroxenites, garnet-pyroxenites, wehrlites, and websterites, as well as megacrysts of clinopyroxene and hornblende.

Data for 66 peridotite and 39 pyroxenite xenoliths are summarized on CaO–Al₂O₃ diagrams in Fig. 22 showing comparisons between Arabian Plate mantle xenoliths, primitive undepleted mantle, and present-day mid-ocean ridge peridotites. Because CaO and Al₂O₃ are removed when peridotite partially melts and are not added during metasomatism, these oxides are very useful for monitoring melt depletion. As noted in Table 3, the mean Arabian peridotite contains about 2% of each oxide. This corresponds to ~15% melt depletion, which is in the range found for peridotites from modern mid-ocean ridges but significantly less than that found for peridotites from beneath modern forearcs. The pyroxenites are greatly enriched in these oxides compared to the peridotites, containing 10–20% of each. Further insight into the depletion experienced by Arabian peridotites is given by plotting spinel Cr# (=100*Cr/(Cr + Al)against olivine compositions for Arabian mantle-peridotite mineral pairs overlain on an olivine–spinel-mantle array and fields for mid-ocean ridge and forearcs peridotites (Fig. 23). The mean Arabian peridotite xenolith has Fo₉₀ olivine and spinel with Cr# = 20, which indicates modest depletion (Stein and Katz, 1989).

Mantle pyroxenites are commonly explained as products of crystal accumulation of mantle-derived magmas, together with variable amounts of trapped interstitial magma. Others may be the products of interactions between magma and peridotite or older pyroxenite wall-rocks (Downes, 2007). Mafic melts have been common twice in the history of western Arabia: during the Neoproterozoic when the crust formed and in the Neogene when the harrats erupted. McGuire

(1988) noted that recrystallization textures in the Saudi Arabian Al-augite-group xenoliths make it very unlikely that these formed by magmatic fractionation of Cenozoic harrat-like melts, implying that Al-augite pyroxenites formed in Neoproterozoic time. In contrast, Medaris and Syada (1999) concluded that pyroxenite xenoliths from Harrat Al Ashaer, Syria formed by a high-pressure crystal accumulation
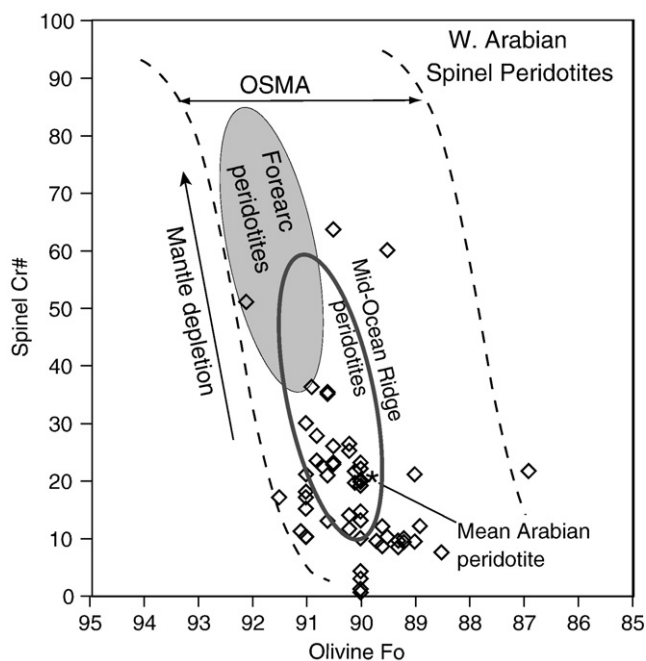

Fig. 23. Relations between forsterite (Fo) contents of olivine and spinel Cr# (=100Cr/Cr + Al) compositions of Arabian spinel–peridotite mantle xenoliths. Field for Olivine–Spinel Mantle Array (OSMA) after Arai (1994); fields for forearc and abyssal peridotites are from Peslier et al. (2002).

from alkali basalt melts, and Thornber (1992) inferred that Al–Ti–Fe-group xenoliths were cumulates related to Neogene alkaline host lavas. Clearly, more work is needed to resolve this controversy.

A different significance was given by Thornber (1992) to the Mg–Cr-spinel peridotites, which were thought to record a "possibly Protero-zoic" (p. 85) process involving melting, internal mobilization and recrystallization of protolith mantle associated with Neoproterozoic crust formation. A depth interval of ~35 km to ~70 km was inferred for the spinel peridotites, suggesting that the mantle lithosphere beneath Harrat Hutaymah is vertically zoned, with Al–Ti–Cr pyroxenites concentrated near the base of the crust and the proportion of spinel-peridotite increasing downward (Fig. 16). Such a gradation calls into question the usefullness of distinguishing between pyroxene-rich xenoliths from the lower crust (e.g. "pyroxene-rich" lower-crustal xenoliths of Al-Mishwat and Nasir (2004)) and upper-mantle pyrox-enites on the basis of whether or not the xenoliths contains plagioclase. In reality, there is likely to be a continuum of pyroxene-rich rocks above and below the western Arabian Moho, with some plagioclase-bearing bodies lying below the Moho and some true pyroxenites, websterites, and wehrlites present in the lower crust. Such an interpretation is consistent with the fact that mantle pyroxenite in Table 3 has much higher Mg# (79 ± 7), Ni (724 ± 1912 ppm) and Cr (827 ± 1761 ppm) contents than do pyroxene-rich lower-crustal xenoliths (Table 2: Mg# = 67 ± 5, 169 ± 64 ppm Ni, and 435 ± 214 ppm Cr). A compositional gradation is consistent, moreover, with the geophysical evidence described in previous sections for a crust–mantle transition zone, a few km thick, beneath western Arabia.

P–T studies indicate that Arabian Plate mantle xenoliths originated near or below the Moho in a temperature range of 800–1050 °C and a large pressure range of 10–33 kbar (1–3.3 GPa). These estimates are based on the pyroxene geothermometers of Wells (1977) and Brey and Köhler (1990), and limited pressure estimates from the methods of Brey and Köhler (1990) and Nickel and Green (1985). Peridotite from Harrat Kishb, for example, re-equilibrated at $T > 1050$ °C and reached a lower limit of around 800 °C (Kuo and Essene, 1986) and Harrat Uwayrid xenoliths equilibrated between 800° and 1100 °C (Kaliwoda et al., 2007). Other studies give temperature ranges for peridotite of 920–1050 °C, with a mean of 994 ± 38 °C (Wells, 1977 method) and 900–1142 °C, with a mean of 1011 ± 67 °C (Brey & Köhler, 1990 method) (Ghent et al., 1980, McGuire, 1988a,b; Stein and Katz, 1989; Nasir, 1992; Medaris and Syada, 1998; Medaris and Syada, 1999; Ismail et al., 2008). Pyroxenite samples show indistinguishable *T* ranges (905–1070 °C, with a mean of 1002 ± 40 °C (Wells, 1977 method); 922–1100 °C with a mean of 1030 ± 63 °C (Brey & Köhler, 1990 method) (Ghent et al., 1980; McGuire, 1988a,b; Nasir, 1992, Medaris and Syada, 1998, Medaris and Syada, 1999, Ismail et al., 2008). These temperature estimates overlap each other and are slightly higher than those for 7 Oman xenoliths studied by Nasir et al. (2006), which yield mean temperature estimates of 970 ± 31 °C and 964 ± 33 °C by the Wells (1977) and Brey and Köhler (1990) methods, respectively.

Many fewer pressure estimates have been made than temperature estimates, because the geobarometric techniques are not generally considered to be reliable for spinel peridotites. Nasir (1992) estimated *P* of 1.32 to 1.52 GPa (~40–50 km depth) for 5 mantle peridotites, using the technique of Köhler and Brey (1990). Kaliwoda et al., (2007) estimated pressures for Harrat Uwayrid spinel peridotites using two approaches. One was based on temperatures estimated by the Brey & Köhler (1990) method in conjunction with maximum pressure estimates based on spinel compositions using the method of Webb and Wood (1986). This gave maximum pressure estimates of 1.5 to 3.3 GPa (~50–100 km depth). The second approach used the two-pyroxene thermometer of Brey and Köhler (1990) and estimated *P* at 10.5 and 16.1 kbar (1.05–1.61 GPa) (~35–53 km depth) with means between 13.7 ± 2.4 kbar (1.37 GPa) and 11.9 ± 1.0 kbar (1.19 GPa), based on the exchange of Ca between diopside and olivine (Köhler and Brey, 1990).

These pressure estimates differ in detail but nevertheless corre-spond to depths near the Moho, strengthening the inference made independently above, that pyroxene-rich lithologies are abundant in the 35–50 km depth range and define a broad crust–mantle transition zone. We note, however, that calculated temperatures for Arabian peridotites and pyroxenites are indistinguishable, suggesting they come from similar mantle depths, and these temperatures are significantly higher than the ~750°–850 °C estimated for lower-crustal xenoliths. It should also be noted that the *P–T* relationship for the Harrat Uwayrid xenoliths (Kaliwoda et al., 2007) is consistent with a conductive heatflow of 80–100 mW/m², much higher than the measured heatflow of ~60 mW/m² discussed earlier. It is controver-sial, however, whether the Uwayrid xenoliths record an ancient (Neoproterozoic) thermal structure or one that has been affected by the Afar plume.

As discussed above, the radiogenic–isotopic compositions of lower-crustal xenoliths and exposed upper crust imply that the lower crust is mostly juvenile Neoproterozoic material and suggests an intimate co-genetic relationship between upper and lower crust. This conclusion also appears to be true for the lithospheric mantle. Lower-crust and mantle lithosphere beneath western Arabia have almost identical initial $^{87}Sr/^{86}Sr$ means and similar ranges (0.7025–0.7035; Fig. 19A,B). The same range is known for most of the juvenile Neoproterozoic upper crust of the Arabian–Nubian Shield (Stern and Abdelsalam, 1998; Stoeser and Frost, 2006), implying that the mantle lithosphere is also juvenile and dates from the Neoproterozoic, further suggesting that the upper crust, lower crust, and mantle are all genetically related. Mantle xenoliths from Yemen, in contrast, are significantly more radiogenic (Fig. 19C), perhaps because the underlying upper mantle contains older, more evolved material complementary to Archean and Paleoproterozoic upper crust there (Whitehouse et al., 2001b), as commented above. Alternatively, the isotopic distinction may reflect modification of Yemen mantle lithosphere by the Afar "mantle plume" (Baker et al. 2002).

A Neoproterozoic age of formation of the lithospheric mantle is supported by Sm–Nd isotopic data for western Arabian Plate mantle xenoliths, but this age is not well-defined. Clinopyroxenes separated from peridotite xenoliths from Harrats Uwayrid, Huataymah, Al Kishb, Lunayyir, and Jizan area (Saudi Arabia), As Shamah (Jordan) (Henjes-Kunst et al., 1990; Nasir and Rollinson, 2009), and Harrat Hutaymah (Thornber, 1992) yield ~700 Ma age. A study by Baker et al. (2002) using their own data combined with that of Henjes-Kunst et al. (1990) and Blusztajn et al. (1995), together with data from Brueckner et al. (1988) for Zabargad Island samples, obtained an age of ~675–700 Ma. Zabargad Island in the Red Sea lies west of the Arabian Plate but is part of the Nubian Shield that prior to Red Sea rifting was contiguous with the Arabian Shield. It is significant therefore that Zabargad peridotite alone yields a poorly-defined Sm–Nd "age" of ~675 Ma (Lancelot and Bosch, 1991) consistent with the Arabian Plate data. Furthermore, Sm–Nd model ages and whole-rock errorchrons indicate that spinel lherzolite and upper-crustal gneisses on the island differentiated from a common depleted-mantle source about 700 Ma (Brueckner et al., 1988). Clinopyroxene separates from Jordan give a slightly younger age of ~600 Ma (Shaw et al., 2007), although Nasir and Rollinson (2009) report ages of ~730 Ma for clinopyroxene from two harzburgites, and ~450–500 Ma for lherzolite clinopyroxene and amphibole from Jordan xenoliths. A considerably younger age of ~430 Ma was obtained by Blusztajn et al. (1995), who combined data from xenolithic clinopyroxenes from Kishb, Uwayrid, Al Birk, Ithnayn, and Hutaymah together with data from Henjes-Kunst et al. (1990). Initial ε_{Nd} are uniformly positive, consistent with a juvenile Neopro-terozoic upper mantle. They include ε_{Nd} values of ~+5.8 ± 1.7 and ~+8.7 for clinopyroxene separates from Saudi Arabia (Henjes-Kunst et al., 1990; Blusztajn et al., 1995), with significantly lower ε_{Nd} of +0.6 and +1.8 for Syrian peridotite clinopyroxenes (Nasir and Rollinson, 2009). Zabargad Island peridotite has an initial ε_{Nd} of ~+6.7 (Lancelot

and Bosch, 1991). In summary, the Sr, Sm, and Nd isotopic data are clearly compatible with the interpretation that the mantle lithosphere sampled by xenoliths from the western part of the Arabian Plate was produced during the Neoproterozoic, about the same time as the upper and lower crust of the Arabian Shield.

Recent Hf isotopic studies on Arabian Plate mantle xenoliths suggest complications to this simple scenario, however, because the ε_{Hf} values are extremely high (0.6 to 165) — in fact, some of the highest ever recorded in mantle samples — and Hf isotopes appear to be decoupled from Nd isotopes in some samples (Shaw et al., 2007). The correlations that exist between Sr, Nd, and Pb isotopic compositions, LILE–LREE enrichments, and HFSE depletions suggest that the samples experienced carbonate-rich metasomatism during Neoproterozoic time. However, Hf isotopic compositions of mantle clinopyroxenes were not affected by metasomatism, and even some strongly metasomatized lithologies record ancient (>1.2 Ga) pre-metasomatic Lu–Hf signatures indicative of a depleted upper mantle that evolved to yield Arabian lithospheric mantle. The Lu–Hf data of Jordanian peridotite clinopyroxenes analyzed by Shaw et al. (2007) yield an errorchron age of ~1.4 Ga, significantly older than Sm–Nd ages discussed above. This age is strongly controlled by 3 high Lu/Hf samples, the other 15 samples defining a lower slope, better approximated by a younger age. Nevertheless, Shaw et al. (2007) concluded that the Lu–Hf isotopic system resisted overprinting by later metasomatic events, resulting in extremely heterogeneous Hf isotopic signatures that are decoupled from other isotopic systems. Shaw et al. (2007) inferred from the Lu–Hf isotopic data that a proto-Arabian lithospheric mantle underwent a major melting event in early Proterozoic–late Archean times (prior to 1.2 Ga), and was subsequently affected by Neoproterozoic metasomatism during the period of upper-crustal island-arc volcanism that led to the formation of the Arabian Shield. Alternatively, the lithosphere of Arabia north of the exposed Shield may contain significant tracts of pre-Neoproterozoic crust, similar to the recent recognition that ~1.1 Ga crust may underlie northern Sinai (Be'eri-Shlevin et al., 2009a).

One final insight into Arabian plate lithospheric evolution is provided by small segregations of quenched melt that are common in Arabian mantle xenoliths. Glass pockets, glass veinlets along grain boundaries, and glass infills along cracks are found in mantle xenoliths from Yemen, Syria, and Saudi Arabia. These have a distinctive chemical signature. Glass samples from Harrat Kishb, Saudi Arabia, and Tel Tanoun, Syria (Kuo and Essene, 1986; Ismail et al., 2008) have high contents of SiO_2 (54.6–62.8 wt.%), Na_2O (4.8–14.9 wt.%), and Al_2O_3 (20.0–25.4 wt.%), whereas TiO_2 (0.05–0.85%), total FeO (0.59–3.3%), and MgO (2.2–3.1%) contents are low, and K_2O contents range from 0.79 to 1.14%. These compositions are broadly andesitic, but the Na/K is unusually high, reminiscent of the ratio found in adakite. Kuo and Essene (1986) concluded that the glass was generated by partial melting in the upper mantle at temperatures >~1000 °C, followed by crystallization of ~10% diopside at lower temperatures. Ismail et al. (2008) inferred that the glass was mostly due to melting of pre-existing amphibole triggered by infiltration of a Na-rich metasomatic fluid, although glass was also observed in amphibole-free harzburgite.

Glass inclusions from peridotite xenoliths in Yemen, in contrast, have a wider chemical composition (Chazot et al., 1996) with 48.9 to 67.3% SiO_2, 5.9–6.1% Na_2O, 16–22.6% Al_2O_3, 1.28–4.28% MgO, and 0.55–2.23% K_2O. The Yemen glass composition furthermore is similar to that of the surrounding residual phases. For these samples, Chazot et al. (1996) inferred two origins: 1) glass rich in Na, P, and Cl was produced by extensive melting of amphiboles; and 2) high-silica glass was produced by small degrees of incongruent melting of pyroxene. It is notable however, that the Yemen glass samples have a very high Sr/Y (mean = 144 ± 122) and $(La/Yb)_N$ (mean = 122 ± 170). Such ratios are characteristic of adakite (Drummond and Defant, 1990), in which regard the glasses from Yemen, Saudi Arabia, and Syria are similar.

The age of the melt pockets is not known. The presence of glass itself suggests that the pockets formed recently, perhaps just prior to entrainment and eruption in Neogene time. However, the glass pockets are completely different in composition from the host basanites, and it is extremely unlikely that the Neogene basanites that transported the xenoliths to the surface were trapped to form the glass inclusions (Chazot et al., 1996; Ismail et al., 2008; Kuo and Essene, 1986; Thornber, 1992). The finding that some of the glasses are adakitic suggests melting of a young, hot subducted slab, and the last time that any subduction zones dipped beneath the Arabian Peninsula was during the Neoproterozoic, other than a possible and somewhat distant south-dipping subduction from Paleo-Tethys along the northeastern flank of Gondwana (present day coordinates) during the Permian onset of separation of the Cimmerian terranes from the Arabian part of Gondwana (Sharland et al., 2001; Stampfli et al., 2006). Clearly, the origin of these glass inclusions warrants further investigation.

6. An important role for delamination in the evolution of the Arabian Plate?

The forgoing sections reveal the important lateral and vertical heterogeneities that have been documented and inferred for the continental lithosphere of the Arabian Plate, but much remains to be determined about how these differences came to be. Crust beneath western Arabia (Arabian Shield) and eastern Arabia (Arabian Platform) are distinct; although both are largely Neoproterozoic constructions: Platform crust stabilized ~700 Ma whereas Shield crust stabilized ~150 m.y. later. These two realms are separated by an important lithospheric suture, the Central Arabian Magnetic Anomaly (CAMA). CAMA separates thinner (<100 km) lithosphere in the west from thicker (~150 km) lithosphere beneath the Platform. In spite of the fact that many workers infer that Arabian Shield uplift and thinner lithosphere reflect Cenozoic processes related to the Afar mantle plume and/or Red Sea opening, the different lithospheric structures (preferred structure shown in Fig. 8C) seem to have been established in latest Neoproterozic time. This conclusion is based not only on the observation that a well-defined Neoproterozoic suture (marked by CAMA) separates the two lithospheric tracts but also because the Shield area has been high-standing all through Phanerozoic time whereas the Platform has been subsided greatly over this time.

Given our strong conclusion that the lithospheric mantle beneath western Arabia is thinner than that beneath eastern Arabia and that this difference reflects Neoproterozoic processes, what may have been the cause? We propose that loss of lithospheric mantle beneath western Arabia is the best explanation. This is sometimes refered to as "delamination" and can involve lower crust as well as lithospheric mantle (Kay and Kay, 1993); in addition to loss of entire slabs of lithospheric mantle, it is thought that warm lithosphere can be lost as "drips", effectively Rayleigh-Taylor instabilities of dense lithosphere (Gögüs and Pysklywec, 2008). Such a process was first suggested for the Neoproterozoic evolution of the region by Black and Liégeois (1993) for N. Africa between Algeria and Hoggar, a region referred to as the Saharan metacraton by Abdelsalam et al. (2002). The concept has recently been applied to the ANS by Avigad and Gvirtzman, (2009).

Avigad and Gvirtzman (2009) noted that rapid and extensive erosional denudation, widespread late-orogenic calc-alkaline and alkaline igneous activity and formation of extensional grabens affected the region ~630–590 Ma. They inferred these processes reflected regional uplift due to a substantial loss of mantle lithosphere from beneath the ANS as a result of late Neoproterozoic orogenic events. The mantle lithosphere was replaced by asthenosphere, which increased the buoyancy of the region, resulting in rapid uplift of the northern ANS to elevations of more than 3 km, followed by rapid erosion and extension. Such delamination may have been restricted to

the Shield because the suture represented by CAMA isolated the sub-Platform lithosphere and kept delamination from propagating to the lihospheric mantle beneath that region. We find this hypothesis to be particularly attractive because it also helps to explain why western Arabian mantle xenoliths are not very depleted. Mantle peridotites associated with modern intra-oceanic arcs — which was the principal process responsible for forming ANS upper- and lower-continental crust — often record extreme depletion because hydrous melting leads to more extensive melting than in other tectonic environments. ANS mantle peridotite xenoliths show only modest depletion, much less than expected for forearc peridotites (Figs. 22 and 23), although strongly depleted arc-like peridotites are found in association with ~750 Ma ANS ophiolites (Azer and Stern, 2007). Loss of highly-depleted lithospheric mantle by delamination or dripping and replacement by asthenospheric mantle (which subsequently cooled to make new lithosphere) is an attractive way to reconcile this paradox. Such an interpretation also helps explain why the lithosphere is relatively thin beneath the ANS. Certainly the general idea that the lithospheric structure varies beneath the Arabian Plate and that differences are particularly marked across the region delineated by the CAMA warrants further investigation.

7. Conclusions

The Arabian Plate represents an excellent example of continental crust and lithosphere formation by plate-tectonic processes. Our effort to synthesize and integrate multiple lines of geoscientific evidence about the nature and evolution of the continental Arabian Plate yields important new insights. Fifteen important points are identified on the basis of our review: 1) Arabian Plate continental crust mostly formed in Neoproterozoic time, with minor relicts of Paleoproterozoic and Archean crust in the southwestern part of the Plate; 2) Most upper crust of the Shield formed by magmatic additions at intraoceanic arcs above several subduction zones, which were active 870–630 Ma and which coalesced to form the Shield as a result of multiple collisions; 3) Post-tectonic (630–570 Ma) granitic and volcanic rocks were subordinate but important contributions to W. Arabian crustal growth; 4) Crust of E. Arabia stabilized considerably earlier (~700 Ma) than that of W. Arabia (~570 Ma); 5) A major, N–S suture of Late Neoproterozoic age is recognized as a strong magnetic anomaly (Central Arabia Magnetic Anomaly, CAMA) between E and W Arabia. CAMA can be traced north to the Arabia–Eurasian collision zone but is lost in the south; 6) Eastern and western Arabia exhibit different subsidence histories, reflecting long-lived differences in lithospheric buoyancy: thinner and more buoyant beneath the Shield; thicker and denser beneath the Platform; 7) A range of geophysical studies indicates that the crust beneath W. Arabia is ~40 km thick, with a well-defined Conrad Discontinuity separating high-velocity lower crust from lower-velocity upper crust. Similar crust appears to characterize all of the Plate west of CAMA, although the crust may thin noticeably to the north; 8) Sparse geophysical studies of crust east of CAMA suggests more complex structure and slightly thicker and more felsic crust; 9) Xenoliths brought to the surface by young basaltic eruptions confirm that the lower crust beneath W. Arabia is mafic and magmatic in origin, with subequal proportions of plagioclase-rich and pyroxene-rich varieties and rare garnet-bearing samples; 10) Lower-crust xenoliths have trace element patterns consistent with the formation of parent magmas above a subduction zone, similar to inferences for the formation of upper crust exposed in the Shield; 11) Isotopic compositions indicate the lower crust is overwhelmingly composed of juvenile additions from the mantle, with Nd model ages that approximate the age of Shield crust; 12) Mantle xenoliths are composed of subequal proportions of spinel peridotite and pyroxene-rich lithologies; 13) The crust mantle boundary (Moho) is probably a broad transition zone, marked by a thick zone of abundant pyroxene-rich lithologies in both the lower crust and upper mantle; 14) Mantle peridotites show modest depletion, much less than might be expected if Arabian crust was extracted from it; and 15) There is strong evidence in the Shield uplift history and lithospheric structure that the W. Arabian Plate experienced substantial lithospheric foundering at the end of Neoproterozoic time.

Our overall understanding of Arabian Plate continental lithosphere has been advancing rapidly over the last 3 decades, but our knowledge of the Plate is heavily weighted towards what we know about the Arabian Shield and its substrate. Our review demonstrates that the crust and mantle lithosphere of the Arabian Platform behaved differently from that beneath the Shield, implying distinct compositions and histories. Our overview also shows that there is insufficient data about Arabian Plate continental lithosphere in the north and northeast (beneath N. Jordan, Syria, S. Turkey, Iraq, Kuwait, the UAE, S. Iran, and the Gulf) to make meaningful conclusions. Concerted, ambitious geoscientific efforts will be needed to fill these gaps in our understanding. We think the following three-stage effort is needed. First, existing potential field data (gravity and magnetics) should be compiled for the entire Plate and interpreted. Where data gaps appear, new surveys should be undertaken to fill these. Second, new field geophysical studies are needed, especially active source seismic-reflection and refraction and heat flow studies. These studies should be designed to image the Plate's crust and lithospheric structure. Two trans-Arabian profiles would be an ideal start, one oriented E–W, from the Red Sea to Oman, the other N–S, from Yemen to Iraq, using modern geophysical techniques to image Arabian Plate crust and lithosphere structure. Third, one or more deep scientific drill holes should be undertaken to sample and study the upper crust of the Arabian Plate away from the Shield, the data, samples, and results of which would be freely available to the geoscientific community.

References

Abd-El-Naby, H., Frisch, W., Siebel, W., 2008. Tectono-metamorphic evolution of the Wadi Hafafit Culmination (central Eastern Desert, Egypt). Implication for Neoproterozoic core complex exhumation in NE Africa. Geologica Acta 6 (4), 293–312.

Abdelsalam, A.G., Liégeois, J.-P., Stern, R.J., 2002. The Saharan metacraton. J. Afr. Earth Sci. 34, 119–136.

Abu-El-Enen, M.M., 2008. Geochemistry and metamorphism of the Pan-African back-arc Mahlaq volcano-sedimentary Neoproterozoic association, W. Kid area, SE Sinai, Egypt. J. Afr. Earth Sci. 51, 189–206.

Al-Amaireh, M., 2007. Petrology, geochemistry and magnetization of Remah volcano, North Eastern Jordan. Am. J. Appl. Sci. 4, 444–448.

Al-Amri, A., Hansen, Nyblade, A., Park, Y., Tkalcic, H., 2008. Structure of the lithosphere and upper mantle across the Arabian Peninsula, Eos. Trans. AGU T23D–03 abstract.

Al-Amri, A.M.S., 1999. The crust and upper-mantle structure of the interior Arabian platform. Geophys. J. Int. 136, 421–430.

Al-Aswad, A.A., 1997. Stratigraphy, sedimentary environment and depositional evolution of the Khuff Formation in south-central Saudi–Arabia Saudi. J. Petrol. Geol. 20 (3), 307–326.

Al-Damegh, K., Sandoval, E., Brazangi, M., 2005. Crustal structure of the Arabian plate: new constraints from the analysis of teleseismic receiver functions. Earth Planet. Sci. Lett. 231, 177–196.

Al-Heety, E.A.M., 2002. Crustal structure of the northern Arabian platform inferred using spectral ratio method. J. Geodyn. 34, 63–75.

Al-Husseini, M., 2000. Origin of the Arabian Plate structures: Amar Collision and Najd Rift. GeoArabia 5, 527–542.

Ali, M., Arai, S., 2007. Clinopyroxene-rich lherzolite xenoliths from Bir Ali, Yemen — possible product of peridotite/melt reactions. J. Mineral. Petrol. Sci. 102, 137–142.

Al-Lazki, A.I., Seber, D., Sandvol, E., Barazangi, M., 2002. A crustal transect across the Oman Mountains on the eastern margin of Arabia. GeoArabia 7, 47–78.

Al-Mishwat, A.T., Nasir, S.J., 2004. Composition of the lower crust of the Arabian Plate: a xenolith perspective. Lithos 72, 45–72.

Al-Saad, D., et al., 1992. Crustal structure of central Syria: the intracontinental Palmyride mountain belt. Tectonophysics 207, 245–358.

Al-Saleh, A.M., Boyle, A.P., 2001. Neoproterozoic ensialic back-arc spreading in the eastern Arabian Shield: geochemical evidence from the Halaban ophiolite. J. Afr. Earth Sci. 33, 1–15.

Al-Zoubi, A., Ben-Avraham, Z., 2002. Structure of the Earth's crust in Jordan from potential field data. Tectonophysics 346, 45–59.

Alavi, M., 2004. Regional stratigraphy of the Zagros fold-thrust belt of Iran and its proforeland evolution. Am. J. Sci. 304, 1–20.

Allen, P.A., 2007. The Huqf Supergroup of Oman: basin development and context for Neoproterozoic glaciation. Earth-Sci. Rev. 84, 139–185.

Allen, P.A., Leather, J., 2006. Post-Marinoan marine siliclastic sedimentatio: the Masirah Bay Formation, Neoproterozoic Huqf Supergroup of Oman. Precambrian Res. 144, 167–198.

Alsinawi, S.A., 2003. Seismicity, seismotectonics, crustal structure, and attentuation data on Iraq. UNESCO-RELEMR (Reduction of Earthquake Losses in the Expanded Mediterranean Region) Workshop on Seismic Hazard Analysis and Data Exchange in the Mediterannean Region, Cyprus.

Amelin, Y., Rotenberg, E., 2004. Sm–Nd systematics of chondrites. Earth Planet. Sci. Lett. 223, 267–282.

Anderson, D.J., Lindsley, D.H., 1988. Internally consistent solution models for Fe–Mg–Mn–Ti oxides: Fe–Ti oxides. Am. Mineral. 73, 714–726.

Anderson, D.L., 1995. Lithosphere, asthenosphere, and perisphere. Rev. Geophys. 33, 125–149.

Angus, D., Wilson, D.C., Sandoval, E., Ni, J.F., 2006. Lithospheric structure of the Arabian and Eurasian collision zone in eastern Turkey from S-wave receiver functions. Geophys. J. Int. 166, 1335–1346.

Arai, S., 1994. Characterization of spinel peridotites by olivine–spinel compositional relationships: review and interpretation. Chem. Geol. 113, 191–204.

Artemieva, I.M., Mooney, W.D., 2001. Thermal thickness and evolution of Precambrian lithosphere: a global study. J. Geophys. Res. B106, 16387–16414.

Avigad, D., Gvirtzman, Z., 2009. Late Neoproterozoic rise and fall of the northern Arabian–Nubian Shield: the role of lithospheric mantle delamination and subsequent thermal subsidence. Tectonophysics 477, 217–228.

Avigad, D., Kolodner, K., McWilliams, M., Persing, H.M., Weissbrod, T., 2003. Origin of northern Gondwana Cambrian sandstone as revealed by SHRIMP dating of zircons. Geology 31, 227–230.

Avigad, D., et al., 2005. Mass-production of Cambro-Ordovician quartz-rich sandstone as a consequence of chemical weathering of Pan-African terranes: environmental implications. Earth Planet. Sci. Lett. 240, 818–826.

Ayres, M.G., Bilal, M., Jones, R.W., Slentz, L.W., Tatir, M., Wilson, A.O., 1982. Hydrocarbon habitat in main producing areas. Saudi Arabia: American Association of Petroleum Geologists Bulletin 66, 1–9.

Azer, M.K., Stern, R.J., 2007. Neoproterozoic (835–720 Ma) serpentinites in the Eastern Desert, Egypt: fragments of fore-arc mantle. J. Geol. 115, 457–472.

Badri, M., 1991. Crustal structure of central Saudi Arabia determined from seismic refraction profiling. Tectonophysics 185, 357–374.

Bahroudi, A., Talbot, C.J., 2004. The configuration of the basement beneath the Zagros basin. J. Petrol. Geol. 26, 257–282.

Baker, J., G, C., Menzies, M., Thirlwall, M., 2002. Lithospheric mantle beneath Arabia: A Pan-African protolith modified by the Afar and older plumes, rather than a source for continental flood volcanism? In: Menzies, M.A., Klemperer, S.I., Ebinger, C.J., Baker, J. (Eds.), Volcanic Rifted Margins, GSA Spec. Paper 362. Geological Society of America, Boulder CO, pp. 67–82.

Be'eri-Shlevin, Y., Katzir, Y., Whitehouose, M.J., Kleinhanns, I.C., 2009. Contribution of pre Pan-African crust to formation of the Arabian–Nubian Shield: new secondary ionization mass spectrometry U–Pb and O studies of zircon. Geology 37, 899–902.

Bird, P., 2002. An updated digital model of plate boundaries. Geochem. Geophys. Geosystems 4 (3), 1027. doi:10.1029/2001GC000252.

Black, R., Liégeois, J.-P., 1993. Cratons, mobile belts, alkaline rocks and continental lithospheric mantle: the Pan-African testimony. J. Geological Society London 150, 89–98.

Blood, M.F., 2000. New Lower Paleozoic exploration plays in southwest Oman: GeoArabia, v. 5, p. Boote, D.R.D., Clark-Lowes, D.D., and Traut, M.W., 1998, Palaeozoic petroleum systems of North Africa, in Macgregor, D.S., Moody, R.T.J., and Clark-Lowes, D.D., eds. Petroleum Geology of North Africa: Geological Society of London Special Publication 132, 7–68.

Blusztajn, J., Hart, S.R., Shimizu, N., McGuire, A.V., 1995. Trace element and isotopic characteristics of spinel peridotite xenoliths from Saudi Arabia. Chem. Geol. 123, 53–65.

Bonavia, F.F., Chorowicz, J., 1992. Northward expulsion of the Pan-African of Northeast Africa guided by a reentrant zone of the Tanzania Craton. Geology 20, 1023–1026.

Bosworth, W., Huchon, P., McClay, K., 2005. The Red Sea and Gulf of Aden basins. J. Afr. Earth Sci. 43, 334–378.

Bowring, S.A., et al., 2007. Geochronological constraints on the chronostratigraphic framework of the Neoproterozoic Huqf Supergroup, Sultanate of Oman. Am. J. Sci. 307, 1097–1145.

Brasier, M., McCarron, G., Leather, J., Allen, P., Shields, G., 2000. New U–Pb zircon dates for the Neoproterozoic Ghubrah glaciation and for the top of the Huqf Supergroup, Oman. Geology 28 (2), 175–178.

Brew, G., Barazangi, M., Al-Maleh, A.K., Sawaf, T., 2001. Tectonic and geologic evolution of Syria. GeoArabia 6, 573–616.

Brey, G.P., Köhler, T., 1990. Geothermobarometry in four-phase lherzolites: II. New thermobarometers, and practical assessment of existing thermobarometers. J. Petrol. 31 (6), 1313–1352.

Brueckner, H.K., Zindler, A., Seyler, M., Bonatti, E., 1988. Zabargad and the isotopic evolution of the sub-Red Sea mantle and crust. Tectonophysics 150, 163–176.

Calvez, J.-Y., Alsac, C., Delfour, J., Kemp, J., Pellaton, C., 1984. Geologic evolution of western, central, and eastern parts of the northern Precambrian Shield, Kingdom of Saudi Arabia. Faculty of Earth Sciences Bulletin 6, 24–48.

Chazot, G., Menzies, M., Harte, B., 1996. Silicate glasses in spinel lherzolites from Yemen: origin and chemical composition. Chem. Geol. 134, 159–179.

Coleman, R.G., 1993. Geologic evolution of the Red Sea. Oxford Monographs on Geology and Geophysics 24. Oxford University Press, New York, p. 186.

Collins, A.S., Pisarevsky, S.A., 2005. Amalgamating eastern Gondwana: the evolution of the Circum-Indian Orogens. Earth-Sci. Rev. 71, 229–270.

Condie, K.C., 1999. Mafic crustal xenoliths and the origins of the lower continental crust. Lithos 46, 85–101.

Cowan, D.R., Kane, M.F., Merghelani, H., Pitkin, J.A., 2005. Regional aeromagnetic/radiometric surveys: a perspective. First Break 3, 17–21.

Dalziel, I.W.D., 1997. Overview: Neoproterrozoic–Paleozoic geography and tectonics: review, hypothesis, environmental speculation. Geol. Soc. Am. Bull. 109, 16–42.

Daradich, A., Mitrovica, J.X., Pysklywec, R.N., Willett, S.D., Foote, A.M., 2003. Mantle flow, dynamic topography, and rift-flank uplift of Arabia. Geology 31, 901–904.

Delfour, J., 1970. Le group de J'Balah, une nouvelle unité du Bouchlier Arabie. Bureau de Recherches Géologiques et Minières Bulletin no. 4, 19–32 Ser. 2, Sec. 4.

Derakshani, R., Faroudi, G., 2005. Existence of the Oman Line in the Empty Quarter of Saudi Arabia and its continuation in the Red Sea. J. Appl. Sci. 5, 745–752.

DESERT-Group, 2004. The crustal strucure of the Dead Sea Transform. Geophys. J. Int. 156, 655–681.

Dixon, T.H., Golombek, M.P., 1988. Late Precambrian crustal accretion rates in northeast Africa and Arabia. Geology 16, 991–994.

Doebrich, J.L., et al., 2007. Geology and metallogeny of the Ar Rayn terrane eastern Arabian shield: evolution of a Neoproterozoic continental-margin arc during assembly of Gondwana within the East African orogen. Precambrian Res. 158, 17–50.

Downes, H., 2007. Origin and significance of spinel and garnet pyroxenites in the shallow lithospheric mantle: ultramafic massifs in orogenic belts in western Europe and NW Africa. Lithos 99, 1–24.

Drummond, M.S., Defant, M.J., 1990. A model for trondhjemite–tonalite–dacite genesis and crustal growth via slab melting: Archean to modern comparisons. J. Geophys. Res. 95 (B), 503–521.

Dyer, R., Husseini, M., 1991. The western Rub' al Khali Infracambrian grabensystem: Society of Petroleum Engineers. Proceedings of the Middle East Oil Show, Bahrain, pp. 505–512.

Edgell, H.S., 1992. Basement tectonics of Saudi Arabia as related to Oil Field Structures. In: Rickerd, M.J., Harrington, H.J., Williams, P.R. (Eds.), Basement Tectonics 9: Australia and Other Regions: Proceedings of the Ninth International Conference on Basement Tectonics. Kluwer Academic Publishers, Dordecht, pp. 169–183.

El-Isa, Z., Mechie, J., Prodehl, C., Makris, J., Rihm, R., 1987. A crustal structure study of Jordan derived from seismic refraction data. Tectonophysics 138, 235–253.

Ellis, D.J., Green, D.H., 1979. An experimental study of the effect of Ca upon garnet–clinopyroxene Fe–Mg exchange equilibria. Contrib. Mineral. Petrol. 71, 13–22.

Esperanca, S., Garfunkel, Z., 1986. Ultramafic xenoliths from the Mt. Carmel area (Karem Maharal Volcano), Israel. Lithos 19, 43–49.

Faqira, M., Al-Hawuaj, A.Y., 1998. Infracambrian salt basin in the Western Rub' al Khali, Saudi Arabia. GeoArabia 3, 93 abstract.

Faqira, M., Rademakers, M., Afifi, A.M., 2009. New insights into the Hercynian Orogeny, and their implications for the Paleozoic Hydrocarbon System in the Arabian Plate. GeoArabia 14, 199–228.

Fouch, M.J., Rondenay, S., 2006. Seismic anisotropy beneath stable continental interiors. Phys. Earth Planet. Int. 158, 292–320.

Fountain, D.M., Salisbury, M.H., 1989. Composition of the continental crust and upper mantle: a review. Earth Planet. Sci. Lett. 56, 263–277.

Förster, A., et al., 2007. The surface heat flow of the Arabian Shield in Jordan. J. Asian Earth Sci. 30, 271–284.

Förster, H.-J., Förster, A., Oberhänsli, R., Stromeyer, D., 2009. Lithospheric composition and thermal structure of the Arabian Shield in Jordan. Tectonophysics.

Galanis, S.P., Sass, J.H., Munroe, R.J., Abu-Ajamieh, M., 1985. Heat Flow at Zerqa Ma'in and Zara and a Geothermal Reconnaissance of Jordan. US Geological Survey, Menlo Park, CA.

Gass, I.G., 1982. Upper Proteozoic (Pan-African) calc-alkaline magmatism in north-eastern Africa and Arabia. In: Thrope, R.S. (Ed.), Andesites. John Wiley & Sons, New York, pp. 591–609.

Gass, I.G., Ries, A.C., Shacleton, R.M., Smewing, J.D., 1990. Tectonics, geochronology and geochemistry of the Precambrian rocks of Oman. In: Robertson, A.H.F., Searle, M.P.,

Ries, A.C. (Eds.), Geology and Tectonics of the Oman Region. Geol. Soc. London, Spec. Pub. 49, London, pp. 585–599.

Gettings, M.E., 1982. Heat-flow measurements at shot points along the 1978 Saudi Arabia seismic deep-refraction line, part II: discussion and interpretation. Saudi Arabia Deputy Minister for Mineral Resources, Jiddah.

Gettings, M.E., Blank, H.R., Mooney, W.D., Healey, J.H., 1986. Crustal structure of southwestern Saudi Arabia. J. Geophys. Res. 91 (B6), 6491–6512.

Gettings, M.E., Showail, A., 1982. Heat-flow measurements at shot points along the 1978 Saudi Arabian deep-refraction line, part I: results of measurements. Saudi Arabia Deputy Minister for Mineral Resources, Jeddah, Saudi Arabia.

Ghent, E.D., Coleman, R.G., Hadley, D.G., 1980. Ultramafic inclusions and host Alkali Olivine Basalts of the Southerrn Coastal Plain of the Red Sea, Saudi Arabia. Am. J. Sci. 280-A, 499–527.

Gnos, E., Peters, T., 2003. Mantle xenolith-bearing Maastrichtian to Tertiary alkaline magmatism in Oman. Geochem., Geophys., Geosystems 4 (9), 8620. doi:10.1029/2001GC000229.

Gok, R., Mahdi, H., Al-Shukri, H., Rodgers, A.J., 2008. Crustal structure of Iraq from receiver functions and surface wave dispersion: implications for understanding the deformation history of the Arabian–Eurasian collision. Geophys. J. Int. 172, 1163–1187.

Grégoire, M., Langlade, J.A., Delpech, G., Dantas, C., Ceuleneer, G., 2009. Nature and evolution of the lithospheric mantle beneath the passive margin of East Oman: evidence from mantle xenoliths sampled by Cenozoic alkaline lavas. Lithos 112, 203–216.

Göğüs, O.H., Pysklywec, R.N., 2008. Near-surface diagnostics of dripping or delaminating lithosphere. J. Geophys. Res. 113 (B11404) doi:10.1029/2007JB005123.

Hacker, B.R., Abers, G.A., Peacock, S.M., 2003. Subduction factory 1. Theoretical mineralogy, densities, seismic wave speeds, and H_2O contents. J. Geophys. Res. 108 (Ba) doi:10.1029/2001JB001127.

Hadley, D.G., 1974. The taphrogeosynclinal Jubaylah group in the Mashhad area, northwestern Hijaz, Kingdom of Saudi Arabia. Saudi Arabian Directorate General of Mineral Resources Bulletin 10, 18.

Hansen, S., Schwartz, S., Al-Amri, A., Rodgers, A., 2006. Combined plate motion and density-driven flow in the asthenosphere beneath Saudi Arabia: evidence from shear-wave splitting and seismic anisotropy. Geology 34, 869–872.

Hansen, S.E., Rodgers, A.J., Schwartz, S.Y., Al-Amri, A.M.S., 2007. Imaging ruptured lithosphere beneath the Red Sea and Arabian Peninsula. Earth Planet. Sci. Lett. 259, 256–265.

Hargrove III, U.S., Stern, R.J., Griffin, W.R., Johnson, P.R. and Abdelsalam, M.G., 2006a. From Island Arc to Craton: Timescales of Crustal Formation along the Neoproterozoic Bi'r Umq Suture Zone, Kingdom of Saudi Arabia, Saudi Geological Survey. in Hargrove, U.S., Crustal evolution of the Neoproterozoic Bi'r Umq suture zone, Kingdom of Saudi Arabia: Geochronological, isotopic, and geochemical constraints. Ph.D thesis, University of Texas at Dallas, Chapter 2, p. 6–174.

Hargrove III, U.S., Stern, R.J., Kimura, J.-I., Manton, W.I., Johnson, P.R., 2006a. How juvenile is the Arabian–Nubian Shield? Evidence from Nd isotopes. Earth Planet. Sci. Lett. 252, 308–326.

Healy, J.H., Mooney, W.D., Blank, H.R., Gettings, M.E., Kohler, W.M., Lamson, R.J., Leone, L.E., 1982. Saudi Arabian seismic deep-refraction profile. Final Project Report: Saudi Arabian Deputy Ministry for Mineal Resources Open-file Report USGS-OF-02-37, 429.

Henjes-Kunst, F., Altherr, R., Baumann, A., 1990. Evolution and composition of the lithospheric mantle underneath the western Arabian Peninsula; constraints from Sr–Nd isotope systematics of mantle xenoliths. Contrib. Mineral. Petrol. 105, 460–472.

Henson, FRS, 1951. Observations on the geology and petroleum occurrences of the Middle East: 3d World Petroleum Cong. Proc., The Hague, sec. 1, pp. 118–140.

Hofmann, A.W., 1988. Chemical differentiation of the Earth: the relationship between mantle, continental crust, and oceanic crust. Earth Planet. Sci. Lett. 90, 297–314.

Howell, D.G., 1995. Principles of Terrane Analysis: New Applications for Global Tectonics. Chapman and Hall 245.

Husseini, M.I., 1990. The Cambro-Ordovician Arabian and adjoining plates: a glacio-eustatic model. J. Petrol. Geol. 13 (3), 267–288.

Husseini, M.I., Husseini, S.I., 1990. Origin of the Infracambrian salt basins of the Middle East. In: Brooks, J. (Ed.), Classic Petroleum Provinces, 50. Geological Society of London Special Publication, London, pp. 279–292.

Ishiwatari, A., 1985. Igneous petrogenesis of the Yakuno Ophiolite (Japan) in the context of the diversity of ophiolites. Contrib. Mineral. Petrol. 89, 155–167.

Ismail, M., et al., 2008. Petrological and geochemical constraints on the composition of the lithospheric mantle beneath the Syrian rift, northern part of the Arabian plate. In: Coltori, M., Grégoire, M. (Eds.), Metasomatism in Oceanic and Continental Lithospheric Mantle. Geological Society, London, pp. 223–251.

Jackson, J., Mckenzie, D., Priestley, K., Emmerson, B., 2008. New views on the structure and rheology of the lithosphere. J. Geol. Soc. London 165, 453–465.

Jacobs, J., Thomas, R.J., 2004. Himalayan-type indenter-escape tectonics model for the southern part of the late Neoproterozoic–early Paleozoic East African–Antarctic orogen. Geology 32, 721–724.

Johnson, P.R., 2003. Post-amalgamation basins of the NE Arabian shield and implications for Neoproterozoic III tectonism in the northern East African orogen. Precambrian Res. 123, 321–338.

Johnson, P.R., Kattan, F.H., 2007. Geochronological dataset for Precambrian rocks in the Arabian Peninsula: a catalogue of U–Pb, Rb–Sr, Ar–Ar, and Sm–Nd ages. SGS-OF-2007-3. Saudi Geological Survey, Jeddah, Saudi Arabia.

Johnson, P.R., Kattan, F.H., Al-Saleh, A.M., 2004. Neoproterozoic ophiolites in the Arabian Shield: field relations and structure. In: Kusky, T.M. (Ed.), Precambrian Ophiolites and Related Rocks. Developments in Precambrian Geology, Elsevier, pp. 129–162.

Johnson, P.R., Stewart, I.C.F., 1995. Magnetically inferred basement structure in central Saudi Arabia. Tectonophysics 245, 37–52.

Johnson, P.R., Woldehaimanot, B., 2003. Development of the Arabian–Nubian Shield: perspectives on accretion and deformation in the East African Orogen and the assembly of Gondwana. In: Yoshida, M., Windley, B.F., Dasgupta, S. (Eds.), Proterozoic East Gondwana: Supercontinent Assembly and Breakup. Geological Society, London, Special Publication, London, pp. 289–325.

Juliâ, J., Ammon, C.J., Herrmann, R.B., 2003. Lithospheric structure of the Arabian Shield from the joint inversion of receiver functions and surface-wave group velocities. Tectonophysics 371, 1–21.

Kaliwoda, M., Altherr, R., Meyer, H.-P., 2007. Composition and thermal evolution of the lithospheric mantle beneath the Harrat Uwayrid, eastern flank of the Red Sea rift (Saudi Arabia). Lithos 99, 105–120.

Kaviani, A., Paul, A., Bourova, E., Hatzfeld, D., Pedersen, H., Mokhtari, M., 2007. A strong seismic velocity contrast in the shallow mantle across the Zagros collision zone (Iran). Geophys. J. Int. 171, 399–410.

Kay, R.W., Kay, S.M., 1993. Delamination and delamination magmatism. Tectonophysics 219, 177–189.

Kennedy, A., Johnson, P.R., Kattan, F.H., 2004. SHRIMP geochronology in the northern Arabian Shield. Part I: data acquisition. Saudi Geological Survey Open File Report, SGS-OF-2004-11.

Kennedy, A., Johnson, P.R., Kattan, F.H., 2005. SHRIMP geochronology in the northern Arabian Shield. Part II: Data acquisition 2004: Saudi Geological Survey Open File Report, SGS-OF-2005-10.

Kennedy, A., Johnson, P.R. and Kattan, F.H., 2009 in press. SHRIMP geochronology in the northern Arabian Shield: part III data acquisition, 2006, Saudi Geological Survey Open File Report, Jeddah.

Kennedy, A., Kozdrok, W., Kattan, F.H., Ziolkowska-Kozdroj, M., and Johnson, P.R., in press. SHRIMP geochronology in the Arabian Shield (Midyan Terrane, Afif Terrane, Ad Dawadimi Terrane) and Nubian Shield (Central Eastern Desert Terrane). Part IV: data acquisition 2008. Saudi Geoogical Survey Open File Report, Jeddah.

Keppie, J.D., Nance, R.D., Murphy, J.B., Dostal, J., 2003. Terhyan, Mediterranean, and Pacific analogues for the Neoproterozoic–Paleozoic birth and development of peri-Gondwanan terranes and their transfer to Laurentia and Laurussia. Tectonophysics 365, 195–219.

Keskin, M., 2003. Magma generation by slab steepening and breakoff beneath a subduction–accretion complex: an alternative model for collision-related volcanism in Eastern Anatolia, Turkey. Geophys. Res. Lett. 30 (24), 8046. doi:10.1029/2003GL018019, 2003.

Khalil, E., 1997. Ocean-arc to continental margin volcanics sequences of the Pan-african Precambrian belt, Egypt. Egypt. J. Geol. 41, 477–528.

Knopoff, L., Fouda, A.A., 1975. Upper-mantle structure under the Arabian Peninsula. Tectonophysics 26, 121–134.

Kolodner, K., Avigad, D., McWilliams, M., Wooden, J.L., Weissbrod, T., Feinstein, S., 2006. Provenance of north Gondwana Cambrian–Ordovician sandstone: U–Pb SHRIMP dating of detrital zircons from Israel and Jordan. Geol. Mag. 143 (3), 367–391.

Konert, G., Afifi, A.M., Al-Harjri, S.A., Droste, H.J., 2001. Paleozoic stratigraphic and hydrocarbon habitat of the Arabian Plate. GeoArabia 6, 407–442.

Kumar, M.R., Ramesh, D.S., Saul, J., Sarkar, D., Kind, R., 2002. Crustal structure and upper mantle stratigraphy of the Arabian Shield. Geophys. Res. Lett. 29 (8). doi:10.1029/2001GL014530.

Kuo, L.-C., Essene, E.J., 1986. Petrology of spinel harzburgite xenoliths from the Kishb plateau, Saudi Arabia. Contrib. Mineral. Petrol. 93, 335–346.

Köhler, T.P., Brey, G., P., 1990. Calcium exchange between olivine and clinopyroxene calibrated as a geothermobarometer for natural peridotites from 2 to 60 kb with applications. Geochimica et Cosmochimica 54, 2375–2388.

Lancelot, J.R., Bosch, D., 1991. A Pan African age for the HP–HT granulite gneisses of Zabargad island: implications for the early stages of the Red Sea rifting. Earth Planet. Sci. Lett. 107, 539–549.

LeGuerroué, E., Allen, P.A., Cozzi, A., Etienne, J.L., Fanning, M., 2006. 50 Myr recovery from the largest negative $\delta^{13}C$ excursion in the Ediacaran ocean. Terra Nova 18, 147–153.

Levin, V., Henza, A., Park, J., Rodgers, A., 2006. Texture of mantle lithosphere along the Dead Sea Rift: recently imposed or inherited? Phys. Earth Planet. Int. 158, 174–189.

Levin, V., Park, J., 2000. Shear Zones in the Proterozoic lithosphere of the Arabian Shield and the nature of the Hales discontinuity. Tectonophysics 323, 131–148.

Loosveld, R.J.H., Bell, A., Terken, J.J.M., 1996. The tectonic evolution of Interior Oman. GeoArabia 1, 28–51.

Matviyenko, V.N., Makhan'kov, O.M., Khazim, D., Khair, Y.E., Asmi, M., 1993. Geothermal conditions in oil- and gas-bearing regions of Syria. Int. Geol. Rev. 35, 453–466.

McDonough, W.F., Sun, S.-S., 1995. The composition of the Earth. Chem. Geol. 120, 223–253.

McGuire, A.V., 1988a. The mantle beneath the Red Sea: xenoliths from western Saudi Arabia. Tectonophysics 150, 101–119.

McGuire, A.W., 1988b. Petrology of mantle xenoliths from Harrat al Kishb: the mantle beneath western Saudi Arabia. J. Petrol. 29, 73–92.

McGuire, A.V., Stern, R.J., 1993. Granulite xenoliths from western Saudi Arabia: the lower crust of the Late Precambrian Arabian–Nubian Shield. Contrib. Mineral. Petrol. 114, 395–408.

Mclennan, S.M., Taylor, S.R., Heming, S.R., 2005. Composition, differentiation, and evolution of continental crust; constraints from sedimentary rocks and heatflow. In: Brown, M., Rushmer, T. (Eds.), Evolution and Differentiation of the Continental Crust. Cambridge U Press, Cambridge, pp. 92–134.

Mechie, J., Prodehl, C., Koptschalitsch, G., 1986. Ray path interpretation of the crustal structure beneath Saudi Arabia. Tectonophysics 131, 333–352.

Medaris Jr., L.G., Syada, G., 1999. Pyroxenite xenoliths from Al Ashaer Volcano, Syria: constraints on the thermal state of the subcontinental Arabian lithosphere. Int. Geol. Rev. 41, 895–905.

Medaris Jr., L.G., Syada, G., 1998. Spinel peridotite xenoliths from the Al Ashaer volcano, Syria: a contribution to the elemental composition and thermal state of subcontinental Arabian lithosphere. Int. Geol. Rev. 40, 305–324.

Meert, J.G., Lieberman, B.S., 2008. The Neoproterozoic assembly of Gondwana and its relationship to the Ediacaran–Cambrian radiation. Gondwana Res. 154, 5–21.

Meert, J.G., Torsvik, T.H., 2003. The making and unmaking of a supercontinent: Rodinia revisited. Tectonophysics 375, 261–288.

Mercolli, I., et al., 2006. Lithostratigraphy and geochronology of the Neoproterozoic crystalline basement of Salalah, Dhofar, Sultanate of Oman. Precambrian Res. 145, 182–206.

Midzi, V., 2005. The receiver structure beneath the Kuwait National Seismic Network. MESF Cyber J. Earth Sci. 3, 1–21.

Miller, N.R., Johnson, P.R., Stern, R.J., 2008. Marine versus non-marine environments for the Jibalah Group, NW Arabian Shield: a sedimentologic and geochemical survey and report of possible metazoa in the Dhaiqa Formation. Arabian J. Sci. Eng. 33 (1C), 55–77.

Mohsen, A., Hofstetter, R., Bock, G., Kind, R., Weber, M., Wylegalla, K., Rümpker, G., DESERT Group, 2005. A receiver function study across the Dead Sea Transform. Geophys. J. Int. 160 (3), 948–960.

Mohsen, A., Kind, R., Sobolev, S.V., Weber, M., DESERT-Group, 2006. Thickness of the lithosphere east of the Dead Sea Transform. Geophys. J. Int. 167, 845–852.

Mokhtar, T.A., Ammon, C.J., Herrmann, R.B., Ghalib, H.A.A., 2001. Surface wave velocities across Arabia. Pure Appl. Geophys. 158, 1425–1444.

Mooney, W.D., Gettings, M.E., Blank, H.R., Healey, J.H., 1985. Saudi Arabian seismic-refraction profile: a traveltime interpretation of crustal and upper mantle structure. Tectonophysics 111, 173–246.

Mooney, W.D., Laske, G., Masters, T.G., 1998. CRUST 5.1: a global crustal model at 5°×5°. J. Geophys. Res. B103, 727–747.

Morgan, P., Gosnold, W.D., 1989. Heat flow and thermal regimes in the continental United States. In: Pakiser, L.C., Mooney, W.D. (Eds.), Geophysical Framework of the Continental United States. Geol. Soc. America, Boulder, CO, pp. 493–522.

Nasir, S., 1992. The lithosphere beneath the northwestern part of the Arabian plate (Jordan): evidence from xenoliths and geophysics. Tectonophysics 201, 357–370.

Nasir, S., 1995. Mafic lower-crustal xenoliths from the northwestern part of the Arabian Plate. Eur. J. Mineralog. 7, 217–230.

Nasir, S., Al-Fuqha, H., 1988. Spinel-lherzolite xenoliths from Aritain Volcano, NE-Jordan. Mineralog. Petrol. 38, 127–137.

Nasir, S., Al-Sayigh, A., Alharthy, A., Al-Lazki, A., 2006. Geochemistry and petrology of Tertiary volcanic rocks and related ultramafic xenoliths from the central and eastern Oman Mountains. Lithos 90, 249–270.

Nasir, S., Rollinson, H., 2009. The nature of the subcontinental mantle beneath the Arabian Shield: mantle xenoliths from southern Syria. Precambrian Res. 172, 323–333.

Nasir, S., Safarjalani, A., 2000. Lithospheric petrology beneath the northern part of the Arabian Plate in Syria: evidence from xenoliths in alkali basalts. J. Afr. Earth Sci. 30, 149–168.

Nehlig, P., Genna, A., Asirfane, F., 2002. A review of the Pan-African evolution of the Arabian Shield. GeoArabia 7, 103–124.

Nelson, B.K., DePaolo, D.J., 1984. Rapid production of continental crust 1.7 to 1.9 b.y. ago: Nd isotopic evidence from the basement of the North American mid-continent. Geol. Soc. Am. Bull. 96, 746–754.

Nicholson, P.G., Janjou, D.L.A., Fanning, C.M., Heaman, L.M., Grotzinger, J.P., 2008. Deposition, age, and pan-Arabian correlation of late Neoproterozoic outcrops in Saudi Arabia (abstract), GEO 2008. Manama, Bahrain.

Nickel, K.G., Green, D.H., 1985. Empirical geothermobarometry for garnet peridotites and implications for the nature of the lithosphere, kimberlites and diamonds. Earth Planet. Sci. Lett. 73, 158–170.

Nyblade, A.A., 1999. Heat flow and the structure of Precambrian lithosphere. Lithos 48, 81–91.

Pallister, J.S., Cole, J.C., Stoeser, D.B., Quick, J.E., 1990. Use and abuse of crustal accretion calculations. Geology 18, 35–39.

Pallister, J.S., Stacey, J.S., Fischer, L.B., Premo, W.R., 1988. Precambrian ophiolites of Arabia: geologic settings, U–Pb geochronology, Pb-isotope characteristics, and implications for continental accretion. Precambrian Res. 38, 1–54.

Park, Y., Nyblade, A.A., Rodgers, A.J., Al-Amri, A., 2008. S wave velocity structure of the Arabian Shield upper mantle from Rayleigh wave tomography. Geochem., Geophys., Geosystems 9 (7). doi:10.1029/2007GC001895.

Pasyanos, M.E., Tkalcic, H., Gök, R., Al-Enzi, A., Rodgers, A.J., 2007. Seismic structure of Kuwait. Geophys. J. Int. 170, 299–312.

Peslier, A.H., Francis, D., Ludden, J., 2002. The lithospheric mantle beneath continental margins: melting and melt-rock reaction in Canadian Cordillera xenoliths. J. Petrol. 43, 2013–2047.

Prodehl, C., 1985. Interpretation of a seismic-refraction survey across the Arabian Shield in western Saudi Arabia. Tectonophysics 111, 247–282.

Reymer, A.P.S., Matthews, A., Navon, O., 1984. Pressure–temperature conditions in the Wadi Kid metamorphic complex: implications for the Pan-African event in SE Sinai. Contrib. Mineral. Petrol. 85, 336–345.

Rieu, R., Allen, P.A., Cozzi, A., Kosler, J., Bussy, F., 2007. A composite stratigraphy for the Neoproterozoic Huqf Supergroup of Oman: integrating new litho-, chemo-, and chronostratigraphic data of the Mirbat area, southern Oman. J. Geol. Soc. London 164, 997–1009.

Rodgers, A.J., Walter, W.R., Mellors, R.J., Al-Amri, A.M.S., Zhang, Y.-S., 1999. Lithospheric structure of the Arabian Shield and platform from complete regional wave group velocities. Geophys. J. Int. 138, 871–878.

Roger, J., Bechennec, F., Janjoud, D., LeMetour, J., Wyns, R., Beurrier, M., 1991. Geologic Map of J'alan, sheet NF 40-8E, Scale 1:100,000, with Explanatory Notes. Directorate General of Minerals, Oman Ministry of Petroleum and Minerals.

Rogers, J.J.W., Santosh, M., 2004. Continents and Supercontinents. Oxford University Press, p. 371.

Roobol, M.J., Ramsay, C.R., Jackson, N.J., Darbyshire, D.P.F., 1983. Late Proterozoic lavas of the Central Arabian Shield: evolution of an ancient volcanic arc system. J. Geol. Soc. London 140 (2), 185–202.

Rudnick, R.L., McDonough, W.F., O'Connell, R.J., 1998. Thermal structure, thickness and composition of continental lithosphere. Chem. Geol. 145, 395–411.

Safarjalani, A., Nasir, S., Fockenberg, T., Massonne, H.-J., 2009. Chemical composition of the upper part of the lower crust beneath the Arabian Plate. Chem. Erde 69, 359–375.

Sandvol, E., Seber, D., Barazangi, M., Vernon, F., Mellors, R., Al-Amri, A., 1998. Lithospheric seismic velocity discontinuities beneath the Arabian Shield. Geophys. Res. Lett. 25, 2873–2876.

Seber, D., Mitchell, B., 1992. Attenuation of surface waves across the Arabian peninsula. Tectonophysics 204, 137–150.

Seber, D., Sandoval, E., Sandoval, C., Brindisi, C., Barazangi, M., 2001. Crustal model for the Middle East and North Africa region; implications for the isostatic compensation mechanism. Geophys. J. Int. 147, 630–638.

Sharkov, Y.V., Laz'ko, Y.Y., Hanna, S., 1993. Plutonic xenoliths from Nabi Matta Explosive Center, Northwest Syria. Geochem. Int. 30, 23–44.

Sharland, P.R., Archer, R., Casey, D.M., Davies, R.B., Hall, S.H., Heward, A.P., Horbury, A.D., Simmons, M.D., 2001. Arabian Plate sequence stratigraphy. GeoArabia Special Publication 2, 371.

Shaw, J.E., Baker, J.A., Kent, A.J.R., Ibrahim, K.M., Menzies, M.A., 2007. The geochemistry of the Arabian lithospheric mantle — a source for intraplate volcanism? J. Petrol. 48 (8), 1495–1512.

Squire, R.J., Campbell, I.H., Allen, C.M., Wilson, C.J.L., 2006. Did the Transgondwanan Supermountain trigger the explosive radiation of animals on Earth? Earth Planet. Sci. Lett. 250, 115–133.

Stacey, J.S., Agar, R.A., 1985. U–Pb isotopic evidence for the accretion of a continental microplate in the Zalm region of the Saudi Arabian Shield. J. Geol. Soc. London 142, 1189–1203.

Stacey, J.S., Stoeser, D.B., Greenwood, W.R., Fischer, L.B., 1984. U–Pb zircon geochronology and geological evolution of the Halaban–Al Amar region of the eastern Arabian Shield, Kingdom of Saudi Arabia. J. Geol. Soc. London 141, 1043–1055.

Stampfli, G.M., Hochard, C., Raumer, J.V., 2006. Reconstructing the Paleozoic Gondwana margin and its redistributon — new aspects. EGU Geophysical Research Abstracts.

Stein, M., 2003. Tracing the plume material in the Arabian–Nubian Shield. Precambrian Res. 123, 223–234.

Stein, M., Katz, A., 1989. The composition of the subcontinental lithosphere beneath Israel: inferences from peridotitic xenoliths. Israel J. Earth Sci. 38, 75–87.

Stein, M., Garfunkel, Z., Jagoutz, E., 1993. Chronometry of peridotitic and pyroxenitic xenoliths: implications for the thermal evolution of the Arabian lithosphere. Geochim. Cosmochim. Acta 57, 1325–1337.

Stern, R.J., 1994. Arc assembly and continental collision in the Neoproterozoic East African Orogen: implications for the consolidation of Gondwanaland. Annual Reviews of Earth and Planetary Sciences 22, 319–351.

Stern, R.J., 2002a. Crustal evolution in the East African Orogen: a neodymium isotopic perspective. J. Afr. Earth Sci. 34, 109–117.

Stern, R.J., 2002b. Subduction zones. Rev. Geophys. 40, 1012. doi:10.1029/2001RG000108.

Stern, R.J., Abdelsalam, M.G., 1998. Formation of continental crust in the Arabian–Nubian shield: evidence from granitic rocks of the Nakasib suture, NE Sudan. Geol. Rundsch. 87, 150–160.

Stern, R.J., Johnson, P.J., Kröner, A., Yibas, B., 2004. Neoproterozoic ophiolites of the Arabian-Nubian Shield. In: Kusky, T. (Ed.), Precambrian Ophiolites. Elsevier, Amsterdam, pp. 95–128.

Stern, R.J., Johnson, P.R., 2008. Do variations in Arabian plate lithospheric structure control deformation in the Arabian–Eurasian convergence zone? Donald D. Harrington Symposium on the Geology of the Aegean. IOP Conf. Series. Earth & Environ. Sci. 2. doi:10.1088/1755-1307/2/1/012005.

Stoeser, D.B., Camp, V.E., 1985. Pan-African microplate accretion of the Arabian Shield. Geol. Soc. Am. Bull. 96 (7), 817–826.

Stoeser, D.B., Frost, C.D., 2006. Nd, Pb, Sr, and O isotopic characterization of Saudi Arabian Shield terranes. Chem. Geol. 226, 163–188.

Stoeser, D.B., Stacey, J.S., 1988. Evolution, U–Pb geochronology, and isotope geology of the Pan-African Nabitah orogenic belt of the Saudi Arabian shield. In: El-Gaby, S., Greiling, R.O. (Eds.), The Pan-African Belt of NE Africa and Adjacent Areas. Friedr. Vieweg & Sohn, Braunschweig, pp. 227–289.

Thornber, C.R., 1992. The petrology, geochemistry and origin of ultramafic inclusions and mafic alkaline volcanics from Harrat Hutaymah, Saudi Arabia. Ph.D. Thesis, University of Colorado, Boulder CO, 233pp.

Tkalcic, H., Pasyanos, M.E., Rodgers, A.J., Gok, R., Walter, W.R., Al-Amri, A., 2006. A multistep approach for joint modeling of surface wave dispersion and teleseismic receiver functions: implications for lithospheric structure of the Arabian Peninsula. J. Geophys. Res. 111 (B11311). doi:10.1029/2005JB004130, 2006.

Vaslet, D., 1987. The Paleozoic (pre-Late Permian) of central Arabia and correlations with neighboring regions. Saudi Arabian Deputy Ministry for Mineral Resources.

Watson, A.D., 1994. Az Zabirah bauxite deposit. In: Collenette, P., Grainger, D.J. (Eds.), Mineral Resources of Saudi Arabia. Saudi Arabian Directorate General of Mineral Resources, pp. 23–36.

Webb, S.A.C., Wood, B.J., 1986. Spinel–pyroxene–garnet relationships and their dependence on Cr/Al ratio. Contrib. Mineral. Petrol. 92, 471–480.

Wells, P.R.A., 1977. Pyroxene thermometry in simple and complex systems. Contrib. Mineral. Petrol. 62, 129–139.

Wever, T., 1989. The Conrad Discontinuity and the top of the reflective crust — do they coincide? Tectonophysics 157, 39–58.

Whitehouse, M.J., Stoeser, D.B., Stacey, J.S., 2001a. The Khida terrane — geochronological and isotopic evidence for Paleoproterozoic and Archean crust in the eastern Arabian Shield of Saudi Arabia (extended abstract). Gondwana Res. 4 (2), 200–202.

Whitehouse, M.J., et al., 2001b. Precambrian basement character of Yemen and correlations with Saudi Arabia and Somalia. Precambrian Res. 105, 357–369.

Wilshire, H.G., Shervais, J.W., 1975. Al-augite and Cr-diopside ultramafic xenoliths in basaltic rocks from the Western United States. Phys. Chem. Solid Earth 9, 257–272.

Windley, B.F., Whitehouse, M.J., Ba-Bttat, M.A.O., 1996. Early Precambrian gneiss terranes and Pan-African island arcs in Yemen: crustal accretion of the Arabian Shield. Geology 24, 131–134.

Wolfe, C.J., 1999. Shear-wave splitting across western Saudi Arabia: the pattern of upper mantle anisotropy at a Proterozoic shield. Geophys. Res. Lett. 26 (6), 779–782.

Wood, B.J., Banno, S., 1973. Garnet–orthopyroxene and othopyroxene–clinopyroxene relationships in simple and complex systems. Contrib. Mineral. Petrol. 42, 109–124.

Worsley, T.R., Nance, R.D., Moody, J.B., 1986. Tectonic cycles and the history of the Earth's biogeochemical and paleoceanographic record. Paleogeography 1, 233–263.

Worthing, M.A., 2005. Petrology and geochronology of a Neoproterozoic dyke swarm from Marbat, South Oman. J. Afr. Earth Sci. 41, 248–265.

Würsten, F., et al., 1991. The uplift history of the Precambrian crystalline basement of the Jabal J'alan (Sur, area). In: Peters, T., Nicolas, A., Coleman, R.G. (Eds.), Ophiolite Genesis and Evolution of the Oceanic Lithosphere, Dordrecht, pp. 613–626.

Zahran, H.M., Stewart, I.C.F., Johnson, P.R. and Basahel, M.H., 2003. Aeromagnetic-anomaly maps of central and western Saudi Arabia. Saudi Geological Survey. Scale 1:2 million. Saudi Geological Survey Open-File Report SGS-OF-2002-8, 6 p., 4 plates.

Ziegler, M.A., 2001. Late Permian to Holocene paleofacies evolution of the Arabian Plate and its hydrocarbon occurences. GeoArabia 6, 445–504.